INTERNAL FRICTION PHENOMENA IN SODIUM CHLORIDE

A thesis submitted in supplication

for the degree of Doctor of Philosophy,

by

David Clive Phillips, B.Sc. (Bristol), M.Sc. (Birmingham).

Department of Metallurgy,
Royal School of Mines,
Imperial College of Science and Technology,
University of London.

July 1968.

ABSTRACT

The internal friction of plastically deformed sodium chloride in the Kc/s range of frequency is due predominantly to the presence of mobile dislocations. After deformation the recovery of internal friction is sensitively affected by the state of dispersion of point defects in the material. Damping measurements have been carried out on pure and cadmium doped crystals of sodium chloride at 90 Kc/s as a function of vibration amplitude, time after deformation and temperature. It has been shown that the recovery of internal friction in Na Cl obeys the theory of Granato, Hikata and Lucke and an attempt has been made to measure the energy of migration of pinning defects which diffuse to the dislocations, and their binding energy with the dislocations. D.C. conductivity and dielectric loss measurements have been employed to determine the state of dispersion of point defects in similar material to that used in the internal friction measurements and the information from these measurements has been combined to identify the mobile pinning defect as the associated divalent cation - vacancy pair.

TABLE OF CONTENTS

Chapter 1.

Introduction and literature survey.

1.1 The aims and scope of this work

The internal friction which arises from dislocation motion in crystals is very sensitively affected by the interaction between the dislocations and other lattice defects. This thesis describes how this phenomenon has been used to study the interaction between dislocations and point defects in single crystal sodium chloride. Measurements of internal friction have been carried out on both pure and cadmium doped crystals as a function of vibration amplitude, temperature, prestrain and time after prestrain, and the results have been interpreted in terms of existing theories.

The physical properties of ionic crystals are strongly affected by the presence of lattice vacancies and the small quantities of impurity ions which exist in real, nominally pure, specimens. The state of dispersion of these point defects is an important factor to consider when interpreting such measurements. Dielectric loss, D.C. conductivity and polarographic analysis measurements have been carried out in conjunction with the internal friction measurements to provide information about the state of dispersion of the point defects, and chemical etching studies have been employed to obtain information about dislocations in the specimens.

This chapter contains a brief review of some of the relevant physical properties of sodium chloride, an introduction to internal friction, and a survey of the previous work on internal friction in sodium chloride. Chapter 2 describes the experimental techniques and apparatus employed in this investigation, and the succeeding chapters

present the results and interpretation of the measurements. The results fall naturally into four sections and each of chapters 3, 4, 5 and 6 presents a separate section together with a discussion of the results of that section and the conclusions obtained from them. Finally chapter 7 seeks to unify the conclusions, discusses them generally and provides suggestions for future work.

1.2 Dislocations in sodium chloride

Sodium chloride (Na Cl) is an ionic solid. Its structure consists of a simple cubic array of alternate positive sodium ions and negative chlorine ions, each surrounded by six nearest neighbours of opposite sign. The ionic radius of Na^+ is 0.95 Å and of Cl^- is 1.81 Å.[1]

Single crystals of Na Cl cleave readily on $\{100\}$ planes and this provides a simple method of producing specimens of the same orientation. When a Na Cl crystal is compressed in a $[100]$ direction at room temperature, deformation occurs by slip in $\langle 110 \rangle$ directions on the $\{110\}$ planes which do not contain the compression direction.[2] There are four equivalent $\{110\}$ $\langle \bar{1}10 \rangle$ slip systems in such a case but deformation does not involve similar amounts of slip on all four. The stress - strain curve of single crystal Na Cl at room temperature typically displays three stages, in a similar way to many f.c.c. metals. (Fig. 1.1). Davidge and Pratt[3] have shown that the most common mode of deformation is by slip commencing on two orthogonal planes, one of which rapidly becomes predominant so that slip occurs principally on a single (major) slip system and this gives rise to a linear stress - strain behaviour in stage I. Stage II is

characterised by the appearance of slip on the oblique systems and is more complex. Density changes occur in both stage I and stage II and, employing a calculation due to Seeger and Haasen, Davidge and Pratt have shown that these changes are too ~~small~~ GREAT to attribute merely to increased dislocation density. They conclude that the density changes are due to the formation of dislocation debris i.e. dislocation dipoles, clusters of point defects and individual point defects. Kear, Taylor and Pratt[4] have demonstrated theoretically how dislocation intersections in Na Cl may produce vacancies. However Taylor and Pratt[5] have carried out conductivity measurements on Na Cl as a function of deformation and were unable to detect the increased conductivity which would be expected if the free vacancy concentration is increased IN TALL SPECIMENS. A possible explanation of the anomaly between the density and conductivity measurements is that dislocation debris is primarily dislocation dipoles and that few free vacancies are formed.

Dislocations in Na Cl differ from those in metals because they can carry an electrostatic charge. Half jogs on $\{1\bar{1}0\}\ \langle 110\rangle$ dislocations can be formed by the binding of vacancies to the core of the dislocation and bear an electric charge equal in magnitude to half the charge of an electron.[6] Eshelby et al[7] considered the thermodynamic equilibrium of edge dislocations, treated as sources and sinks of vacancies, and showed that they would in general bear a nett electric charge in the form of an excess of half jogs of one sign because of the different concentrations of positive and negative vacancies. In order to maintain electric neutrality in the bulk of the crystal the charged dislocation jogs are surrounded by a charge cloud of vacancies of

opposite sign. Depending on how close the jogs are together, this can result in two extreme cases, one in which the dislocation is surrounded by a space charge cylinder of vacancies, and the other in which there are localised regions of charge which might act as pinning points on the dislocation.

1.3 Point defects in Na Cl

The predominant thermally produced point defect in Na Cl, the Schottky defect, consists of a cation vacancy plus an anion vacancy. Thermally produced cation and anion vacancies must exist in equal numbers in the bulk of the crystal in order to maintain electrostatic neutrality. Interstitial ions are rare because of their high energy of formation.(8)

Additional vacancies exist in real Na Cl crystals due to the presence of substitutional polyvalent ions and the condition of maintenance of bulk electrostatic neutrality. Electrical conductivity at temperatures below 400°C is due almost exclusively to the motion of cation vacancies, indicating that diffusion of this species is considerably easier than that of anion vacancies because of the difference in ionic size. For this reason cation vacancy formation will be considered in more detail than anion vacancy formation. Divalent metal ions may be introduced substitutionally into the Na Cl lattice, and in order to achieve electrostatic neutrality an equal number of cation vacancies must be created. Association can occur between the divalent cations and the cation vacancies to produce impurity - vacancy pairs which can act as electrical and mechanical

dipoles.[9][10] Different types of dipole can exist depending on the relative proximity of the impurity and the vacancy e.g. nearest neighbour dipole and next nearest neighbour dipole. Further association can also occur to produce higher aggregates, and electron microscopy[11] and X-ray studies[12] have revealed the existence of a precipitated phase in Na Cl alloyed with thousands of mole parts per million (m.p.m.) of divalent cation. The actual state of dispersion of the divalent cation impurities and cation vacancies depends on the concentration of impurity, temperature and heat treatment of the crystal, but in general a real Na Cl crystal may be expected to contain at room temperature divalent ions and cation vacancies in all forms ranging from unassociated to possibly precipitate. Two techniques which may be used to study the state of dispersion are electrical conductivity and dielectric loss, and something will be said of them here.

1.4 The electrical conductivity of Na Cl

Electrical conductivity in Na Cl is almost purely ionic and although it is possible that there is a small electronic contribution this contribution is not important in the present work and will be ignored. The ionic conductivity (σ_c) is related to the concentration (n) and the mobility (μ) of the cation vacancies by

$$\sigma_c = n e \mu \qquad 1.1$$

where e is the electronic charge and

$$\mu \propto \frac{1}{T} \exp\left(\frac{-E_m^{\boxplus}}{kT}\right) \qquad 1.2$$

where T is temperature, k is Boltzmann's constant and $E_m^{\boxplus}$ is the

activation energy for motion of the cation vacancy. Thus

$$\sigma_c \propto \frac{n}{T} \exp.\left(-\frac{E_m^{\boxplus}}{kT}\right) \qquad 1.3$$

and if n is temperature independent, a conductivity plot of $\ln\sigma_c T$ v. $1/T$ yields a straight line whose slope is $-E_m^{\boxplus}/k$. In practice the conductivity plot of real Na Cl consists of several stages of differing slopes,[13][14] which may be approximated into three regions (Fig. 1.2).

The conductivity of stage I is an intrinsic property of the Na Cl lattice and is due predominantly to the thermally produced cation vacancies, while the contribution due to the cation vacancies produced by virtue of the presence of substitutional divalent impurities is negligible. In this region of intrinsic conductivity the cation vacancy concentration is given by

$$\frac{n}{N} \propto \exp.\left(\frac{-E_s}{2kT}\right) \qquad 1.4$$

where N is the concentration of cation lattice sites and E_s is the energy of formation of a Schottky defect. The slope of stage I is thus $-(E_m^{\boxplus} + E_s/2)/k$. At about 400°C a transition occurs from stage I to stage II as the temperature dependent concentration due to Schottky defects becomes equal to the concentration of free vacancies due to the substitutional divalent cations. In stage II the concentration of cation vacancies remains constant and equal to the concentration of divalent cation impurities and the slope of this stage is $-E_m^{\boxplus}/k$. Stage III is more complicated than stages I and II and is very dependent on the concentration of impurity and the thermal history

of the specimen. Initially, as the temperature is decreased below that of stage II, association of cation impurities and cation vacancies decreases the free vacancy concentration. This association reaction may be described by the law of mass action :

$$\underset{\text{impurity}}{M^{++}} + \boxplus \rightleftharpoons \underset{\text{impurity - vacancy pair}}{M^{++}.\boxplus}$$

$$\frac{p}{(1-p)^2} = Z_a \sigma \exp\left(\frac{E_a}{kT}\right) \qquad 1.5$$

where σ is the concentration of divalent impurity, p is the fraction of impurity associated with vacancy to form nearest neighbour pairs, Z_a is the number of distinct orientations of the pair and E_a is the binding energy of the pair. Thus the slope of stage III is $-(E_m^{\boxplus} + E_a/2)/k$. In doped specimens the conductivity plot can steepen at lower temperatures and this has been explained in terms of impurity precipitation,[14] then at lower temperatures still the original stage III slope is regained as the kinetics of precipitation are slowed. The behaviour is too complicated to discuss here but the important fact to note is that conductivity at room temperature is due to impurity induced cation vacancies, and that the conductivity at a given temperature is proportional to the free cation vacancy concentration.

1.5 Dielectric Relaxation in Na Cl

The electric dipole formed by the association of a divalent cation impurity and a cation vacancy on near lattice sites has several possible equivalent orientations in the lattice, and may rotate to the

energetically most favourable position in an electric field. On application of an alternating electric field there is an energy absorption from the field due to the rotation of the dipoles and this is manifested as a phase lag δ of the rotating dipoles behind the electric field. Debye has developed a model describing dielectric relaxation in dipolar solids which enables dielectric loss to be related to the frequency (ω) of the applied field. This relationship is

$$\tan\delta = K_d \frac{\omega\tau}{1+\omega^2\tau^2} \qquad 1.6$$

for the relaxation of dipoles with a single relaxation time τ. K_d is a constant. This model describes the behaviour of many dipole systems in ionic solids, and estimates of the concentration of free dipoles may be obtained from the height of the Debye peak which is given by

$$(\tan\delta)_{max.} = p \frac{2\pi e^2 c}{3a\ kT} \qquad 1.7$$

where c is the mole fraction of divalent ions and p is the fraction of divalent ions associated with vacancies in the form of free dipoles. Cook and Dryden [9][15][16] and Quin[17] have studied dielectric loss in Na Cl doped with Mn^{++} and Ca^{++} and have found that on quenching specimens from above 200°C most of the divalent ions are associated with cation vacancies to form free dipoles. By studying the decrease in height of the loss peak as a function of time they conclude that

dipoles initially aggregate in a third order reaction to form trimers, i.e. a combination of three dipoles. Complexes of higher order then grow, and in equilibrium at room temperature most of the divalent ions and cation vacancies are associated in these higher complexes.

1.6 Internal friction

Internal friction is the capacity of a vibrating solid to dissipate its mechanical energy of vibration by processes within, and characteristic of, the solid. The subject has been extensively reviewed[18][19][20] and will be only briefly introduced here. In practice the damping of vibrations of a solid generally arises from external effects such as loss of energy by atmospheric friction and through the supporting members attached to the solid, as well as internal friction. The former effects may be minimised by careful experimental design so that damping due to internal friction may be studied unambiguously. This is frequently accomplished by vibrating a solid in one of its simple vibration modes and suspending it in vacuo at vibration nodes. By suspending at vibration nodes, energy losses along the supports are minimised, and removal of the atmosphere prevents atmospheric friction. Damping within the solid may then be measured by studying either the resonance curve of the specimen in forced vibrations to obtain the resonance Q factor, or the decay of free vibrations to obtain the logarithmic decrement (usually termed simply, decrement)Δ. These quantities are related simply to more fundamental measures of internal friction, dW/W and ϕ, where dW is the loss of vibration energy per cycle and W is the maximum stored

vibration energy, and ϕ is the phase lag angle of oscillating strain behind oscillating stress.

If f_r is the resonant frequency in forced vibrations and f_1 and f_2 are the frequencies at which the amplitude of vibration falls to $1/\sqrt{2}$ of the maximum value (Fig. 1.3)

$$\frac{1}{Q} = \frac{f_2 - f_1}{f_r} \qquad 1.8$$

Alternatively, if a specimen is vibrating freely and the amplitude of vibration decreases from Θ_1 to Θ_2 in 1 cycle, the decrement is given by

$$\Delta = \ln\left(\frac{\Theta_1}{\Theta_2}\right) \qquad 1.9$$

For a specimen in which the internal friction is small and amplitude independent, and the strain homogeneous[18]

$$\frac{1}{Q} = \frac{\Delta}{\pi} = \frac{dW}{2\pi W} = \phi \qquad 1.10$$

Internal friction is a result of the non-elastic behaviour of a real solid. In such a material under stress the strain is greater than it would be if the material was perfectly elastic. This causes a decrease $\triangle E$ in the apparent value of the elastic modulus E_{el} and leads to a real modulus E. Internal friction ϕ and modulus defect $\triangle E/E$ are closely related, as shown by Nowick. In general if an oscillatory stress

$$\sigma = \sigma_1 \exp(i\omega t)$$

is applied to a solid, an oscillatory strain is produced which can be divided into two parts, an elastic part

$$\varepsilon' = \varepsilon_1' \exp.i\omega t$$

and a non-elastic part

$$\varepsilon'' = (\varepsilon_1'' - i\,\varepsilon_2'') \exp.\, i\omega t \quad .$$

Because internal friction and modulus defect are usually very small

$$|\varepsilon''| \ll |\varepsilon'|$$

and it may be seen (Fig. 1.4) that the angle of lag of strain behind stress is

$$\phi \approx \frac{\varepsilon_2''}{\varepsilon_1'} \qquad 1.11$$

The measured dynamic modulus E is given by

$$E = \frac{\sigma_1}{\varepsilon_1' + \varepsilon_1''} \approx \frac{\sigma_1}{\varepsilon_1'} \left(1 - \frac{\varepsilon_1''}{\varepsilon_1'}\right)$$

or

$$E = E_{el.} \left(1 - \frac{\varepsilon_1''}{\varepsilon'}\right)$$

Thus $$\frac{\Delta E}{E} = \frac{E_{el} - E}{E} = \frac{\varepsilon_1''}{\varepsilon_1'} \qquad 1.12$$

Hence internal friction ϕ is a result of the component of strain out of phase with stress, while the modulus defect $\Delta E/E$ depends on

the component in phase with stress.

Mechanisms of internal friction may be roughly divided into two classes. The first contains relaxation processes in which the internal friction is frequency dependent and to a first approximation amplitude independent. These typically display one or more peaks when internal friction is plotted against frequency, and each peak is defined by one or more relaxation times each of which is related to temperature by an Arrhenius equation. An example of this type of behaviour in Na Cl is the anelastic peaks due to mechanical dipole orientation[10] which is the mechanical analogue of the dielectric loss peaks due to electric dipoles. The second class contains hysteretic phenomena in which internal friction is amplitude dependent but, to a first approximation, frequency independent.

1.7 General features of the Kc/s. amplitude dependent internal friction in Na Cl

The internal friction measurements described in this thesis have been carried out at about 90 Kc/s as a function of amplitude, and are directed to investigate the second class of mechanisms rather than the first. Internal friction at this frequency, in plastically deformed crystalline solids, is due mainly to the presence of mobile dislocations.[21] For example, Whitworth[22] has shown that the decrement of a well annealed pure Na Cl crystal at 90 Kc/s is about 10^{-5} at low amplitudes rising to about 10^{-4} at an amplitude of 4×10^{-5}, while the decrement of slightly impure specimens is amplitude independent in this range. Pure Na Cl is much softer than impure Na Cl and it is difficult to avoid

introducing dislocations into pure specimens during handling but this difficulty can be overcome with impure specimens. Whitworth has therefore suggested that it is possible that in a truly undeformed, pure Na Cl crystal the decrement is less than 10^{-5} and is amplitude independent at least up to a strain amplitude $\varepsilon = 4 \times 10^{-5}$. Deformation of a crystal increases the decrement and decreases the modulus at all amplitudes. For example, a plastic compression of 1% increases the decrement of a pure specimen from 10^{-5} to 5×10^{-4} at low amplitudes. Further, the decrement and modulus of such a specimen vary with amplitude of vibration. At low amplitudes decrement and modulus remain constant but as the amplitude is raised above about 10^{-6} the decrement increases to values which can be in excess of 10^{-2}, while the modulus decreases. These changes are monotonic over the ranges so far studied in Na Cl. When a pure specimen is vibrated at amplitudes in excess of about 10^{-4} dislocation multiplication occurs, increasing the damping and decreasing the modulus. No significant dislocation multiplication has been observed at lower amplitudes.

After plastic deformation, damping and modulus recover toward their original values on irradiation, on annealing and even on standing at room temperature.[23][24][25] The decreases in damping and increases in modulus occur at all amplitudes. This change is clearly due either to the annihilation of the fresh dislocations or to their immobilisation by interacting among themselves or with point defects.

Continuous vibration of deformed crystals at amplitudes lower than that at which dislocation multiplication occurs can cause changes in internal friction. For example, Whitworth[22] reports that on

vibrating in the amplitude dependent region specimens which had been lightly annealed after deformation, small increases in internal friction occurred during the vibration.

The general features of internal friction described above are common to many crystalline solids, although variations do occur. Before discussing previous work in this field in detail, it will be convenient here to describe some of the theories which have been proposed to explain these features.

1.8 Theories of internal friction

It is probable that no one simple model will adequately account for the whole amplitude range in any material, even if the state of dislocation density and point defect distribution is accurately known. Interpretation is further complicated because in general the vibration strain distribution in the solid is not homogeneous but can vary along its length, so that in different regions of a specimen different mechanisms might be operative. The theory which has been developed furthest and applied most frequently is that due to Granato and Lucke (G-L theory). Most of the work on Na Cl and other crystalline solids has been interpreted in terms of this theory although there are several physical limitations to the model. On the other hand Nowick has suggested a simple phenomenological model which has been qualitatively detailed by Whitworth and seems physically more probable at high strain amplitudes than the G-L model. Unfortunately it has not been developed quantitatively.

Nowick[26] has suggested that the internal friction of lightly

deformed crystals is due to a hysteresis in the motion of dislocations because of their interaction with obstacles, such as point defects, which lie in their slip planes. This has been developed into a quantitative theory by Weertman [27] for the case where the interaction between dislocations and impurities is due to long range elastic stresses. Whitworth[22] has stated that rough calculations show that the Weertman theory does not account for the flow stress or damping of Na Cl but he suggests that the Nowick model might be applicable if dislocations have a strong short range interaction with the obstacles, such as might arise from electrostatic interaction between the dislocations and obstacles. Application of a stress to a dislocation lying in its slip plane and pinned by fairly immobile defects will cause it to bow out between the obstacles and perhaps break away from some of them. However it will not move far before being pinned by another obstacle and thus it moves along the slip plane in a series of jumps. On reversing the stress the stress - dislocation strain curve will exhibit a hysteresis, and as increased stress will cause longer lengths of dislocation line to move and produce a larger hysteresis, the model predicts an amplitude dependence of internal friction.

Granato and Lucke have developed a theory originally due to Koehler who pointed out that dislocations in a crystal under the influence of an alternating stress will oscillate in the manner of a stretched string. The equation of motion of the dislocation line has the general form

$$A \frac{\partial 2x}{\partial t^2} = \sigma b + G \frac{\partial 2x}{\partial y^2} - B \frac{\partial x}{\partial t} - \sigma_p b - \varrho(y) \frac{d E_B}{d x}$$

where the dislocation is considered to lie initially in a straight line along the y axis, and displacements perpendicular to y are measured along the x axis. A is the effective mass of the dislocation; σ the applied stress; b the burgers vector; C the effective tension of the dislocation; B the damping constant; σ_p the Peierls stress; $\rho(y)$ the density of pinning defects along x = o; and $E_B(x)$ is the interaction energy between a single pinning defect and the dislocation. Teutonico, Granato and Lucke have solved this equation for two simple extreme cases but the results are too complicated to test experimentally.[28] However Granato and Lucke[29] have also solved the equation, ignoring the last two terms. The most important limitation of this is that they effectively ignore the fact that thermal activation can aid the motion of a dislocation. It is this solution which has been extensively used in the interpretation of experimental results. The model which they employ to establish the constants in the differential equation assumes that a crystal contains dislocations which are pinned by two types of pinning defects, a strong pinning species from which the dislocation can not break away, and a weak pinning species from which breakaway can occur when the resolved force of the dislocation on the pinner reaches a critical value. The weak pinning defects are usually considered to be point defects which interact with the dislocations by a Cottrell mechanism, while the strong pinning species is usually considered to be dislocation nodes. The latter assumption requires that the crystal should contain a network of dislocations, but this is not an essential condition for the model to be applicable as any mechanism which acts as a strong pinner relative

to the weak pinners is suitable. For example, crosslip occurs readily in Na Cl and the point where a dislocation leaves its slip plane to produce crosslip could act as a strong pin.

For simplicity the strong pinning points are assumed to determine a constant dislocation loop length L_n and the weak pinning points to determine smaller loop lengths which initially have an exponential size distribution and an average length L_c. On application of a stress the dislocation bows out between the pinning points until the stress reaches a level at which breakaway can occur from one of the weak pinning defects in that loop. Catastrophic breakaway from all the other weak pinning defects in that loop then follows because the first unpinning occurs when the stress is sufficient to unpin the longest segment, thus creating a longer free length and continued unpinning. Increasing the stress further causes the unpinned loop to act as a Frank-Read source. Fig. 1.5 illustrates the different stages of breakaway and Fig. 1.6 the stress - dislocation strain behaviour of a single dislocation. This model does not consider dislocation interactions with defects other than those lying along the original line of the dislocation, and it might be suspected that it would break down either when there is a sufficiently high concentration of pinning defects in the lattice or when the dislocation line moves through large enough distances to interact with pinning defects off the original line. Under these conditions a Nowick - Whitworth model might be more applicable.

The G-L theory predicts two different energy loss mechanisms. At low amplitudes, before breakaway occurs, there is a loss due to the dynamic nature of the measurements, arising because the motion of the

dislocations is damped. This loss has a resonance character and is frequency dependent while amplitude independent. A second, hysteretic loss is superimposed on the dynamic loss after breakaway. Fig. 1.7 illustrates roughly the form of the damping v. strain amplitude curve. At low amplitudes the dynamic decrement Δ_I and modulus defect $(\Delta E/E)_I$ are constant, while at higher amplitudes the decrement Δ and modulus defect $\frac{\Delta E}{E}$ are assumed to be the sum of the constant dynamic values and the decrement Δ_H and modulus defect $(\Delta E/E)_H$ due to hysteresis.

$$\Delta = \Delta_I + \Delta_H \qquad 1.13$$

$$\frac{\Delta E}{E} = \left(\frac{\Delta E}{E}\right)_I + \left(\frac{\Delta E}{E}\right)_H \qquad 1.14$$

For homogeneous strain the theory predicts that

$$\Delta_H = r\left(\frac{\Delta E}{E}\right)_H = \frac{A_1}{L_c^2 \varepsilon} \exp\left[-\frac{A_2}{\varepsilon L_c}\right] \qquad 1.15$$

$$\Delta_I = A_3 L_c^4 \qquad 1.16$$

$$\left(\frac{\Delta E}{E}\right)_I = A_4 L_c^2 \qquad 1.17$$

where

$$A_1 = 2.5 \Omega \Lambda L_n^3 K\eta a/\pi^2 \qquad 1.18$$

$$A_2 = K\eta a \qquad 1.19$$

$$A_3 = 120 \Omega \Lambda B \omega/\pi^3 C \qquad 1.20$$

$$A_4 = 6 \Omega \Lambda/\pi^2 \qquad 1.21$$

Here r is a constant of the order of unity; Ω is an orientation factor which takes into account the fact that the shear stress on the slip planes is less than the applied stress; Λ is the dislocation density; K is a parameter which depends upon orientation and anisotropy; η is the Cottrell misfit parameter measuring the magnitude of the lattice dilation at the point defect; a is the lattice parameter; ϵ is the strain amplitude; B is a damping constant; ω is the frequency; and C is the dislocation line tension. Equation 1.15 has to be modified for non homogeneous strain distributions. In most of the previous work, and in the present work, the experimental arrangement is such that it is usually assumed that the strain distribution is described by a simple cosine standing wave.[30] This leads to

$$\Delta_H = r\left(\frac{\Delta E}{E}\right)_H = \left(\frac{2}{\pi A_2}\right)^{\frac{1}{2}} \frac{A_1}{\epsilon^{\frac{1}{2}} L_c^{3/2}} \exp\left(-\frac{A_2}{\epsilon L_c}\right) \quad 1.22$$

The G-L theory attributes the amplitude dependent part of the internal friction to a hysteresis in the stress v. dislocation strain behaviour after breakaway. However the possibility exists that the dynamic loss is also amplitude dependent. This could arise because after breakaway the weak pinning length L_c of a dislocation is increased to L_n and the Δ_I and $(\Delta E/E)_I$ terms increase accordingly. Heiple and Birnbaum[31] report that Trott has made an exact calculation of amplitude dependent viscous damping and has shown that this can cause large increases in the damping with increasing strain amplitude. Rogers[32] has also considered this problem and has shown that the dynamic loss is amplitude dependent after breakaway. Alefeld[33] has considered the different problem of the motion of pinned, kinked

dislocations and has shown that an amplitude dependence can occur, due to the presence of the kinks, at amplitudes which are less than or comparable to the breakaway strain. It is thus to be expected that at low amplitudes in the amplitude dependent region the G-L theory would break down because of its neglect of thermal activation and these other sources of amplitude dependence. On this reasoning the G-L theory would tend to underestimate Δ_H at low amplitudes and this is in fact invariably observed.

Despite its shortcomings the G-L theory has been used widely with a large measure of success to interpret the behaviour of many materials. The theory has been extended to explain the recovery of internal friction due to the migration of point defects and, as this has been used in the interpretation of the present work, something will be said of it here.

If the dislocation loop length L_c, defined by the weak pinning defects, decreases with time because of the migration of additional point defects to the dislocations, then equations 1.15, 1.16 and 1.17 are time dependent because of their dependence on L_c. Granato, Hikata and Lucke[34] (G H L theory) assumed the existence of two different types of weak pinning defect, a mobile species of concentration c_{10} and an immobile species of concentration c_{20}. Only the mobile defects migrate to the dislocation and do so with a Cottrell - Bilby time dependence

$$c_1(t) = c_{10} \frac{8\alpha}{a^2} \left(\frac{ADt}{kT} \right)^{2/3} \qquad 1.23$$

where $c_1(t)$ is the concentration of mobile defects which have

migrated to the dislocation after time t, α is a constant, A is a parameter measuring the strength of Cottrell attraction and D is the diffusion coefficient. Initially the dislocations are pinned by both types of defect whose concentrations on the dislocations are the same as in the bulk. After a time t the migrating mobile defect alters the loop length so that in the early stages of recovery, equations 1.20, 1.21 and 1.22 are modified to

$$\Delta_H = r\left(\frac{\Delta E}{E}\right)_H = \frac{A_1}{L_c^2 \varepsilon} \exp\left[-\frac{A_2}{a\varepsilon}(c_{10} + c_{20})\ (1 + \beta t^{2/3})\right] \qquad 1.24$$

$$\Delta_I = \frac{A_3\ a^4}{(c_{10} + c_{20})^4} \qquad \frac{1}{[1 + \beta t^{2/3}]^4} \qquad 1.25$$

$$\left(\frac{\Delta E}{E}\right)_I = \frac{A_4\ a^2}{(c_{10} + c_{20})^2} \qquad \frac{1}{[1 + \beta t^{2/3}]^2} \qquad 1.26$$

where

$$\beta = \frac{c_{10}}{c_{10} + c_{20}} \qquad \frac{8\alpha}{a^2} \left(\frac{AD}{kT}\right)^{2/3} \qquad 1.27$$

The changes in internal friction which are frequently observed during continuous vibrations of crystals have been considered by several workers. Yamafuji and Bauer,[35] and Alefeld[36] have considered the effect on the G-L theory of permitting the weak pinning defects to diffuse along the dislocation core under an applied stress. This leads to a redistribution of the pinning defects and an increase in the internal friction. Whitworth,[22] on the other hand, has suggested that the Nowick - Whitworth model can explain the increases without recourse

to the redistribution of pinning defects.

1.9 Previous work on amplitude dependent internal friction in Na Cl

The earliest work on amplitude dependent internal friction in Na Cl was published by Frankl[21] in 1953. He interpreted his results in terms of a qualitative model of dislocations interacting with vacancies. Granato and Lucke[30] considered Frankl's published data, together with other published data on metals, and concluded that there was a reasonable agreement with their theory. It can be seen from equation 1.21 that according to this theory $\log \varepsilon^{\frac{1}{2}} \Delta_H$ v. $1/\varepsilon$ should yield a straight line (G-L plot). They tested the data by calculating G-L plots and approximated them to straight lines, from whose slopes and intercepts they calculated as many as possible of the parameters in their theory. The linearity (or lack of it) of a G-L plot is not in itself a good test as deviations from linearity can be expected at low amplitudes in real materials because of the limitations of the theory already stated. These reasons, together with the exaggeration of small deviations which occur on a semi-log plot lead to large deviations from linearity as shown in Figs. 1 and 2 of reference (30). Deviations from linearity at low amplitudes are to be expected, the plot perhaps tending asymptotically to a straight line at larger values of strain amplitude, and the largest value of the slope being nearest to that predicted by the theory. A typical G-L plot for Na Cl at room temperature is never a straight line over its whole range, possibly for these reasons.

There are two major difficulties involved in Granato and Lucke's analysis of the data. The first of these is that the constant K in

equation 1.15 has either to be a priori calculated or a value assumed. For Cottrell pinning K is about $\frac{1}{2}$ but this leads to values of L_c which are approximately equal to L_n. They considered that this was not consistent with their initial assumptions and therefore assumed a value of K = 1/50 which leads to values of L_c a factor of ten less than L_n. Secondly, for several reasons they were led to conclude that the dynamic loss $\triangle_I$ and the hysteretic loss $\triangle_H$ could not be ascribed to the same dislocation loops. Bauer and Gordon[24] however have carried out a series of experiments involving the measurement of damping as a function of amplitude after various amounts of prestrain and X irradiation doses. They measured dislocation densities by etchpit counts and, by assuming that the measured densities were the correct values to substitute in the G-L theory for both $\triangle_I$ and $\triangle_H$, were able to obtain all the parameters in the theory without assuming a value for K. This led to values of L_c which were of the same order of magnitude as L_n and implies that K is about $\frac{1}{2}$. Bauer and Gordon also found reasonably straight line G-L plots and showed that $\left(\frac{\triangle E}{E}\right)_I$ and $\triangle_I$ increase linearly with measured dislocation density as predicted by the theory.

Frankl[21] and Whitworth[37] showed that over a wide amplitude range $\triangle_H = r\,(\triangle E/E)_H$ where r is a constant for a particular specimen as predicted by the G-L theory. Their values of r were about 3 to 6 as opposed to the value of about 1 which Granato and Lucke predicted. Whitworth concluded from his experiments that the G-L theory was not obeyed by Na Cl.

Strumane et al[38] measured the amplitude dependence of damping as

a function of temperature and obtained G-L plots which approximated to straight lines at high amplitudes. Because the slope and intercept of a G-L plot depend on L_c, they should vary with temperature. If the weak pinning defect equilibrium concentration (C_{eq}) on the dislocation varies as

$$C_{eq.} = C_o \exp\left(\frac{E_B}{kT}\right) \qquad 1.28$$

where C_o is the bulk concentration and E_B is the binding energy between pinner and dislocation, then

$$L_c \propto \exp\left(-\frac{E_B}{kT}\right) \qquad 1.29$$

and from equation 1.15 the slope and intercept of a G-L plot,* $\ln \xi \Delta_H$ v. $1/\xi$, should be respectively proportional to $1/L_c$ and $\ln(1/L_c^2)$. Hence a plot of the logarithm of the slope or the intercept against $1/T$ should yield a straight line whose slope gives the binding energy E_B. This linear behaviour was in fact observed and the energies obtained from the slope and intercept data were -0.045 ± 0.005 eV and -0.037 ± 0.006 eV which agreed well with each other but were negative. Strumane et al. explained the apparent negative nature of the binding energy by assuming that the bulk concentration (C_o) of the weak pinners is temperature dependent i.e.

$$C_o \propto \exp\left(-\frac{E_f}{kT}\right) \qquad 1.30$$

where E_f is the formation energy of the weak pinner, and thus the energies obtained from the slopes are not E_B but $E_B - E_f$ where $E_f > E_B$.

* STRUMANE ET AL. CONSIDER IT APPROPRIATE TO USE THE HOMOGENEOUS STRAIN EQUATION TO DERIVE A G-L PLOT.

Some work has also been carried out on the recovery of internal friction on room temperature annealing and irradiation. Gordon and Nowick[23] have shown that X-irradiation increases the modulus and decreases the internal friction of Na Cl crystals. Similar changes also occur on standing the crystals at room temperature and are collectively known as the Koster effect after their discoverer in metals. They have shown that the modulus increase produced in Na Cl by X irradiation corresponds exactly to the modulus decrease produced by plastic deformation, thus indicating that the recovery process consists of the immobilisation of freshly introduced dislocations. Granato, Hikata and Lucke[34] have analysed the published data of Gordon and Nowick on room temperature annealing in terms of their own theory, outlined above. The data fitted the predicted relationships well thus confirming that immobilisation of the dislocations in Na Cl during room temperature annealing is due to the diffusion of weak pinners to the dislocations. It is worth noting that again a value of K had to be assumed and a value of 1/50 gave a derived dislocation density of $1.1 \times 10^{9} cm^{-2}$ while 1/5 gave $1.1 \times 10^{7} cm^{-2}$. The specimen had been prestrained 4% and the smaller dislocation density is more reasonable for such a specimen, which implies that the larger value of K is the better value. Sivertsen[25] has studied the effect of ^{60}Co γ irradiation on amplitude independent internal friction in Na Cl and has found a dosage time dependence which implies that the amplitude independent decrement and modulus defect are related to the dislocation loop lengths by a fourth power and a square relationship respectively, as is predicted by the Granato - Lucke theory.

No previous work has been published on the quantitative effects

of impurity addition and temperature variation on the recovery of internal friction in Na Cl but Blistanov, Shaskol'skaya and their co workers[39][40][41] have investigated such behaviour in the very similar material LiF. They found that their results agreed well with the predictions of the Granato, Hikata and Lucke theory. For example, the amplitude independent decrement Δ_I, plotted as a function of time at room temperature in the form $\Delta_I^{-\frac{1}{4}}$ v. $t^{2/3}$ yielded good straight lines after the first seven minutes of recovery. During the first seven minutes recovery was faster than predicted. Among other interesting effects which they observed was a variation of the recovery parameter β with prestrain, and an increase in the rate of recovery on the addition of divalent impurities.

To sum up previous work, it appears that despite the physical limitations of the model the Granato - Lucke theory provides a useful explanation of the behaviour of internal friction in Na Cl, especially the recovery behaviour.

1.10 Identification of the weak pinning defect

There is no reason to suppose, a priori, that one specific type of point defect is responsible for all the pinning effects described above. The results of the previous experiments fall naturally into two classes, those where the pinning defects have been produced by irradiation and those where the pinning defects have been those which exist in the unirradiated material. In its unirradiated state Na Cl contains impurities and vacancies distributed as discussed earlier, while irradiation produces additional vacancies, interstitials and clusters of these primary defects. A comparison may perhaps be drawn to the

effects of irradiation and divalent doping on the hardening of alkali halides. Johnston et al,[42] for example, have attributed these similar hardening effects to two different asymmetric defects. They attribute irradiation hardening to the production of interstitials, while divalent doping produces mechanical dipoles, both defects have tetragonal symmetry and thus give rise to similar hardening effects.

Bauer and Gordon[43] have shown by an elegant series of experiments that the weak pinning defect produced on irradiating Na Cl with X rays is a dislocation jog closely associated with an F centre. Strumane and Batist have suggested that the pinning defect in unirradiated Na Cl is the cation vacancy, but they have not proposed a specific pinning mechanism. Their results however only show that the bulk concentration of the weak pinner is temperature dependent and no unambiguous identification has been made of the weak pinner in unirradiated pure and doped Na Cl.

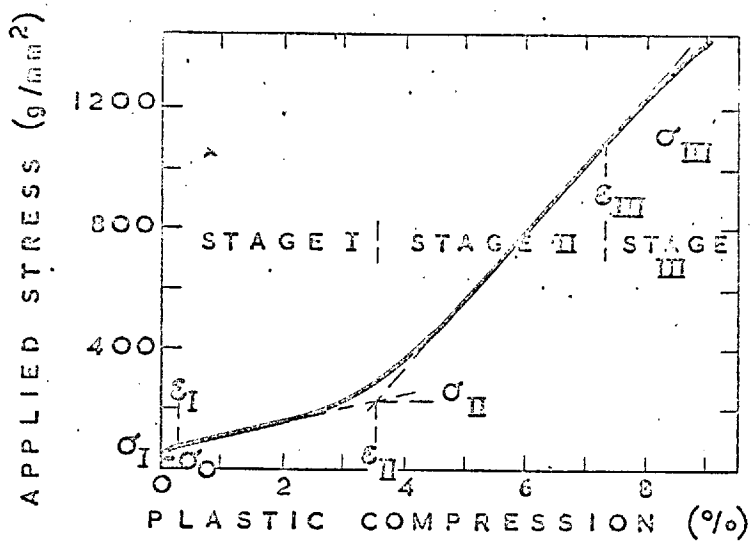

FIG. 1·1. STRESS-STRAIN BEHAVIOUR OF SINGLE CRYSTAL NaCl. (AFTER DAVIDGE & PRATT)

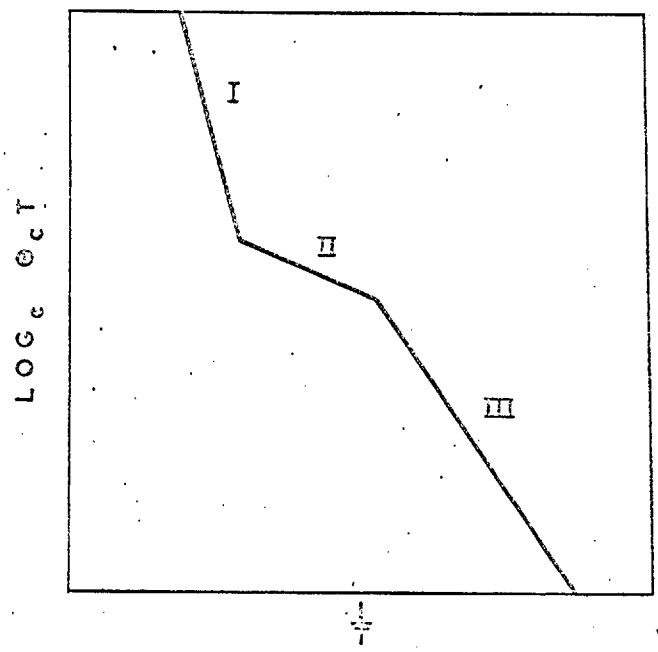

FIG. 1·2. SCHEMATIC DIAGRAM OF CONDUCTIVITY PLOT OF NaCl

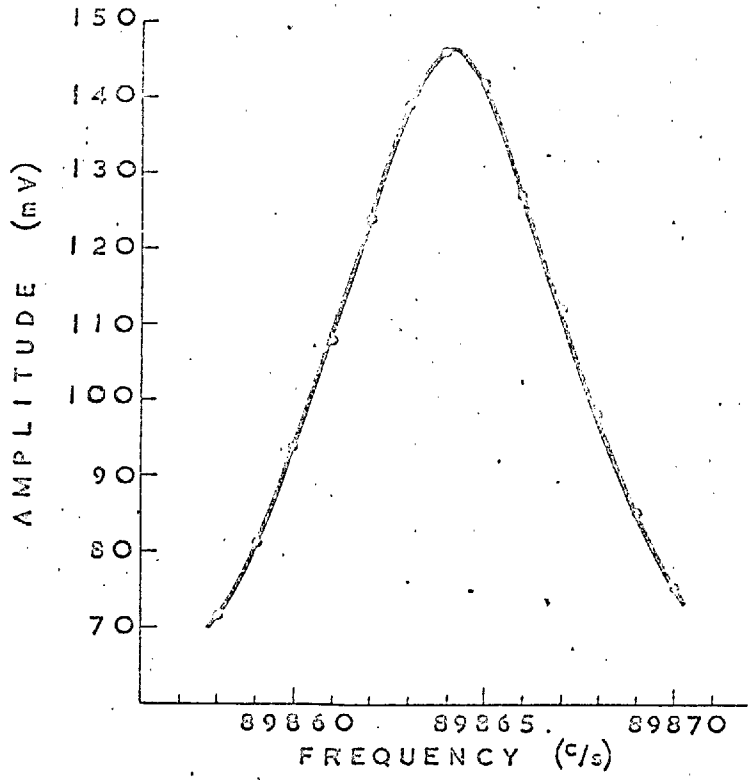

FIG. 1·3. TYPICAL RESONANCE CURVE. A MARX OSCILLATOR WITHOUT A SPECIMEN ATTACHED, DRIVEN AT 300mV

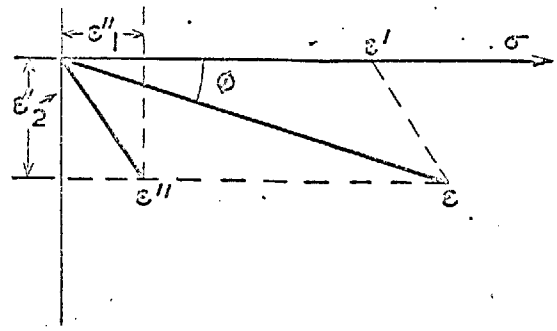

FIG.1·4. PHASE RELATIONSHIPS BETWEEN THE STRESS AND THE ELASTIC AND NON-ELASTIC STRAIN (AFTER NOWICK)

THE GRANATO-LÜCKE MODEL

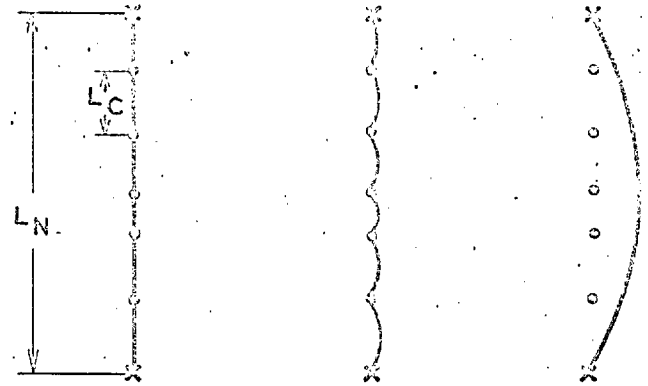

FIG. I.5. DISLOCATION BOWING AND BREAKAWAY

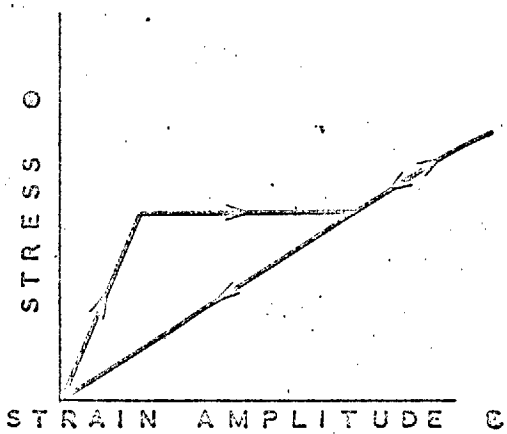

FIG. I.6. STRESS-DISLOCATION STRAIN CURVE FOR A DISLOCATION

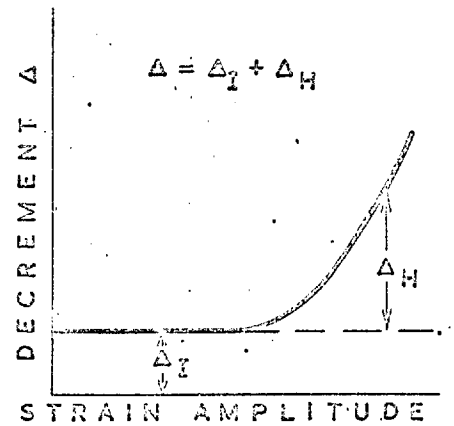

FIG. I.7. VARIATION OF DECREMENT WITH STRAIN AMPLITUDE

Chapter 2.

Experimental Techniques.

2.1 Internal friction measurements

2.1 (a) General principles

Internal friction and modulus measurements have been carried out as a function of vibration amplitude by the composite oscillator technique originally developed by Marx.[44] The Marx oscillator is basically a single unit consisting of three parts, each of which is cut to resonate at the same frequency, which in this work was about 90 Kc/s. Fig. 2.1 shows the various parts of the oscillator. The first part is a piezoelectric α- quartz crystal which is excited into its fundamental longitudinal mode by an A.C. voltage (V_d) applied at the resonant frequency. This crystal is used to drive the entire oscillator, and its amplitude of vibration is determined by the drive voltage (V_d) and the total damping of the oscillator. The second part is another, similar, α - quartz crystal which measures the response of the oscillator to the drive crystal vibration by piezoelectrically transforming the mechanical energy of the oscillator into an electric signal (V_g) which can be displayed on a voltmeter. The third part is the specimen itself. The oscillator is supported in position by attachments at displacement nodes and can be regarded as mechanically free, while the joints between the components occur at strain nodes and do not contribute greatly to the damping of the oscillator.

In the neighbourhood of the fundamental mechanical mode the composite oscillator is electrically equivalent to a series RLC circuit in parallel with a capacitance. From this analogue Marx has derived relationships between the amplitude (ξ_g) of the gauge crystal, the decrement (Δ_t) of the oscillator, V_d and V_g. These have the general

form,

$$\mathcal{E}_g = K_1 V_g \qquad 2.1$$

$$\Delta_t = K_2 \frac{V_d}{V_g} \qquad 2.2$$

where K_1 and K_2 are constants which may be measured by a calibration procedure to be described below. The decrement (Δ_s) and strain amplitude ($\mathcal{E}_s$) of the specimen are related to the measured values $\mathcal{E}_g$ and Δ_t by

$$\Delta_s = \frac{m_t \Delta_t - m_q \Delta_q}{m_s} \qquad 2.3$$

$$\mathcal{E}_s = \mathcal{E}_g \frac{l_g}{l_s} \qquad 2.4$$

where m_q is the mass of driver and gauge crystals, m_s is the mass of the specimen and $m_t = m_q + m_s$; l_s, l_g are the lengths of specimen and gauge crystals respectively; and Δ_q is the decrement of the driver-gauge crystal combination. The Young's modulus (E) of a specimen vibrating in its fundamental mode in free - free longitudinal vibrations is related to the frequency (f) of vibration by

$$f = \frac{1}{2l} \sqrt{\frac{E}{\rho}} \qquad 2.5$$

where ρ is its density and l its length. If the frequency (f_s) of a specimen is within 5% of the driver-gauge frequency (f_q) it is closely approximated from the observed frequency (f_t) of the three component

unit by the equation

$$f_s = \frac{m_t f_t - m_q f_q}{m_s} \qquad 2.6$$

In general the measured modulus of a specimen differs from its elastic modulus because of the presence of a dislocation contribution to the strain. The modulus defect in the amplitude independent range is then, from equation 2.5

$$\left(\frac{\Delta E}{E}\right)_I = 2\,\frac{(f_{el.} - f_I)}{f_I} \qquad 2.7$$

where $f_{el.}$ is the resonant frequency which the specimen would have if it were perfectly elastic and f_I is its actual frequency. Similarly, in the amplitude dependent range

$$\left(\frac{\Delta E}{E}\right)_H = 2\,\frac{(f_I - f_H)}{f_H} \qquad 2.8$$

where f_H is the frequency of the specimen at an amplitude in the amplitude dependent range.

It was frequently necessary to carry out internal friction measurements at temperatures other than room temperature. In order to accomplish this without heating or cooling the quartz crystals a long, low damping, fused quartz bar was inserted between the driver-gauge crystals and the specimen. In this way the specimen could be held far enough from the quartz crystals to heat or cool it without greatly altering the temperature of the quartz crystals. The quartz bar had to be cut to the correct size to enable it to resonate at the same frequency with an integral number of half wave lengths, and the

decrement and modulus of the specimen were calculated from simple modifications of equations 2.3 and 2.6.

2.1 (b) Calibration of the oscillator.

The constants K_1 and K_2 in equations 2.1 and 2.2 contain the values of the components of the equivalent electric circuit of the oscillator, the dimensions of the quartz crystals, the piezoelectric coefficients and the frequency of the crystals. Marx has obtained the numerical forms of these equations for 18.5° X-cut crystals and has described how calibration may be carried out by an impedance bridge technique. In the present work both 18.5° and 5° X-cut crystals were employed and the numerical forms which Marx obtained are not applicable to the latter. A method of calibration which does not involve knowing the piezoelectric coefficients and therefore allows for inaccuracy in orientation of the crystal cut was generally used. The calibration procedure was carried out on the oscillator without a specimen attached.

The constant K_2 was obtained by measuring V_g as a function of frequency around the resonant frequency f_r at constant V_d, then the width of this resonance curve at $1/\sqrt{2}$ of peak height gave Q^{-1} and thus Δ_q of the driver-gauge combination (v. equations 1.8 and 1.10 and Fig. 1.3). Thus Δ_q and V_d/V_g at resonance were known, leading to K_2. The constant K_1 was obtained by employing equation (11) of the Marx paper.

$$\xi_d^2 = \frac{V_d^2}{2 R l_d^2 f_r^3 m_q \Delta_q}$$

where R is the electrical resistance of the driver crystal at the

resonant frequency f_r, ε_d is its amplitude and l_d its length. The resistance of the driver crystal was measured at its resonant frequency by an impedance bridge technique and hence ε_d obtained. But, because of the similarity of driver and gauge crystals $\varepsilon_d = \varepsilon_g$, and this leads to K_1. The errors in this procedure made K_1 and K_2 usually reproducible to $\pm$ 5%. The 18.5° crystals were also calibrated by the method indicated by Marx and excellent agreement was obtained.

2.1 (c) Practical details.

It has already been mentioned that the quartz crystals used in this work were of two orientations, 18.5° X-cut and 5° X-cut. Coupling between longitudinal and shear modes is minimised by the 18.5° cut and for this reason that orientation has been most frequently used by other workers, however 5° are more readily obtained from manufacturers and are in practice equally suitable. Each oscillator was formed from two similar crystals which were supplied cut to resonate at about 90 Kc/s. and frequency matched to better than 0.5 %. The 18.5° crystals were 2.85 cm. long and the 5° crystals 3.13 cm. long, both having the same 0.5 cm. square cross section. Each oscillator was formed by attaching two crystals end to end with their electric axes at right angles so that electrical coupling was minimised. The joint between them was made with Araldite epoxy resin. Full face electrodes were coated on to the driver crystal and $\frac{1}{3}$ face electrodes on to the gauge crystal by painting with Dag colloidal suspension of silver or graphite in alcohol. Mechanical support of the crystals and electrical contact to the electrodes were obtained by attaching fine phosphor bronze wires to the centre of the crystals at the electrode faces, before coating

on the electrodes, by means of small blobs of a thermo-setting silver preparation, or conducting cement, manufactured by Johnson, Matthey & Co. Ltd. Fig. 2.2 is a photograph of the driver-gauge crystals and specimen mounted in the experimental rig.

The fused quartz rods employed in measurements at temperatures other than room temperature were of 0.5 cm square cross section and were cut by means of a diamond slitting saw to a length of 22.4 cm., which corresponds to $3\frac{1}{2}$ wavelengths. Fig. 2.3 shows the arrangement of quartz crystals, fused quartz rod and specimen. The oscillator, dummy and specimen were mounted in a chamber which could be evacuated, and the specimen at the end of the dummy was in a constant temperature enclosure. Temperatures above room temperature were obtained by means of a furnace which was controlled to better than 1°C by an Ether anticipatory controller. For low temperature measurements a constant temperature bath was substituted for the furnace, and constant low temperatures were obtained by a series of cold mixtures, at 0°C by ice and water, -29.8°C by Isceon 12, -78°C by Isceon 12 and solid Co_2, -196°C by liquid N_2. No one adhesive was suitable for attaching the specimens to the dummy rod over the whole temperature range, and a variety of empirically determined adhesives were used. The criterion used in selecting an adhesive was that it should rapidly form a strong bond at the testing temperature and yet be easily broken on returning to room temperature, this excludes more conventional adhesives such as the epoxy resin type. At room temperature, and at 0°C, and for attaching the dummy rod to the piezoelectric crystals, beeswax was used

as the adhesive. Beeswax melts at about 70°C and this is easily accomplished with a hot air blower. For temperatures up to 60°C beeswax and resin was suitable and at temperatures in excess of this Bostik 1160, a high temperature adhesive, was used. At -78°C and -196°C silicon vacuum grease forms a strong bond, while at -30°C a typist's material, Gestetner spotting out fluid, fitted the criterion excellently.

Fig. 2.1 is a block diagram of the electric circuit and Fig. 2.4 is an overall photograph of the apparatus. A Muirhead - Wigan D-890-A oscillator was used to excite the quartz crystals into vibration and Solartron VF 252 feedback voltmeters measured the drive and gauge voltages. Frequency was measured to an accuracy of 0.1 c/s. at 90 Kc/s. by means of an Advance TC 10 Counter. At 90 Kc/s. the Muirhead - Wigan D-890-A oscillator is not altogether satisfactory for this type of work as small, accurate, predetermined changes of frequency cannot be readily effected. To overcome this the Muirhead - Wigan oscillator was used to provide a variable frequency signal of about 3 Kc/s. and this was mixed with a constant frequency signal of 87 Kc/s. to provide a 90 Kc/s. side band which was filtered out and used as the driving signal. At 3 Kc/s., incremental changes of 1 c/s. may be made in the Muirhead - Wigan output frequency by a decade switch, and changes of less than 1 c/s. may be effected by turning a continuous, variable control through a total of 360° of rotation for 1 c/s. Thus with this arrangement small, accurate changes of frequency of 0.1 c/s. could be made at 90 Kc/s. The same mixing unit also contained an amplifier and attenuators for varying the size of the drive signal, and

terminated in a cathode follower circuit which gave a low output impedance. This is necessary because at resonance the impedance of the composite oscillator is greatly decreased to about 10 KΩ for a decrement of 10^{-4}. The mixing unit was designed by R.W. Whitworth and built for his investigation[37] of internal friction in Na Cl.

The composite oscillators were calibrated before every experiment because it was found that the calibration constants tended to alter over periods of the order of days, and after a few weeks of use it was necessary to remake the cement contacts and coat new electrodes on the electrode faces. In air the decrement of an oscillator was about 1.5×10^{-4} and this could be reduced to about 0.8×10^{-4} on evacuating the chamber containing the oscillator, thus a vacuum was advisable when measuring low damping specimens. Usually the decrement of the oscillator was constant over the amplitude range used in these experiments, but where it did vary with amplitude slightly, this amplitude dependence was allowed for in the calculation of the specimen decrement.

Several factors affected the accuracy of the damping measurements. It has already been mentioned that the calibration was reproducible to better than 5 %. From equation 2.3 it can be seen that the error in the calculated specimen decrement depends on the weighted errors in the total decrement and the decrement of the quartz crystals, the weighting factors arising from the dependence of the calculated specimen decrement on the masses of the various components. Modifying equation 2.3 for the presence of the dummy bar of mass m_d and decrement Δ_d leads to

$$\Delta_s = \frac{m_t}{m_s}\Delta_t - \left(\frac{m_q}{m_s}\Delta_q + \frac{m_d}{m_s}\Delta_d\right) \qquad 2.7$$

Typical values of the masses and decrements were $m_d = 9.6$ gm., $m_q = 4.1$ gm., $m_s = 1.4$ gm., $\Delta_d = 3 \times 10^{-4}$, $\Delta_q = 1.5 \times 10^{-4}$. Thus when a dummy bar was used

$$\Delta_s \approx 10\Delta_t - 25 \times 10^{-4}$$

and without a dummy

$$\Delta_s \approx 4\Delta_t - 5 \times 10^{-4}$$

A dummy bar was only used with specimens which had been deformed at least 2 % and had a decrement of the order of 10^{-2}, while the lowest damping specimens had decrements of the order of 10^{-3}. Thus the systematic error involved in the calculation of Δ_s during any experiment because of an error in the measured values of Δ_d and Δ_q is small compared with the $\pm$ 5 % systematic error possible in Δ_t because of the calibration procedure. The random error involved in Δ_s during any experiment depended on the accuracy of the voltmeters and was about $\pm$ 2 %. Another systematic error was introduced because of the unknown but small contribution to damping from the joints between the components, this was assumed to be negligible. Finally, very occasionally a small error was introduced because of an abrupt, small change in the background damping of the apparatus. This only affected Δ_I however as Δ_H was obtained by subtracting two values of Δ_s, both of which contained the background damping.

Frequency measurements on the other hand suffered from two different faults. Firstly the sharpness of a resonance curve is determined by the damping of the system and for high damping of the order of 10^{-2} it was frequently impossible to define the resonant frequency to better than $\pm$ 1 c/s. Secondly, the resonant frequency depends far more strongly on temperature than does the decrement because it is related to the length, density and elastic modulus of a specimen, all of which are temperature dependent. Thus small changes in temperature produce large changes in frequency. In these experiments it was necessary to measure the changes in frequency which had occurred between two successive measurements. At temperatures other than room temperature the scatter in the frequency measurements often obscured any systematic change and thus too much reliance could not be placed on these measurements. For these reasons the damping measurements are considered more useful and reliable than the frequency measurements.

Each internal friction measurement usually took less than ten seconds to carry out.

2.2 Preparation of specimens

2.2 (a) Fabrication

Na Cl crystals were grown in air by a modified Kyropoulos technique. This technique has been described in detail by Harrison.[45] Large Na Cl single crystals, or boules, were nucleated on a water cooled seed crystal and pulled from molten Na Cl in a silica beaker. The crystal growing apparatus is illustrated schematically in Fig. 2.5. Employing this technique, crystals of approximately 9 cm x 3 cm x 3 cm

were grown. The starting material for pure crystals was Analar grade Na Cl while some Cd^{++} doped crystals were also grown by adding small quantities of Analar grade $CdCl_2$ to the melt.

Internal friction specimens were cleaved with razor blades from the boules, where possible at right angles to the direction of growth in order to minimise the variation of impurity concentration along the specimen. This was not always possible as the thickness of the boule was sometimes insufficient. The specimens were of 0.5 cm square cross section and their length depended on the temperature of test and the amount by which they were to be prestrained. For comparison, a Na Cl specimen which resonates at 90 Kc/s at 25°C is 2.52 cm. long, while at -196°C it is 2.74 cm, and at 100°C it is 2.44 cm. It was sometimes found necessary to polish the surfaces of a specimen in order to remove cleavage steps. Polishing was carried out by hand on a silk cloth which had been slightly damped with water. No differences were observed in the behaviour of polished specimens and specimens which had been so well cleaved as to not require polishing. Frequency matching between the internal friction specimens and the quartz crystals was better than 1 %. Fig. 2.6 is a photograph of an internal friction specimen alongside a boule.

2.2 (b) Heat treatment and prestrain

Two standard heat treatments were applied to most of the specimens used in this work. The first consisted of slowly heating a specimen to 600°C, maintaining it at that temperature for one hour and then cooling it to room temperature over a period of 30 hours. This treatment removes internal stresses and completely immobilises existing

dislocations within the specimen. Such specimens are referred to in the text as annealed. Experiments on the annealed crystals were carried out within a few hours of the end of the anneal. The second heat treatment was similar to the first with the difference that cooling was halted at some temperature and, after two hours at that temperature, the specimen was removed from the furnace and allowed to cool to room temperature in a matter of minutes. Such specimens are referred to as quenched. Experiments were started on quenched specimens within a half hour of quenching.

Internal friction specimens were deformed, after heat treatment and prior to testing, in compression along their lengths in an Instron machine at a strain rate of 10^{-4} mins.$^{-1}$ at room temperature.

2.3 Specimen analysis

2.3 (a) Impurity content.

The maximum limit of impurities in Analar grade Na Cl is given in table 2.1 at the end of this chapter. It is probable that there are smaller quantities of impurities in the crystals grown from Analor grade Na Cl because of the difference in solubility of impurities in the solid and liquid states, and possibly because of a slagging reaction suggested by Newey.(46)

No analysis has been carried out on the nominally pure specimens used in this work, but analyses have been carried out on very similar specimens by other workers. Whitworth(47) has reported that a general spectrographic survey revealed the presence of Ca, K, Al, Mg, Si and Fe, and no other impurity. Flame emission spectroscopy revealed (in

mole parts per million) Ca 25 to 45, K 15 to 30; atomic absorption spectrometry revealed Mg about 7; chemical techniques revealed Al about 13, Si less than 2, Fe less than 1. He warns that these Ca, Al and Mg concentrations are about five times higher than the upper limit obtained from arc spectrographic analyses. The discrepancy between these values is rather confusing, however Quin[17] has carried out dielectric absorption studies on similar crystals which had been air quenched and has concluded that there was less than five mole parts per million of divalent impurity associated with vacancies in the form of impurity vacancy dipoles immediately after quenching. His work on Ca^{++} doped Na Cl indicates that if there were as much as 25 to 45 m.p.m. of Ca^{++} in the nominally pure crystals, sufficient should have associated with vacancies on quenching to have given considerably in excess of 5 m.p.m. of dipoles. This implies that there is a lot less than 25 to 45 m.p.m. of Ca in nominally pure specimens and probably the arc spectrographic analysis value is more correct, at least for calcium.

The cadmium doped specimens used in the present work were analysed polarographically for Cd^{++} content to ar accuracy of better than 4 % by the Analytical Services Laboratory at Imperial College. Internal friction experiments were carried out on specimens from two Cd^{++} doped boules, one of which contained about 60 m.p.m. of Cd^{++} and the other about 120 m.p.m. There was a variation of Cd^{++} content through each boule however, and more exact values are given where appropriate in the sections dealing with the experimental results.

2.3 (b) Free vacancy content - D.C. conductivity measurements.

In section 1.4 it was shown that relative values of free vacancy

concentrations in different samples of Na Cl may be obtained from conductivity measurements made at the same temperature, while if the mobility of the vacancy is known, absolute values of the free vacancy concentration can be calculated. D.C. conductivity measurements have been carried out at room temperature on both pure and Cd^{++} doped specimens which had been heat treated in a similar manner to the internal friction specimens. Because the conductivity of Na Cl at room temperature is due predominantly to the presence of extrinsic cation vacancies, these measurements yield information about the concentration of free cation vacancies and free divalent cations.

Na Cl is an insulator and the conductivities measured in these experiments ranged from $10^{-16}\Omega^{-1}$ cm^{-1} to $5 \times 10^{-15}\Omega^{-1}$ cm^{-1}. The circuit used to measure these low conductivities is illustrated schematically in Fig. 2.7. A measured, stable, D.C. voltage of up to 500 volts was applied to the specimen and the current thus produced was passed through a standard 10 KMΩ or 100 KMΩ resistor. The potential difference produced across the standard resistor was then measured with an E.I.L. 33 c Vibron electrometer. Specimen resistances ranged from $10^{13}\Omega$ to $10^{15}\Omega$ and were thus much larger than the standard resistances so that it was valid to approximate

$$R_{spec.} = \frac{V_{app.}}{V_E} R_s$$

where $R_{spec.}$ and R_s are the resistances of the specimen and the standard, and $V_{app.}$ and V_E are the applied and induced voltages.

Conductivity specimens were obtained from the same boules as the internal friction specimens. Plates, several millimetres thick,

were cleaved from the boules as near the internal friction specimens as possible to minimise impurity variation. The plates were heat treated in the appropriate manner and thin plates, about 0.5 m.m. thick, were cleaved from the centre of them. Each plate surface was painted with Dag colloidal suspension of graphite in alcohol to form a conducting electrode, and then the plates were cleaved to form conductivity specimens about 7 m.m. square and 0.5 m.m. thick. It was considered advisable to heat treat the material in the form of the relatively thick plates, rather than in the form of the small conductivity specimens, in order to reduce impurity loss from the specimens during heat treatment. Specimen areas were measured with a travelling microscope and thickness with a micrometer.

The specimens were held between brass electrodes insulated by P.T.F.E. and alumina insulators as depicted in Fig. 2.8. Precautions were taken to prevent errors due to current leakage. These included passing a flow of dried argon over the specimen during measurement to prevent current leakage due to a damp atmosphere, and regularly cleaning insulators with carbon tetrachloride. Another precaution, to ensure that true ionic conductivity was being observed, and not space charge effects, involved the measurement of conductivity at different applied voltages and the verification of Ohm's law for each specimen.

The random errors in the conductivities obtained by this technique arose from the errors in measurement of the specimen dimensions and resistance and were less than $\pm$ 5 %, while there may have been a rather larger systematic error in the standard resistance values. However the scatter in conductivities measured off similar specimens

was sometimes larger than this, being as much as ± 18 % once, probably due to variation of impurity content.

2.3 (c) Dipole concentration - Dielectric loss measurements.

In section 1.5 it was stated that a divalent cation and a cation vacancy associated on near lattice sites can give rise to a dielectric absorption peak. The relative concentrations of associated pairs, or dipoles, which existed in the Cd^{++} doped specimens used in this work, have been estimated from dielectric absorption measurements carried out by means of an impedance bridge technique. Dielectric absorption, expressed as the tangent of the loss angle (δ) is related to the conductance (G mhos), the capacitance (C farads) and the frequency (f c/s.) by

$$\tan \delta = \frac{G}{2 \pi f C}$$

Thus if the conductance and capacitance of a specimen are measured at a given applied field frequency, the dielectric absorption can be calculated.

Fig. 2.9 is a schematic diagram of the apparatus. The impedance bridge was a Wayne - Kerr B221 universal bridge which had been modified to measure conductances an order of a magnitude lower than the standard model. On the most sensitive range the bridge could be used to measure conductances to an accuracy of ± 1 x 10^{-6} μmho and capacitances to ± 1 x 10^{-3} $\mu\mu$f. Measurements were carried out over a frequency range from 60 c/s to 2000 c/s using an external source and detector. The source was a D-650-B Muirhead - Wigan decade oscillator which supplied a 30 volt signal with a frequency accuracy of ± 0.2 % or

$\pm$ 0.5 c/s, whichever was the greater. The output signal from the bridge was amplified by a Furzehill P.A.80 low noise preamplifier with a gain of 30 and detected by a Wayne Kerr A321 waveform analyser which could detect signals of less than 10^{-6} volts. Specimens under test were measured in a Wayne Kerr D321 permittivity jig which was enclosed in a thermostatically controlled chamber with a temperature stability of $\pm$ 0.05°C in 24 hours.

Again, specimens were cleaved from the same boules as the internal friction specimens, in the form of plates cut perpendicularly to the boule axis and about 2 mm. thick. Thin, plate-like specimens were necessary because the dimensions of a specimen determines its capacity and it was essential, because of the small values of tan δ to be measured, that the capacity be large and hence the conductance measurable. No electrodes were coated on the specimens, but they were placed between the plates of the permittivity jig which were screwed tightly on to them.

When the conductance and capacitance of a specimen were measured as a function of frequency, it was found that the capacitance altered only slightly over the whole range, while the conductance varied considerably, so that the variation in dielectric loss was reflected in the conductance and not the capacitance. The measurements reported here were carried out at the limit of accuracy of the apparatus and typically the measured conductances were of the order of 20 x 10^{-6} μmho. After measuring the conductance with the specimen in the permittivity jig it was necessary to correct for the conductance of the jig itself by measuring the conductance without a specimen and with the jig plates set at approximately the same capacitance, which was

typically about 7$\mu\mu$f. The conductance of the jig itself was not very much less than in the case where a specimen was between the jig plates, say 15 x 10^{-6} μmho. Thus the correct conductance of the specimen would be (20 - 15) x 10^{-6} μmho. However the error on each measurement was about $\pm$ 0.5 x 10^{-6} and thus a typical measured value of specimen conductance was (5 $\pm$ 1) x 10^{-6} μmho. The errors in these dielectric loss measurements were thus large and are shown explicitly on the dielectric loss curves in the appropriate section to follow.

2.4 Dislocation densities

The dislocation densities of the internal friction specimens were not measured directly but were estimated from measurements carried out on similar specimens which had undergone the same heat treatments and deformations. Each specimen was cleaved perpendicularly to the deformation axis at $\frac{1}{4}$, $\frac{1}{2}$ and $\frac{3}{4}$ of the length and the cleaved surfaces were etched with a solution of 1 part of methyl alcohol and 2 to 4 parts of glacial acetic acid. Photomicrographs were taken of two regions of each etched surface at a magnification of x 540 and dislocation etchpit densities were determined from the photographs. Fig. 2.10 is a typical photomicrograph of an etched surface. Dislocation densities increased with impurity content, the following values* being obtained for 2 % deformed specimens, pure (0.58 $\pm$ 0.11) x 10^7; 60 m.p.m. Cd^{++} (0.89 $\pm$ 0.15) x 10^7, 120 m.p.m. Cd^{++} (1.21 $\pm$ 0.16) x 10^7, and there was a tendency for the dislocation densities measured at $\frac{1}{4}$ and $\frac{3}{4}$ of the length to be slightly higher than those measured at $\frac{1}{2}$ length.

*units are $cm.^{-2}$

The procedure described above measures the screw dislocation density Λ_s not the total dislocation density Λ, because only screw dislocations intersect the cleaved planes. Screw dislocations are less mobile than edge dislocations in Na Cl and hence the screw dislocation density is greater than that of the edge dislocations. However dislocation density measurements[3] appear to indicate the opposite because the etching of planes which are intersected by both edge and screw dislocations reveal anomalously high dislocation densities. This is due to the formation during deformation of dislocation debris, which etches in a similar way to dislocations when planes containing edge dislocations are etched but not when planes containing screw dislocations are etched. It is for this reason that this procedure has been followed. The true dislocation density can be determined if the relative mobilities of screw and edge dislocations are known and there is reason to believe that the latter are about ten times more mobile than the former in pure Na Cl.[48] This being the case Λ will be only slightly greater than Λ_s but in any case $\Lambda_s < \Lambda < 2\Lambda_s$ and the measured dislocation density is a good approximation to the true dislocation density.

Fig. 2.11 shows the measured etch pit densities, plotted with Davidge and Pratt's data. It will be noticed that at 2 % deformation the dislocation density of a Cd^{++} doped crystal is greater than that of a pure crystal, while at 6 % the reverse is true. The dislocation density of a pure Na Cl crystal increases rapidly at compressive strains above about 3 % as the material enters stage II of work hardening. However the addition of divalent impurity increases the strain at which

stage II commences. At 6 % deformation the 60 m.p.m. Cd doped specimens were still in stage I of work hardening, and this probably explains why their dislocation densities were lower at that strain than those of the pure crystals.

Table 2.1. Maximum limit of impurities in 'analar' grade Na Cl expressed as % by weight.

Free acid	0.05 ml. N/1
Free alkali	0.05 ml. N/1
Sulphate	0.003
NO_3	0.002
PO_4	0.0005
Fe	0.0005
Pb	0.001
Ba	0.003
Ca and Mg	0.005
K	0.01
NH_4	0.001
As	0.0001

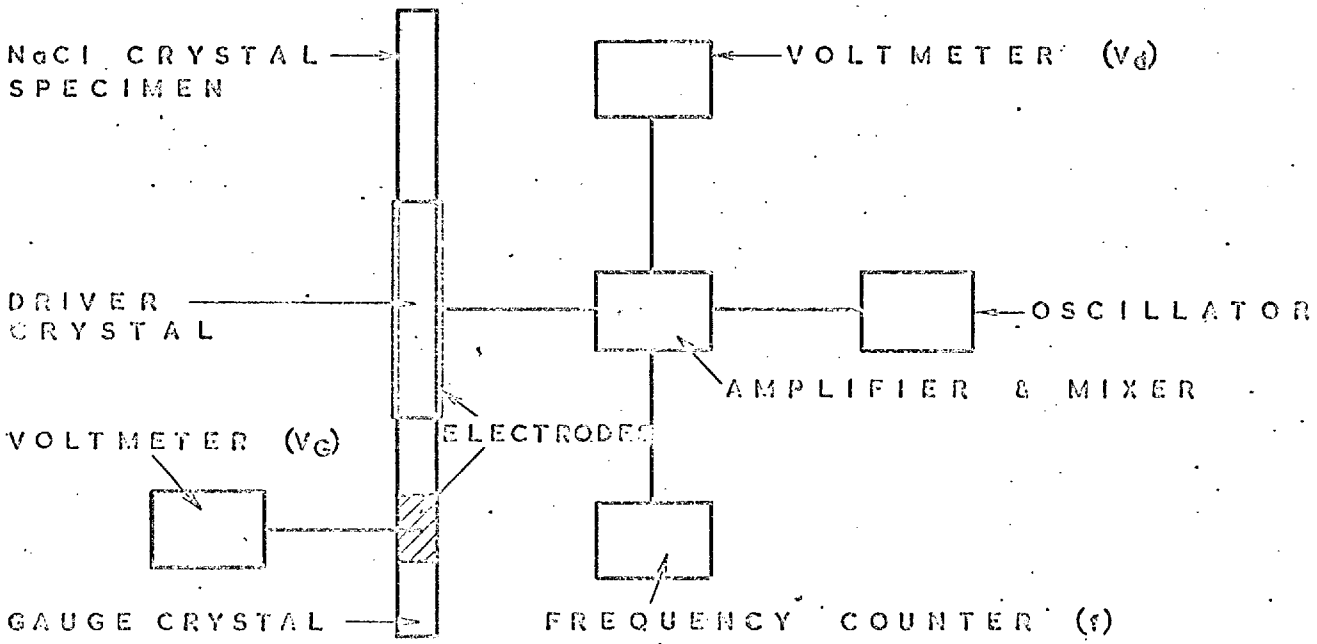

FIG. 2-1. SCHEMATIC DIAGRAM OF COMPOSITE OSCILLATOR AND ASSOCIATED CIRCUITRY

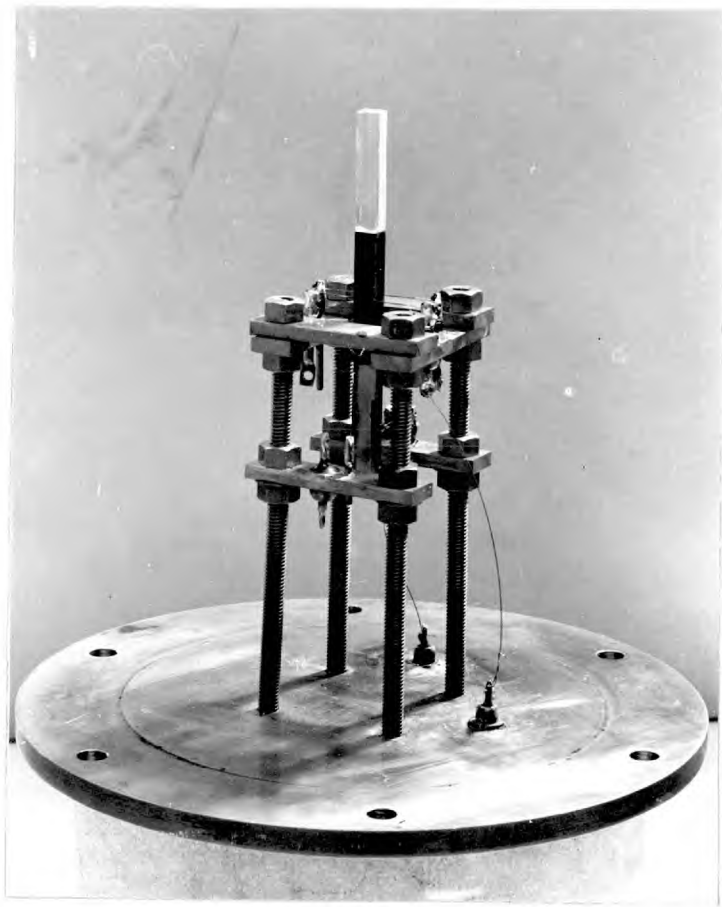

Fig. 2.2. The composite oscillator and a specimen mounted in the experimental rig.

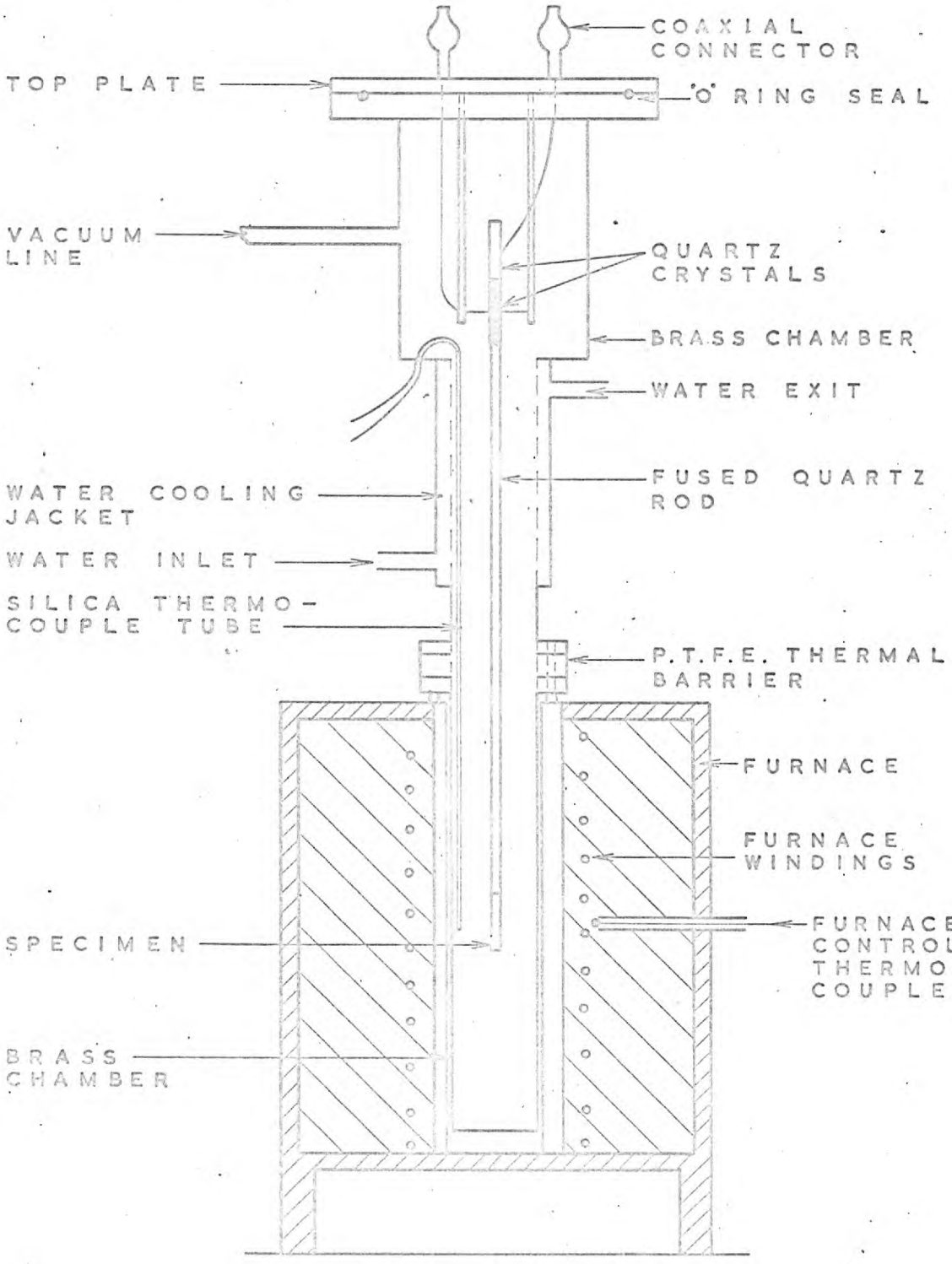

FIG. 2.3. THE INTERNAL FRICTION APPARATUS

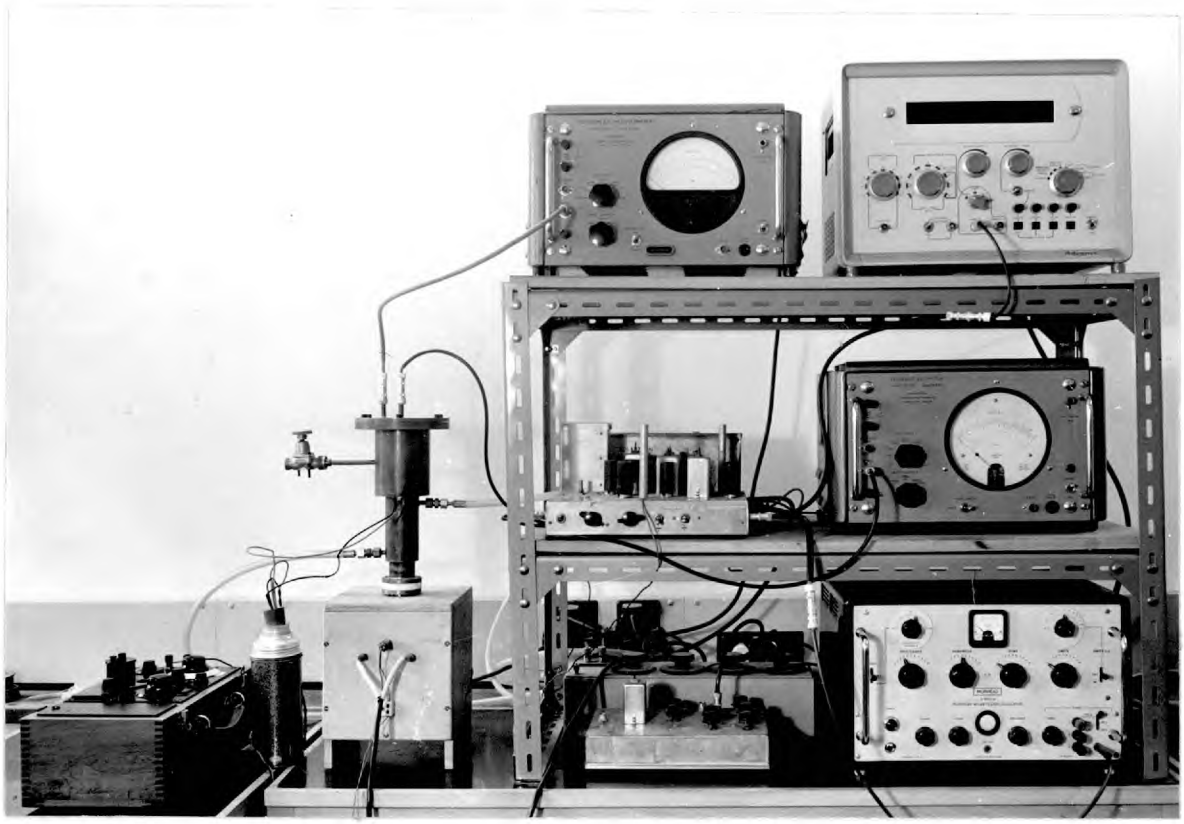

Fig. 2.4. The internal friction apparatus.

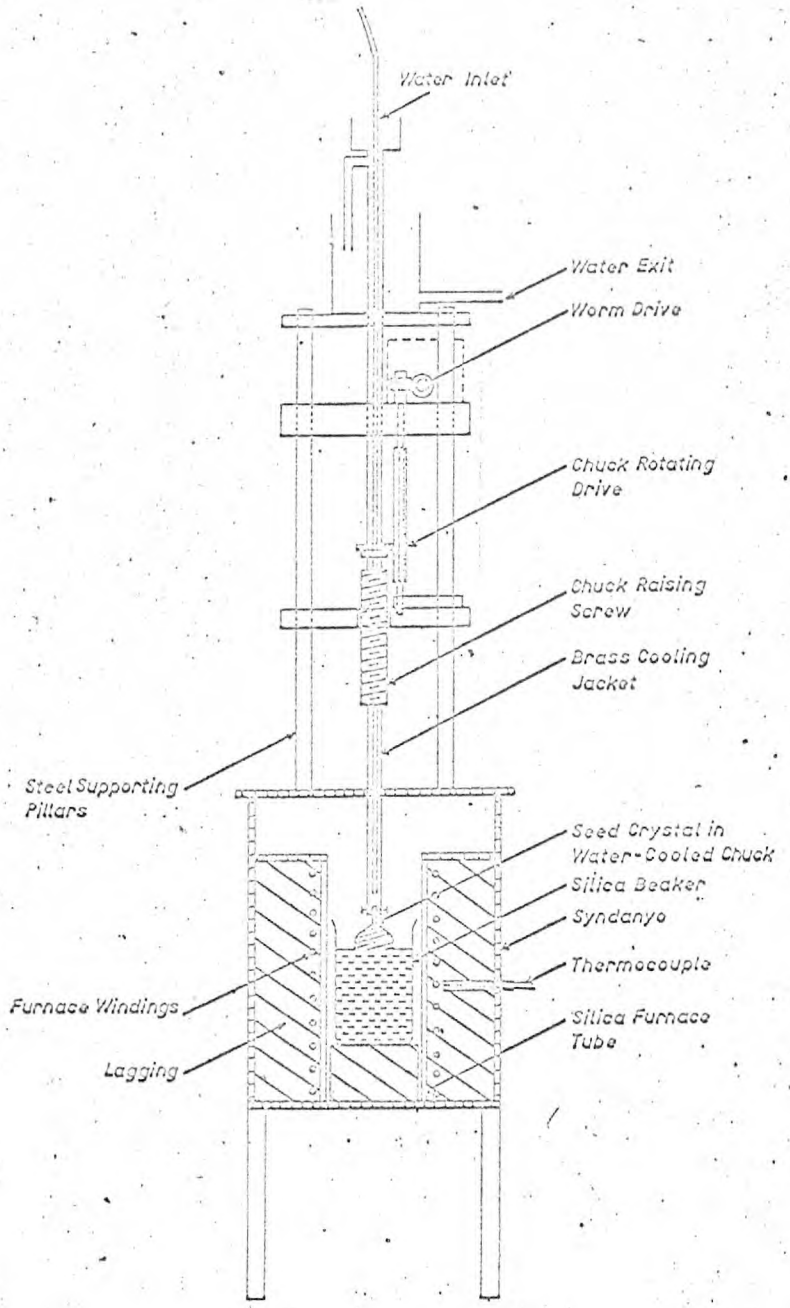

FIG.2.5. The Crystal Growing Apparatus.

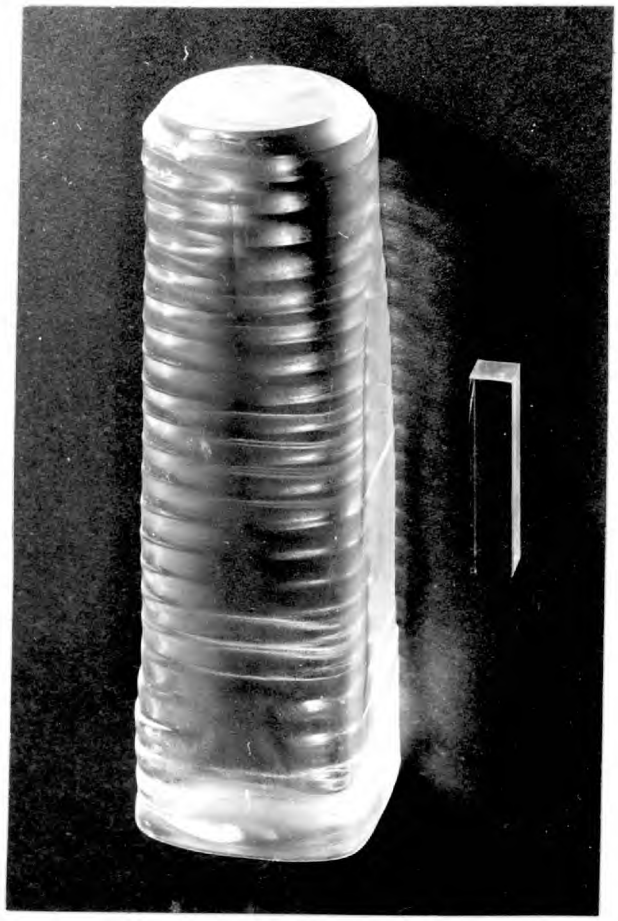

Fig. 2.6. A Na Cl boule and an internal friction specimen.

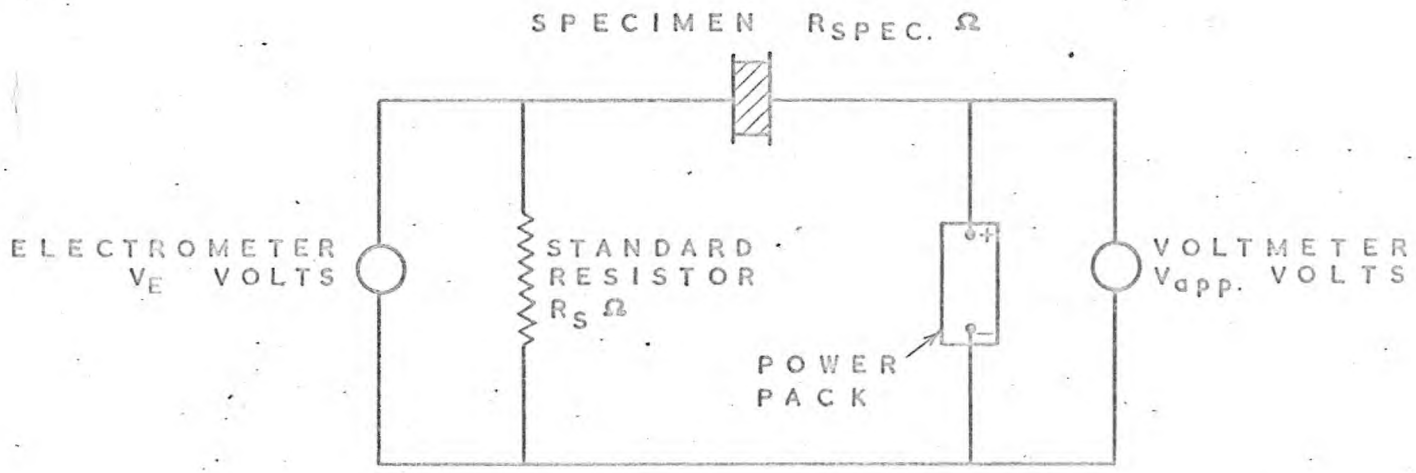

FIG. 2·7. BASIC CONDUCTIVITY CIRCUIT

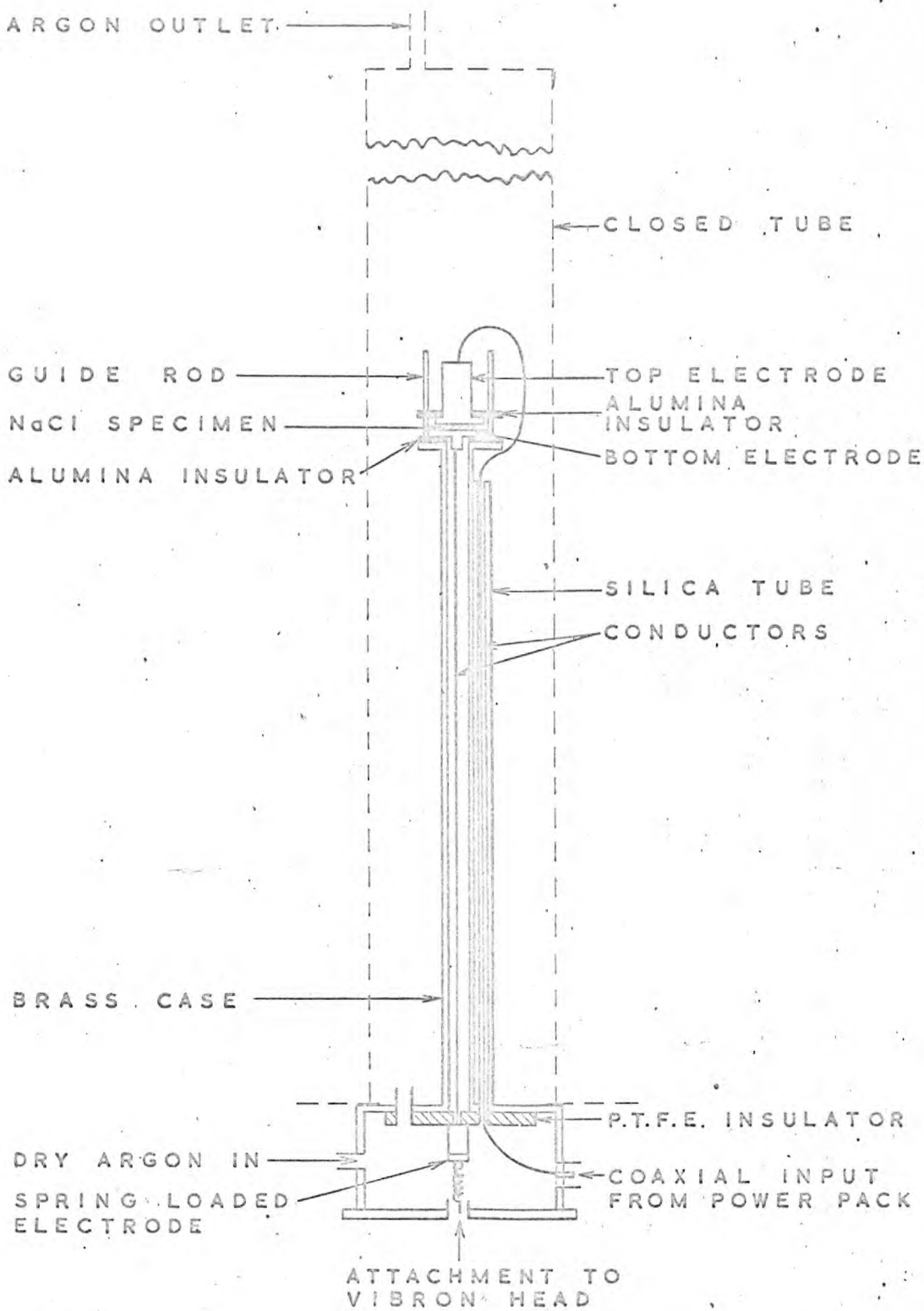

FIG. 2.8. SCHEMATIC DIAGRAM OF CONDUCTIVITY RIG

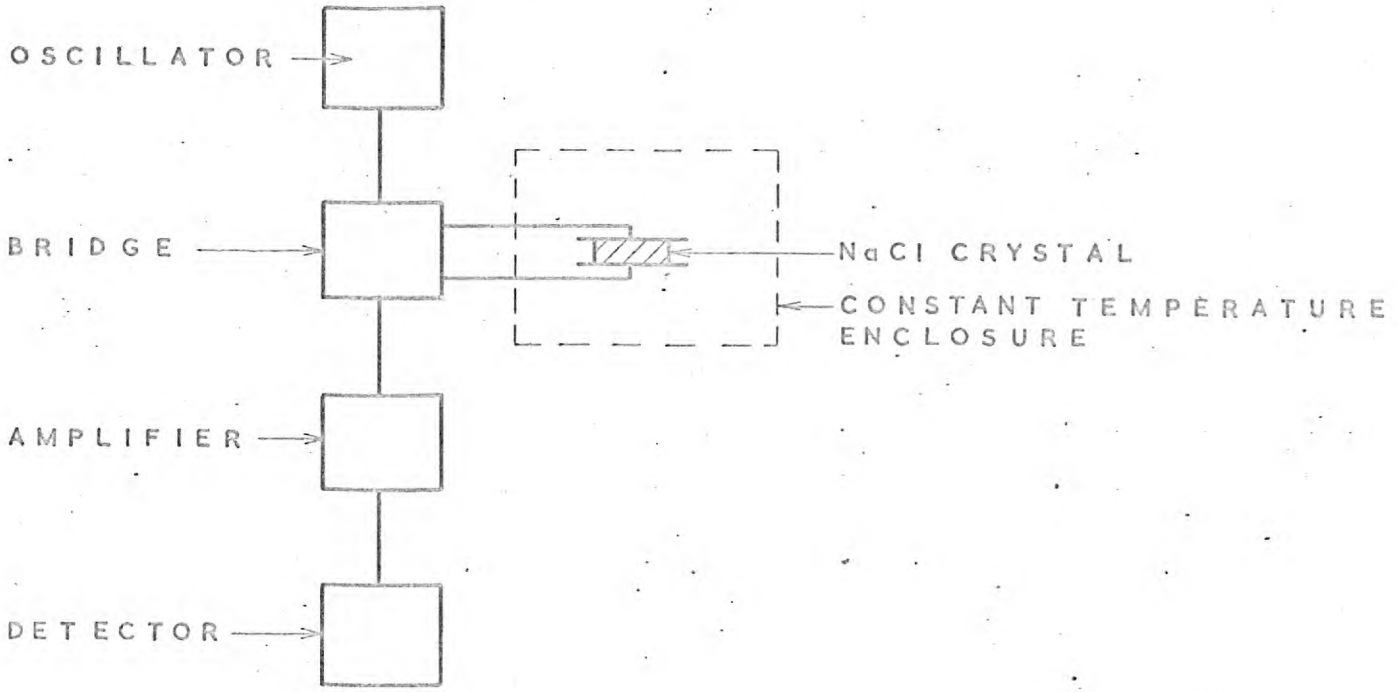

FIG. 2.9. BLOCK DIAGRAM OF DIELECTRIC LOSS APPARATUS

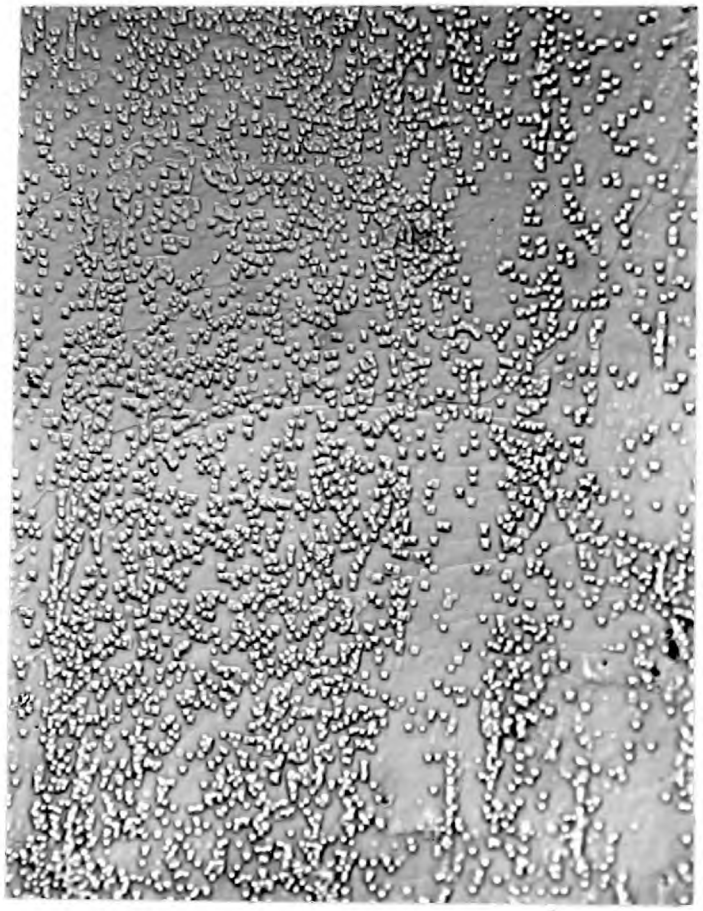

Fig. 2.10. Dislocation etchpits (x 540) on a 2 % deformed, pure Na Cl crystal.

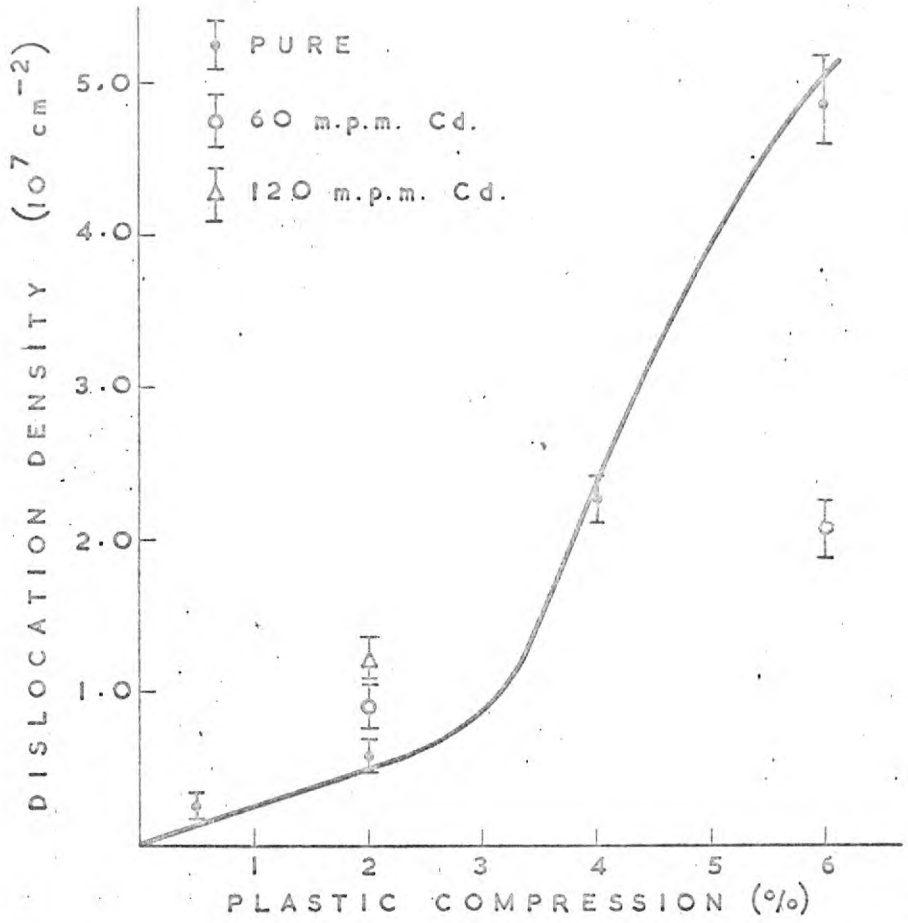

FIG. 2·11. DISLOCATION DENSITIES IN NaCl (SOLID LINE, DATA OF DAVIDGE & PRATT OFF PURE NaCl)

Chapter 3

General features of the internal friction

3.1 Changes of damping and modulus with amplitude at room temperature

The smallest amplitude at which measurements have been carried out was about 10^{-8} and from this amplitude to some other higher amplitude the decrement and resonant frequency are independent of amplitude. The decrement in the amplitude independent region increases with prestrain and thus with dislocation density for pure and Cd^{++} doped annealed specimens as shown in Figs. 3.1 and 3.2. It is necessary to specify that the decrement measurements displayed there were carried out ten minutes after deformation, as the decrement decreases, and the modulus increases, with time after deformation.

On increasing the amplitude of vibration above a critical amplitude ε_1 the damping begins to increase and the resonant frequency to decrease with increasing amplitude. This amplitude ε_1 depends upon the purity of the specimens and typically for a 2 % deformed, annealed pure specimen is about 5×10^{-7} while for a 2 % deformed specimen containing about 60 m.p.m. of Cd it is about 1×10^{-5}. It is difficult to accurately determine ε_1 experimentally but it appears to be quite reproducible for similar specimens, e.g. two different pure specimens had estimated values of ε_1 of 3×10^{-7} and 5×10^{-7} while two doped specimens had estimated values of 1×10^{-5} and 1.5×10^{-5}. ε_1 also depends on the deformation as is shown by comparing the values of the 2 % deformed pure specimens with that of a very lightly deformed specimen which was estimated as 2×10^{-6}. It is not known what amount of deformation the latter had suffered in terms of strain or dislocation density, but its amplitude independent decrement was 9×10^{-5} which indicates a very light deformation. There did not

appear to be any significant change in ε_1 on ageing a 2 % deformed annealed pure specimen although the amplitude independent decrement decreased appreciably, thus 15 minutes after deformation the decrement was 4.4×10^{-3} and decreased to 1.9×10^{-3} after 1600 minutes, while it was not possible within the accuracy of the measurements to detect a change in ε_1 from the value of 5×10^{-7}. This means that any change must have been less than 2×10^{-7}. Fig. 3.3 shows the behaviour described above.

When the amplitude of vibration of a pure annealed specimen which had been deformed and then aged at room temperature was increased in the amplitude dependent region, it was frequently observed that at amplitudes greater than a value ε_2 vibration induced changes took place in the damping and resonant frequency. This was manifested as a decrease in the oscillator gauge voltage V_g on driving the oscillator at a constant drive voltage V_d in this amplitude region and this implies an increase in damping, while the resonant frequency f_r decreased implying a decrease in modulus. When this happened V_g was measured as soon as possible after the application of V_d and the oscillator was kept vibrating at resonance under the same applied voltage until V_g had stopped varying, then the final value of V_g was recorded. The increase in damping and decrease in modulus which occur on vibrating a specimen at an amplitude in excess of ε_2 do not continue indefinitely but commence rapidly and slow down until they are no longer observable, and these changes increase with increasing amplitude. If a specimen is vibrated at an amplitude between ε_1 and ε_2 for times of a few minutes no change of damping or frequency

occur and the damping v. amplitude curve obtained on increasing strain amplitudes to that amplitude is retraceable on decreasing strain amplitude. However on vibrating at an amplitude greater than ε_2 the damping is increased at all amplitudes in the amplitude dependent region but is not increased in the amplitude independent region. The vibration induced changes are not permanent but the damping and modulus rapidly recover to their original values on standing at room temperature. As with ε_1, ε_2 is rather difficult to determine accurately experimentally, but typically a 2 % deformed annealed pure crystal displayed a value of ε_2 of 5×10^{-6}, 360 minutes after deformation and this value had not changed appreciably 1300 minutes later, while the corresponding values of amplitude independent decrement and decrement at ε_2 were 23×10^{-4} and 122×10^{-4}, and 19×10^{-4} and 70×10^{-4} respectively.

Similar vibration induced changes occur in divalent doped crystals at increased strain amplitudes. For example, a 2 % deformed annealed crystal containing about 60 m.p.m. of Cd^{++} had a value of ε_2 of about 4×10^{-5} at a decrement of 30×10^{-4} and an amplitude independent decrement of 7.5×10^{-4} (Fig. 3.4). A lightly deformed, annealed specimen containing about 20 m.p.m. of Ca^{++} showed the effect so rapidly that on increasing V_d in this region, V_g was actually decreased to a lower value than in the preceding measurement in the short time necessary for measurement, which gave the impression of a double valued decrement v. amplitude curve.

This phenomenon was not studied in detail. However it is worth noting that vibration induced changes were observed over the

temperature range -196°C to 150°C and the rate at which the damping and modulus recovered to their original values increased with increasing temperature. Unless otherwise stated in the text, all measurements reported in the amplitude dependent region have been carried out at amplitudes below that at which vibration induced effects begin.

3.2 Discussion

The general features of the behaviour described above are consistent with those observed by other workers. Internal friction is amplitude independent below a critical amplitude and the amplitude independent decrement increases with prestrain and dislocation density. The data shown in Figs. 3.1 and 3.2 should be treated with some caution as recovery occurs after deformation and some evidence will be presented that the rate of recovery varies with prestrain so that the results do not accurately reflect the values of amplitude independent decrement immediately after deformation. However they clearly show that damping increases linearly with dislocation density at low dislocation densities, and decreases with impurity concentration. This is qualitatively consistent with the predictions of the G-L theory as stated in equations 1.16 and 1.20. Damping does not increase linearly with screw dislocation density over the whole range of deformation from 0% to 6 % in pure Na Cl and this appears to contradict the G-L theory. However the slope of the work hardening curve of Na Cl steepens at about 3 % (Fig. 1.1) as the material enters stage II of work hardening which is characterised by increased intersection of dislocations and interaction with dislocation debris. Thus although the dislocation density is

increased, the mean dislocation loop length is decreased and it is to be expected that the damping at strains in excess of 3 % will be decreased below the value obtained by a linear extrapolation of the low deformation data. The mean loop length should also be decreased by increased inpurity concentration and in fact the decrement of a Na Cl crystal containing 60 m.p.m. of Cd^{++} is decreased by a factor of about 10 below that of a pure Na Cl crystal with the same dislocation density. Because of the dependence of Δ_I on the fourth power of the weak pinner length this implies that the weak pinner concentration is increased by a factor of 1.8. Without knowing the purity of a 'pure' crystal (v. Chapter 2.3), or the state in which the additional Cd^{++} interacts with the dislocation as a weak pinner (i.e. as free Cd^{++} ion, aggregate, etc.) it can only be concluded that this is not an unreasonable value.

The qualitative nature of the observations of the vibration induced changes limits their analysis. These changes are similar to the type I changes observed by Whitworth[22] in pure Na Cl, and the apparent double valued decrement v. amplitude behaviour of the Ca^{++} doped specimen is similar to that observed by Frankl[21] and Birnbaum.[49] Theories of vibration induced changes in internal friction have been mentioned in Chapter I but there is insufficient evidence to test any of them. However it is worth noting that the observed behaviour is consistent with the suggestion in Chapter I that the G-L model might be applicable at amplitudes below that at which a Nowick-Whitworth model might apply. The former corresponds to the amplitude dependent region below ε_2 and the latter to amplitudes greater than ε_2 where the vibration induced changes occur by the mechanism suggested by Whitworth. The observation

that there is an amplitude dependent region where vibration induced changes do not occur is of some importance in the following experiments as it permitted measurements of internal friction to be carried out during recovery without seriously affecting the recovery process.

Some information may be obtained by comparing the recovery of the critical amplitude ε_1 with that of the amplitude independent decrement Δ_I. Blistanov and Shaskol'skaya have studied the recovery of internal friction in LiF by observing the change in ε_1 with time. They have shown that if the recovery theory of Granato, Hikata and Lucke is correct then ε_1 should vary with time as $(1 + \beta t^{2/3})$, while the theory itself predicts that Δ_I should vary as $(1 + \beta t^{2/3})^{-4}$. Hence ε_1 and $\Delta_I^{-\frac{1}{4}}$ should have the same time dependence and a relative change in $\Delta_I^{-\frac{1}{4}}$ should be accompanied by a comparable relative change in ε_1. Above it was shown that a change of Δ_I from 44×10^{-4} to 19×10^{-4} was not accompanied by any significant change in ε_1. According to this theory a change in Δ_I of that amount should increase ε_1 by a factor of about 1.2 which would certainly not be observed within the accuracy of the present measurements. Thus this behaviour is consistent with the G-L model of internal friction.

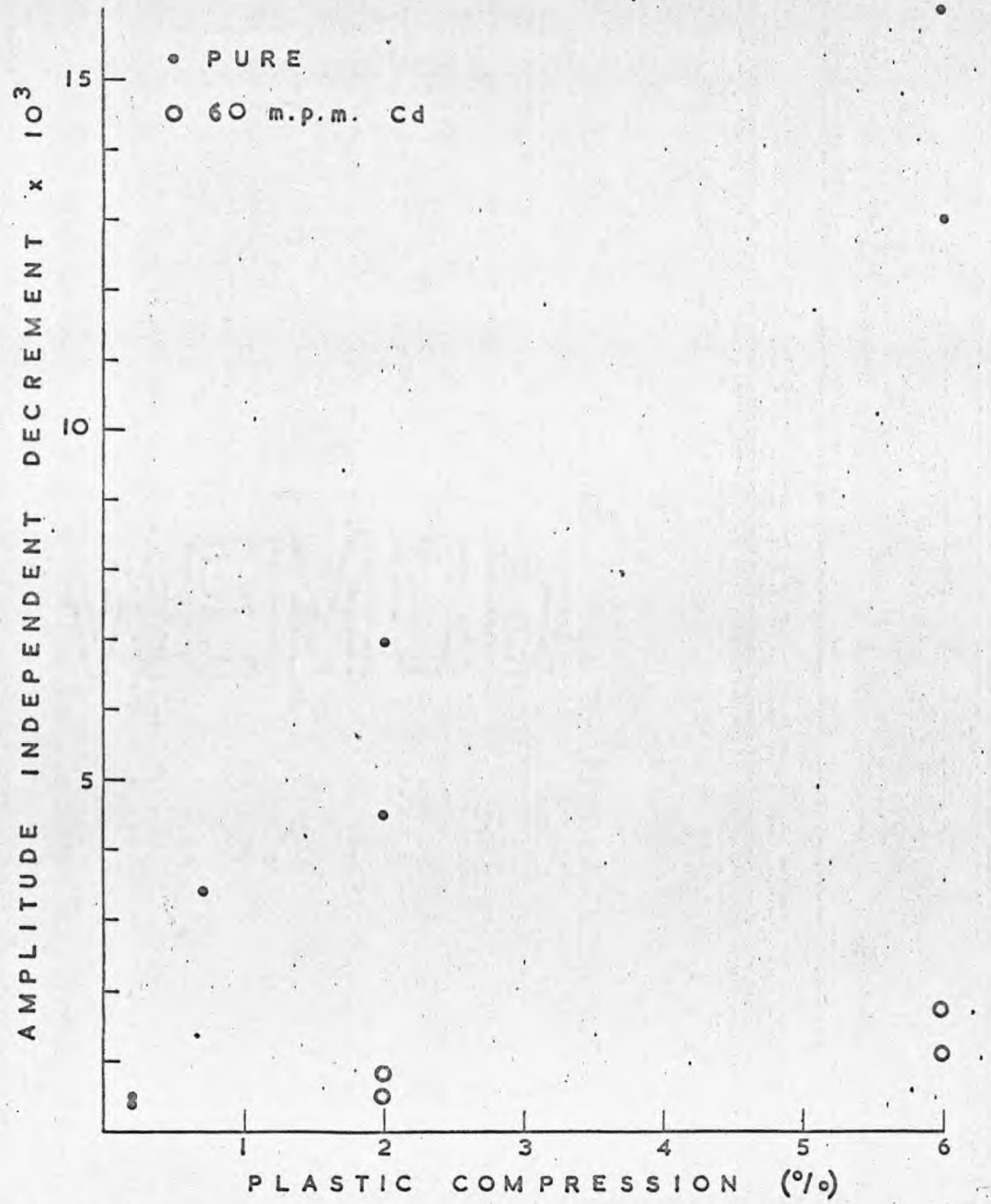

FIG. 3·1. VARIATION OF Δ_I WITH PRESTRAIN AT ROOM TEMPERATURE. (Δ_I MEASURED 10 MINUTES AFTER DEFORMATION)

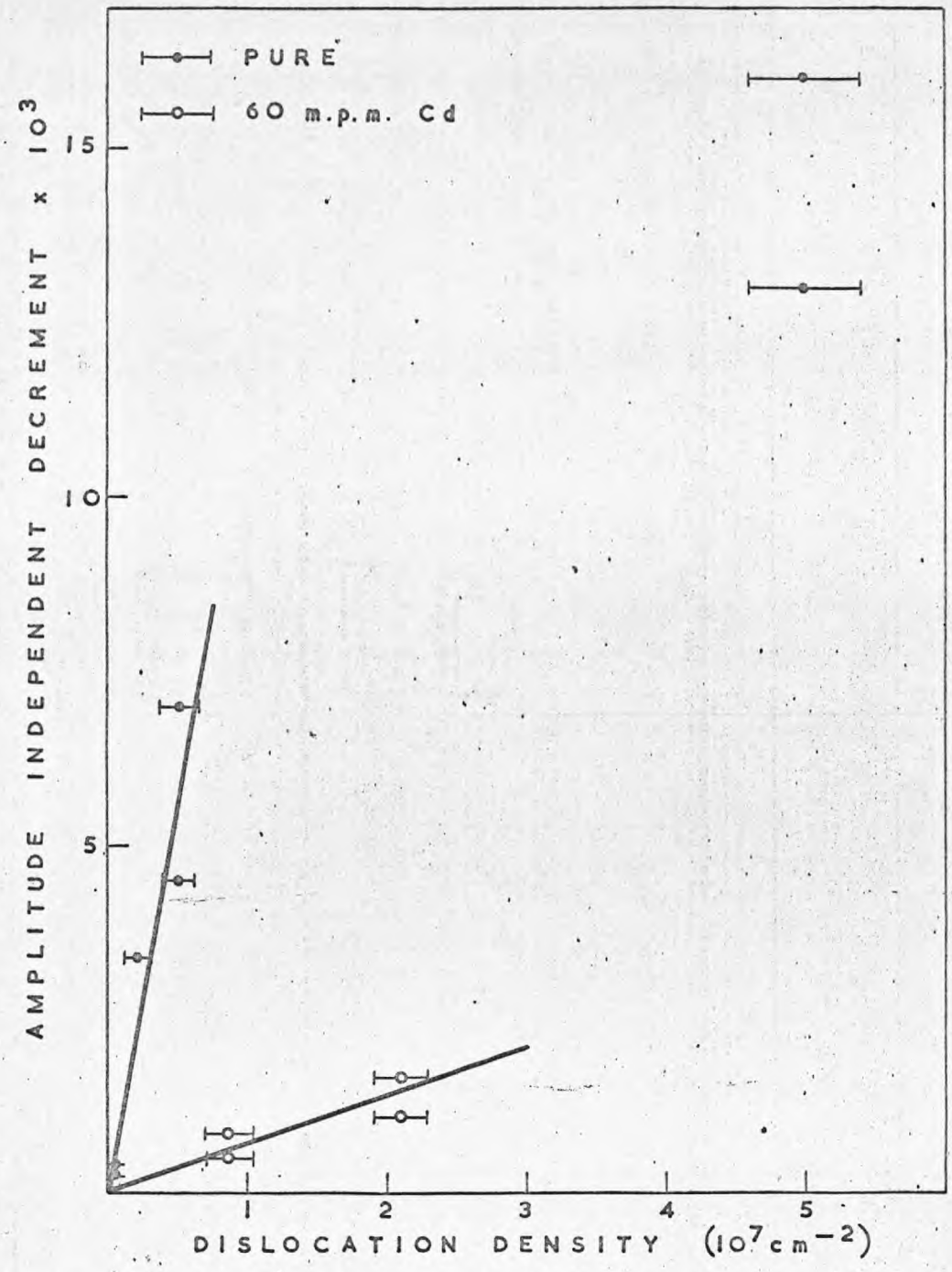

FIG. 3·2. VARIATION OF Δ_I WITH DISLOCATION DENSITY AT ROOM TEMPERATURE. (Δ_I MEASURED 10 MINUTES AFTER DEFORMATION)

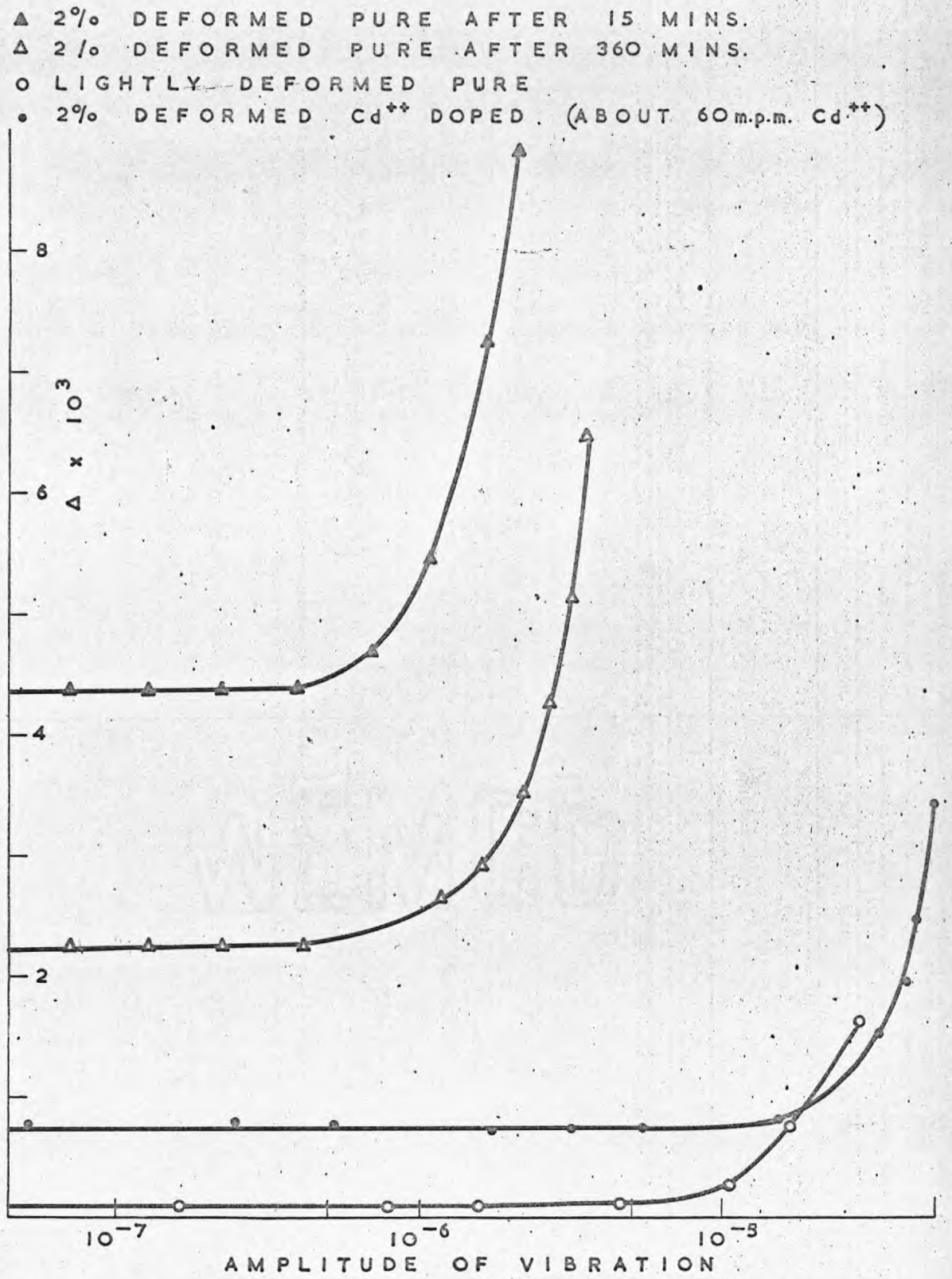

FIG. 3.3. EFFECT OF DEFORMATION, RECOVERY AND Cd^{++} ADDITION ON ε_1

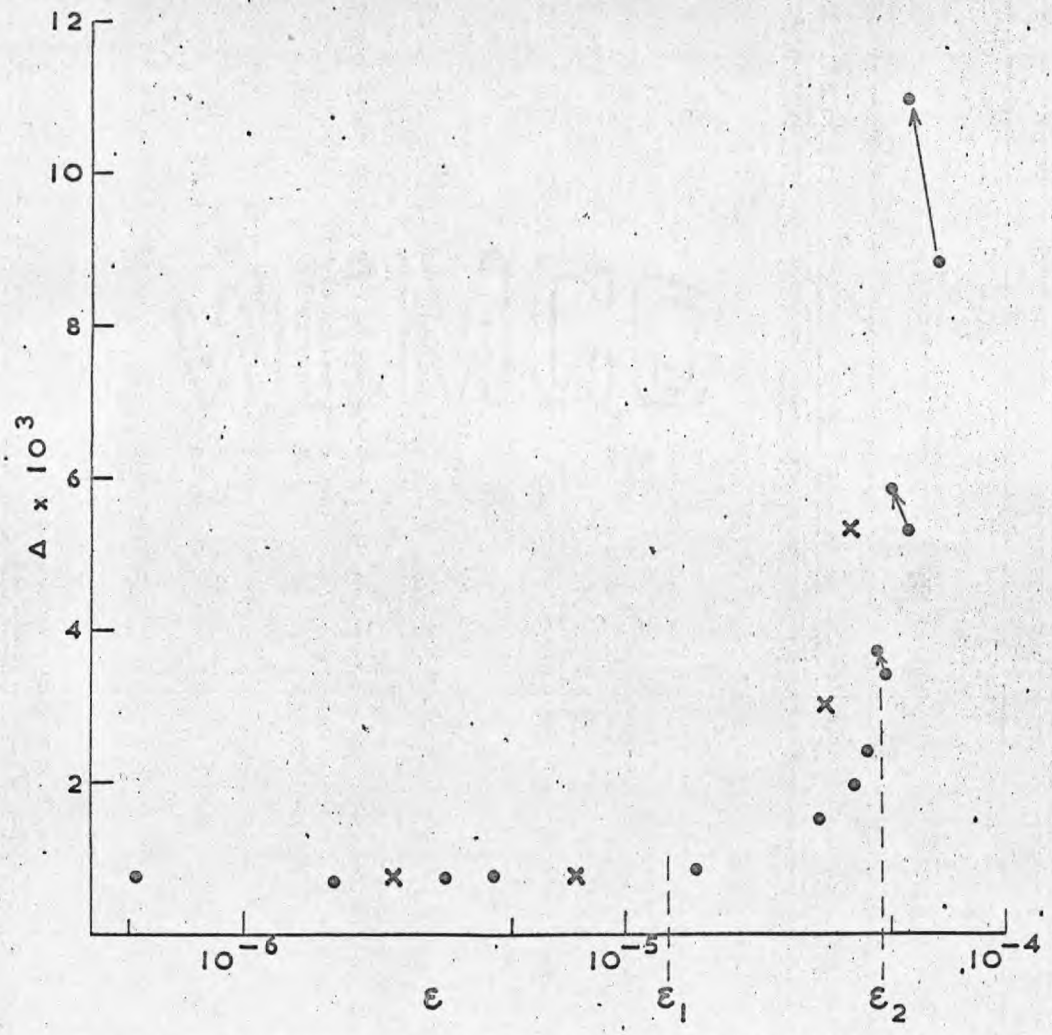

• MEASUREMENTS TAKEN ON INCREASING AMPLITUDE
× MEASUREMENTS TAKEN ON DECREASING AMPLITUDE
ARROWS INDICATE CHANGES OF INTERNAL FRICTION

FIG. 3.4. VIBRATION INDUCED CHANGES IN INTERNAL FRICTION IN A CRYSTAL CONTAINING ABOUT 60 m.p.m. OF Cd, 2 % DEFORMED.

Chapter 4

Recovery of internal friction.

4.1 General procedure

The variation of damping and modulus with time after deformation was studied in the following manner. Immediately after deformation at room temperature the specimen was mounted on the composite oscillator and placed in the internal friction chamber which was already at the testing temperature. At temperatures other than room temperature the specimen took up to ten minutes to reach equilibrium and so measurements at these temperatures were not taken until up to fifteen minutes after deformation. Measurements were then carried out as a function of time measured from half way through the period of deformation. Each measurement was carried out at one of two gauge voltages which were constant for that specimen, one was in the amplitude independent region and the other was in the amplitude dependent region. The driving voltages and the resonant frequencies necessary to produce these gauge voltages were recorded and thus the decrement Δ_I at a constant amplitude in the amplitude independent region, and the decrement Δ at a constant amplitude in the amplitude dependent region, together with information about the modulus at those amplitudes were obtained as a function of time.

4.2 Recovery of pure Na Cl as a function of temperature

All measurements in this section were carried out on 2 % deformed, annealed pure specimens.

Fig. 4.1 shows typical recovery behaviour of Δ and Δ_I at 53°C and -78°C, and Fig. 4.2 shows the recovery of Δ, Δ_I and frequency at 24°C. For the reasons already stated in the chapter on experimental techniques little reliance can be placed on frequency

measurements at temperatures other than room temperature and that data will not be presented here. It is clear that the recovery of damping is strongly temperature dependent, and this suggests a thermally activated process such as the diffusion of weak pinners to dislocations as suggested by Granato, Hikata and Lucke. Following the assumption that Δ may be dissociated into two parts, Δ_I and Δ_H, where $\Delta = \Delta_I + \Delta_H$, these quantities will be considered separately.

Fig. 4.3 shows the behaviour of Δ_I as a function of time at room temperature plotted in the coordinate system $\Delta_I^{-\frac{1}{4}}$ v. $t^{2/3}$, and Fig. 4.4 shows the behaviour of Δ_I in the same coordinate system at different temperatures. According to the GHL theory, equation 1.25, $\Delta_I \propto (1 + \beta t^{2/3})^{-4}$ and a plot of $\Delta_I^{-\frac{1}{4}}$ v. $t^{2/3}$ should lead to a straight line in the early stages of recovery before saturation of the dislocation begins to occur. Fig. 4.3 shows that this linear relationship is obeyed after an initial period when the recovery is faster than predicted. The data shown in Fig. 4.4 do not show the $t^{2/3}$ stage as well as the room temperature data, but this is consistent with recovery being divided into three stages. In each of these experiments recovery was observed for about six hours and during this time at 53°C the initial rapid stage, the $t^{2/3}$ stage and the onset of saturation occurred; at room temperature and 0°C only the rapid and $t^{2/3}$ stages occurred; while at the lower temperatures the rapid stage did not proceed to conclusion. Where the $t^{2/3}$ stage did occur, the recovery parameter β can be obtained from the slopes and the intercepts of the lines.

Fig. 4.5 shows the behaviour of Δ_H at room temperature plotted

as $\log \Delta_H$ v. $t^{2/3}$. In accordance with the GHL theory, equation 1.24, this shows a linear stage, and as for the amplitude independent data the $t^{2/3}$ stage is preceded by an initial more rapid stage and followed by a slower stage. Fig. 4.6 shows the behaviour of Δ_H during recovery over the temperature range 53°C to -80°C and the three stages of recovery are observed here as for the Δ_I data. The rate of recovery of Δ_H depends on the amplitude at which it is measured. For example at 0°C the slopes $M = d(\log \Delta_H)/d(t^{2/3})$ of the linear stages of the recovery data of two different specimens with exactly similar histories were 2.7×10^{-3} (mins.)$^{-2/3}$ and 5.0×10^{-3} (mins.)$^{-2/3}$ at respective amplitudes ε of 3.5×10^{-6} and 2.1×10^{-6}. If a recovery parameter is defined as a quantity which is a measure of the recovery rate and is the same for specimens of similar histories then the above, typical, example shows that the quantity M is not as useful as the product ε M. The M values differ by a factor of almost two while the ε M values agree within 10 %. This result is consistent with the GHL theory and encourages the use of ε M as a recovery parameter.

According to the GHL theory the recovery parameters β and ε M are related to more fundamental properties of the material by the equations

$$\beta = \frac{c_{10}}{c_{10} + c_{20}} \frac{8\alpha}{a^2} \left(\frac{AD}{kT}\right)^{2/3} \qquad 1.27$$

and

$$\varepsilon M = 0.434 \; K \eta \; c_{10} \; \frac{8\alpha}{a^2} \left(\frac{AD}{kT}\right)^{2/3} \qquad 4.1$$

Equation 4.1 is derived from equation 1.24, and the diffusion coefficient

D is related to the temperature by

$$D = D_o \exp.\left(\frac{-E_m}{kT} \right)$$

where E_m is the migration energy. Thus $\log \beta^{3/2} T$ and $\log (\varepsilon M)^{3/2} T$ when plotted against $1/T$ should yield straight lines whose slopes give the diffusion energy E_m. Figs. 4.7 and 4.8 show the recovery parameters plotted in this way as a function of temperature and the slopes of the best straight lines, fitted by a least squares method, give

(amplitude independent data) $E_m = 0.70 \pm 0.12$ eV.

(amplitude dependent data) $E_m = 0.72 \pm 0.09$ eV.

Only the data for 53°C, 24°C and 0°C have been used in these calculations as it is not certain that the $t^{2/3}$ stage had been attained at the lower temperatures.

4.3 Recovery of pure Na Cl as a function of prestrain and thermal history

The rate of recovery of damping of pure Na Cl is sensitively related to the prestrain and thermal history of the specimen. Fig. 4.9 shows the variation of the recovery parameter εM with prestrain for annealed pure specimens. Table 4.1 compares the values of the recovery parameter εM of specimens which had been quenched from 200°C and 350°C and then deformed 2 %, with the recovery parameter of 2 % deformed annealed specimens.

Table 4.1

Variation of ξM with heat treatment

Heat treatment	ξM (minutes)$^{-2/3}$
Annealed	$2.62 \ 10^{-8}$ 2.94×10^{-8}
200°C quenched	6.09×10^{-8}
350 C quenched	2.05×10^{-7}

4.4 Recovery of Cd^{++} doped Na Cl

The effect of alloying a Na Cl crystal with Cd^{++} is to increase the speed with which recovery of internal friction proceeds. This is clearly shown in Fig. 4.10 which is a recovery curve at room temperature after a 2 % deformation of an annealed specimen containing 69 m.p.m. of Cd^{++}. Figs. 4.11 and 4.12 show the data plotted as $\triangle_I$ and $\triangle_H$ in the appropriate coordinates for testing the GHL theory. Recovery in doped specimens was studied at 24°C and 0°C, but at -30°C the rate of recovery was so slow that it could not be measured in the times employed in this research. As for the pure specimens, recovery can be divided into three stages. Fig. 4.13 and Fig. 4.14 show the recovery parameters, obtained from the $t^{2/3}$ stage, plotted with temperature to give the migration energies, and the values obtained are

(amplitude independent data) $E_m = 0.72$ eV $\pm$ 0.22 eV.

(amplitude dependent data) $E_m = 0.72$ eV $\pm$ 0.06 eV.

As for pure Na Cl, the recovery of a doped crystal depends on the thermal history of the crystal prior to its deformation. The heat treatment applied to the 'annealed' crystals used in this work does not produce an equilibrium state of dispersion of pinning defects, as is shown by the fact that the recovery parameter of a specimen which had been annealed and then allowed to stand at room temperature for a year before deformation was a lot less than that of a specimen which was tested within a day or two of annealing. Quenching a doped specimen immediately before deformation made recovery so rapid that it was difficult to measure with any accuracy. As might be expected the recovery rate increased with Cd^{++} content. Table 4.2 summarises this information in terms of the measured recovery parameters ξ M obtained with 2 % deformed crystals.

Table 4.2

Variation of ξ M with heat treatment and doping

Specimen	ξ M $(\text{minutes})^{-2/3}$
Annealed specimens containing (a) 69 m.p.m. Cd^{++} (b) 58 m.p.m. Cd^{++}	(a) 1.63×10^{-6} (b) 1.40×10^{-6}
Annealed specimen containing (a) about 120 m.p.m. Cd^{++} (b) 112 m.p.m. Cd^{++}	(a) 4.91×10^{-6} (b) 3.51×10^{-6}
Unannealed specimens aged at room temperature for 1 year and containing (a) 124 m.p.m. Cd^{++} (b) 115 m.p.m. Cd^{++}	(a) 5.90×10^{-7} (b) 3.71×10^{-7}
Specimens containing about 60 m.p.m. Cd^{++} and 120 m.p.m. Cd^{++} quenched from 200°C.	Recovery too fast to measure $\therefore > 5 \times 10^{-6}$

4.5 Determination of the time exponent

The preceding analysis of the recovery data is based on the theory of Granato, Hikata and Lucke, which in turn assumes that the interaction between weak pinners and dislocations is by a Cottrell - Bilby mechanism resulting in a $t^{2/3}$ time dependence. The time exponent, which is assumed to be 2/3, could in general have some other value x which would depend on the actual mechanism of interaction between pinners and dislocations. Thus if it is not assumed that the mechanism is a Cottrell - Bilby one, the more general relationships between decrement and time would lead to $\log \triangle_H$ v. t^x and $\triangle_I^{-\frac{1}{4}}$ v. t^x being straight lines.

In this general case, equation 1.24, reduces to

$$\log \triangle_H = X - y\, t^x \qquad 4.2$$

where X, y and x are constants which could best be calculated by a numerical technique employing a computer and using all the data obtained in this work. This has not been carried out but one set of results has been analysed in a less detailed way to find x. Equation 4.2 leads to

$$\log \left\{ \frac{d}{dt} (\log \triangle_H) \right\} = \text{Constant} + (x - 1)\log t \quad .$$

Fig. 4.15 shows the data obtained on room temperature recovery of a specimen containing 125 m.p.m. of Cd^{++} unannealed and deformed 2 %, plotted as $\log \triangle_H$ v.t. This specimen was selected because recovery occurred fast enough that changes in ambient temperature were small, and yet not so fast that it was not possible to make accurate

measurements. The slope $d(\log\Delta_H)/dt$ has been obtained at successive times t by approximating the slope of the curve to that of the straight line joining two experimental points on the curve equal short times from t. Fig. 4.16 shows a plot of $\log\{d(\log\Delta_H)/dt\}$ v. $\log t$. The best straight line fitted to these points by a least squares method has slope -0.27 ± 0.08, which implies a value of the time exponent x of

$$x = 0.73 \pm 0.08$$

4.6 Behaviour of the Δ v. ε curves on ageing

Fig. 4.17 shows a series of Δ v. ε curves obtained off one 2 % deformed, annealed, pure specimen measured at various times up to 1600 minutes after deformation. Fig. 4.18 shows some of this data plotted as $\log \varepsilon^{\frac{1}{2}}\Delta_H$ v. $1/\varepsilon$ to give a G-L plot. The G-L plot is clearly not linear over the whole of its range but at higher amplitudes tends to linearity more than at lower amplitudes. According to the G-L theory a G-L plot should yield a straight line whose negative slope is inversely proportional to the mean length L_c between weak pinners. Fig. 4.19 shows the G-L plots obtained from the data shown in Fig. 4.17 plotted over only the upper amplitude range where the results approximate best to straight lines. This data was obtained at the highest amplitudes at which vibration induced changes of internal friction did not occur. The negative slopes clearly increase with time in agreement with the concept that L_c decreases with ageing.

4.7 Discussion of recovery data

The data presented above show that over a wide range of recovery the variables damping, time and temperature obey the functional relationships predicted by the theory of Granato, Hikata and Lucke. The evidence thus strongly supports their model of point defects migrating to and immobilising dislocations. Recovery can be divided into three stages. Initially recovery of both $\triangle_H$ and $\triangle_I$ proceeds more rapidly than predicted, and at room temperature this rapid stage finishes about forty minutes after deformation for pure Na Cl. The published data of Gordan and Nowick[23] on the recovery of damping of Na Cl at room temperature do not show this rapid stage, but their published measurements did not commence until 90 minutes after deformation, when the rapid stage is completed. However Blistanov et al.[39][41] have observed the rapid stage in the recovery of amplitude independent damping in LiF at room temperature and it there ended about 7 minutes after deformation. They suggested that rapid recovery might be due to the redistribution of dislocations immediately after deformation, but an alternative explanation is that point defects which are initially close to the dislocations move through the distorted region near the dislocation core more rapidly than distant point defects diffuse through the bulk. The evidence however is insufficient to unambiguously identify the rapid recovery mechanism. After the rapid stage, recovery can be explained by the $t^{2/3}$ time dependence of the GHL model. This slows down with increased time, as is typical of processes involving diffusion to a dislocation, as the point defect concentration gradient in the vicinity of the dislocation core increases.

The GHL theory was developed from the Granato - Lucke theory of internal friction. Both theories have been outlined in Chapter 1, but to recapitulate, the G-L theory of internal friction relates the mean dislocation loop length to Δ_H and Δ_I and the form of this relationship is unique to the G-L theory so that recovery which obeys the GHL theory is strong support for the G-L theory. Further support for the G-L theory is given by the increasing negative slopes of the G-L plots as recovery proceeds, which is shown in Fig. 4.19.

The GHL theory is based on a model in which dislocations are initially pinned by strong pinners and two types of weak pinners of which one has a bulk concentration c_{10}, is mobile and can diffuse, and the other of bulk concentration c_{20} is immobile. The theory can be easily extended to cover other simple cases such as one type of mobile weak pinner and no immobile weak pinner, or two types of mobile weak pinner with different diffusion energies. Such assumptions do not alter the form of the dependence of Δ_I and Δ_H on $t^{2/3}$ and similar functional relationships are obtained with the only important differences being exhibited in the recovery parameters β and εM. The GHL model (call this case (a)) produces recovery parameters with the values

$$\beta = \frac{c_{10}}{c_{10}+c_{20}} \quad \frac{8\alpha}{a^2} \left(\frac{AD}{kT}\right)^{2/3}$$

$$\varepsilon M = K \eta \, c_{10} \quad \frac{8\alpha}{a^2} \left(\frac{AD}{kT}\right)^{2/3} \times 0.434$$

The assumption that there is no immobile defect is equivalent to

equating c_{20} to zero and makes β independent of concentration of pinning defect while leaving ξM unaltered (case (b)). On the other hand, assuming two mobile defects with different diffusion energies (case (c)) leads to

$$\beta = \frac{x_1 c_{10} + x_2 c_{20}}{c_{10} + c_{20}}$$

$$\xi M = x_1 c_{10} + x_2 c_{20}$$

where x_1 and x_2 are the respective $\frac{8\alpha}{a^2}\left(\frac{AD}{kT}\right)^{2/3}$ factors for the two defects. Figs. 4.7 and 4.13 show that the difference between β values of pure and doped specimens at the same temperature is less than a factor of 2, and as this factor is determined by the scatter on the experimental data, the difference might be less or even zero. On the other hand the ξM values of doped specimens are increased by an order of magnitude over those of pure specimens as can be seen from Figs. 4.8 and 4.14 and tables 4.1 and 4.2. It is reasonable to assume that the addition of divalent impurity increases the concentration of mobile pinner in a crystal and thus these observations are in agreement with the general predictions of the GHL theory whichever of the three cases is operative. For if it is case (a) then provided $c_{10} \gtrsim c_{20}$ for pure crystals, $\beta_{\text{doped}} \approx \beta_{\text{pure}}$ and ξM is proportional to c_{10}. If it is case (b) then $\beta_{\text{doped}} = \beta_{\text{pure}}$ and ξM is proportional to c_{10}. While if it is case (c) then provided $x_1 c_{10} \gtrsim x_2 c_{20}$ for pure crystals, then $\beta_{\text{doped}} \approx \beta_{\text{pure}}$ and ξM is approximately proportional to c_{10}. Figs. 4.7 and 4.8

might be expected to deviate from linearity if case (c) holds but there is not sufficient data to show any small non-linearity, and no evidence for large non-linearity. This could mean that there are several pinner types with very nearly equal diffusion energies, or that one type has an energy sufficiently lower than the others to dominate the diffusion.

The $t^{2/3}$ time dependence of recovery in the GHL theory arises from their use of the Cottrell-Bilby relation. In general if the interaction energy E_B between a point defect and a dislocation is spatially related to the distance d between the point defect and the dislocation by

$$E_B \propto \frac{1}{d^{\nu}}$$

then the initial time dependence of recovery in terms of the number of pinners n(t) which have arrived at a dislocation after time t is (51)

$$n(t) \propto t^{2/\nu + 2}$$

Where $\nu = 1$, e.g. the elastic interaction between an edge dislocation and an impurity atom due to the difference in size between the impurity atom and the matrix atoms, the time dependence is $t^{2/3}$. Where $\nu = 2$, e.g. the elastic interaction between a screw dislocation and an impurity atom due to the size difference, the time dependence is $t^{\frac{1}{2}}$. The present work shows that the time dependence of recovery is $t^{2/3}$ rather than $t^{\frac{1}{2}}$ and thus implies a first order interaction between pinners and dislocations. Brown and Pratt(50) have also observed a $t^{2/3}$ time dependence of recovery in strain ageing experiments on Cd doped Na Cl. They measured the increase in yield stress on ageing a strained crystal

and assumed that the increase was a linear function of the number of point defects which had migrated to the dislocation.

The variation of the recovery parameter ξ M with prestrain of pure Na Cl could arise in several ways. Blistanov et al.[41] have observed a similar variation in the recovery parameter β of LiF and have suggested that it is due to a variation in the concentration of the low mobility point defect c_{20} with prestrain. They attribute this to an increase in vacancy concentration and dislocation intersection points with increasing deformation. This does not seem an unreasonable explanation and, although it might be argued that the GHL theory predicts that ξ M should be independent of c_{20}, it must be remembered that the theory does not take into account the variation of the geometry of the dislocation intersection configuration with strain that occurs in a real material. ξ M appears to be a minimum at a strain near to that at which the transition from stage I to stage II of work hardening occurs, and this suggests that the variation in ξ M is connected with the change in mean loop length with increasing strain. It is interesting to note that Brown and Pratt observed a maximum in the strain ageing effect of Cd^{++} doped Na Cl at a strain corresponding to the transition from stage I to stage II, while the present work indicates a minimum in the recovery rate of pure Na Cl at a strain corresponding to the transition from stage I to stage II. Another possible explanation of the variation of ξ M is that it is a reflection of a variation in c_{10}. Unfortunately the scatter in the low strain results was too large to obtain any complementary information about $c_{10}/(c_{10} + c_{20})$, but the coincidence between the findings of Blistanov

et al and of the present work suggests that careful measurements of β as a function of prestrain in Na Cl might show a similar variation. Such measurements would shed light on this problem.

The diffusion energy obtained for both pure and Cd^{++} doped specimens from amplitude dependent data and amplitude independent data agree well, suggesting that the same, or similar, weak pinner or pinners are responsible in both cases. Further, the increase in $\mathcal{E}$ M values with increased Cd^{++} content show that the concentration of mobile pinners is related to the presence of divalent ions, while the variation of $\mathcal{E}$ M with heat treatment shows that c_{10} depends on the state of dispersion of the impurity. This suggests that the predominant mobile pinner is a divalent ion, a cation vacancy, a cation vacancy - divalent ion pair, or a higher aggregate.

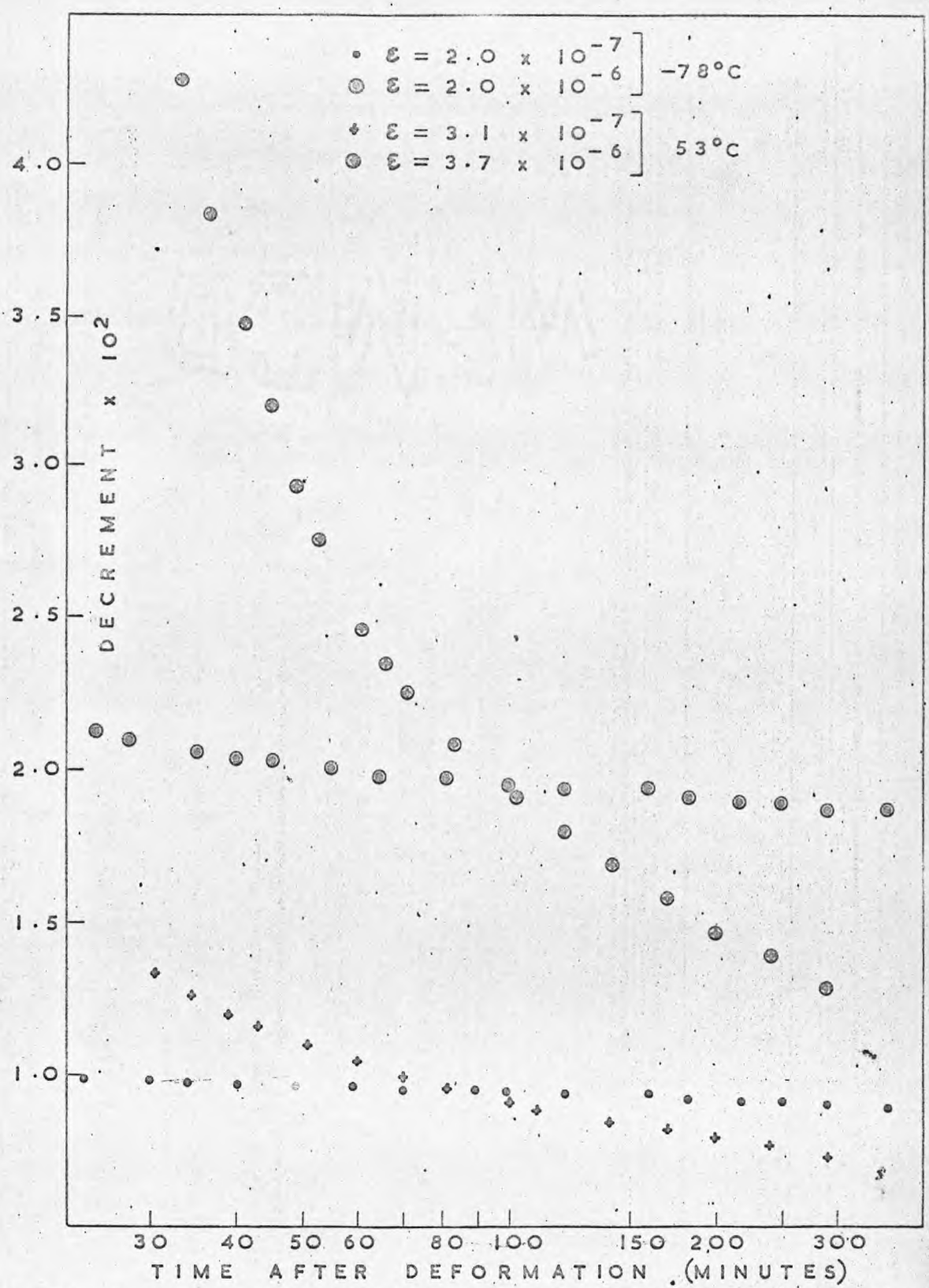

FIG. 4.1. RECOVERY OF Δ AND Δ_I OF 2% DEFORMED, ANNEALED, PURE NaCl CRYSTALS AT -78°C. AND 53°C.

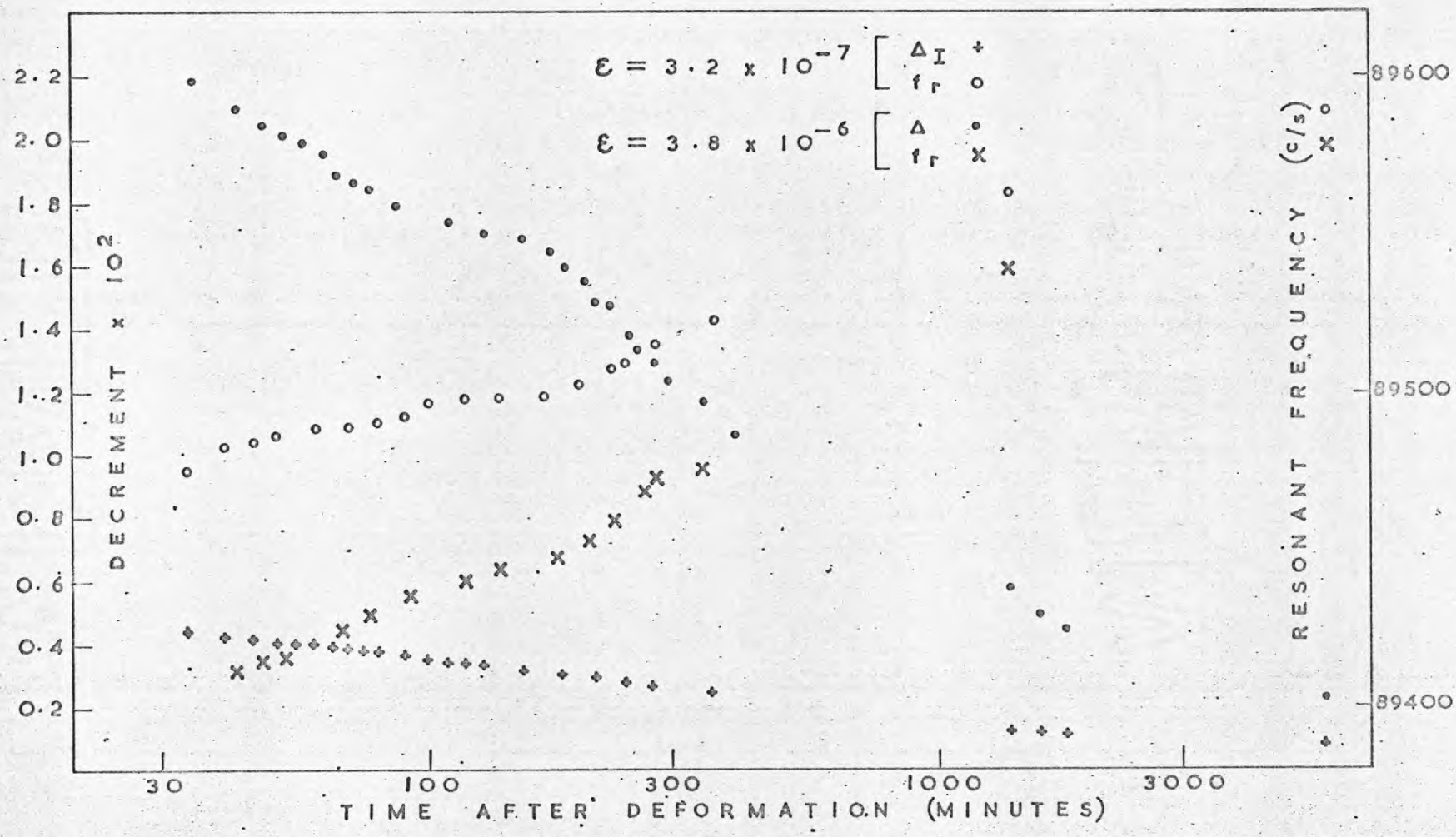

FIG. 4.2. RECOVERY OF DAMPING AND FREQUENCY OF A 2% DEFORMED, ANNEALED, PURE NaCl CRYSTAL AT 24°C.

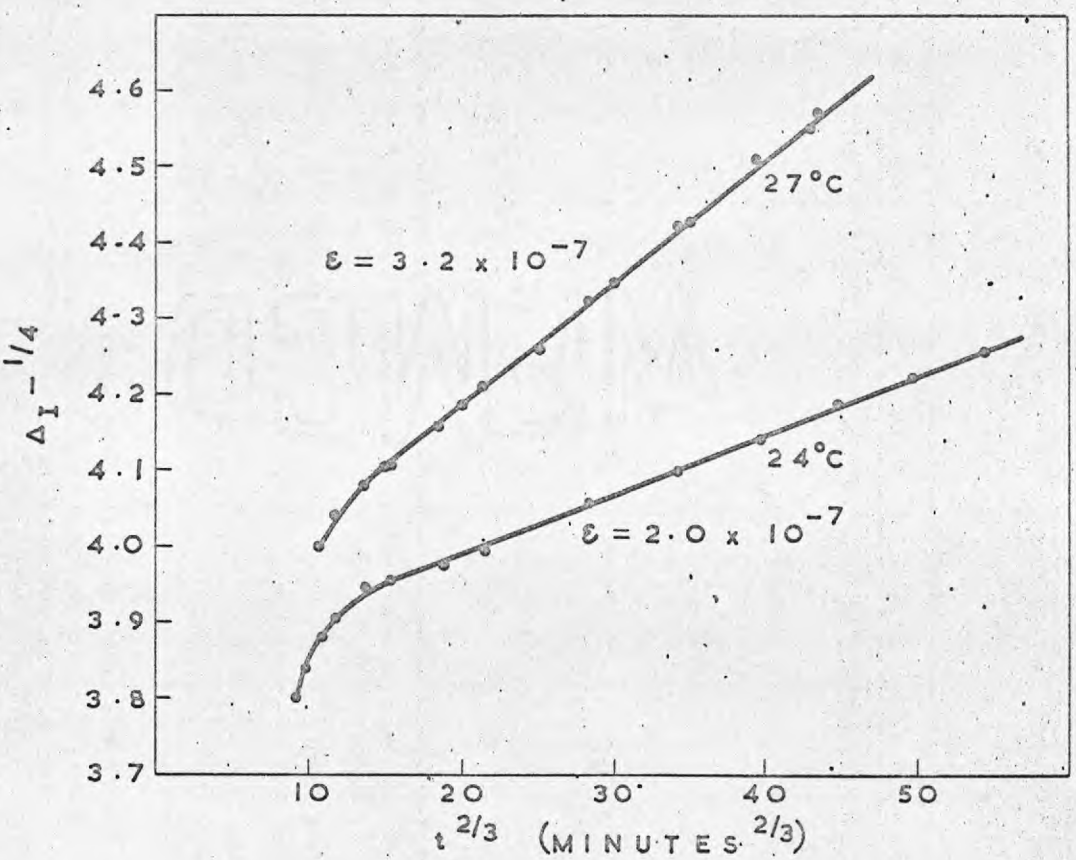

FIG. 4·3. ROOM TEMPERATURE RECOVERY OF AMPLITUDE INDEPENDENT DECREMENT. BOTH SPECIMENS 2% DEFORMED, ANNEALED, PURE CRYSTALS.

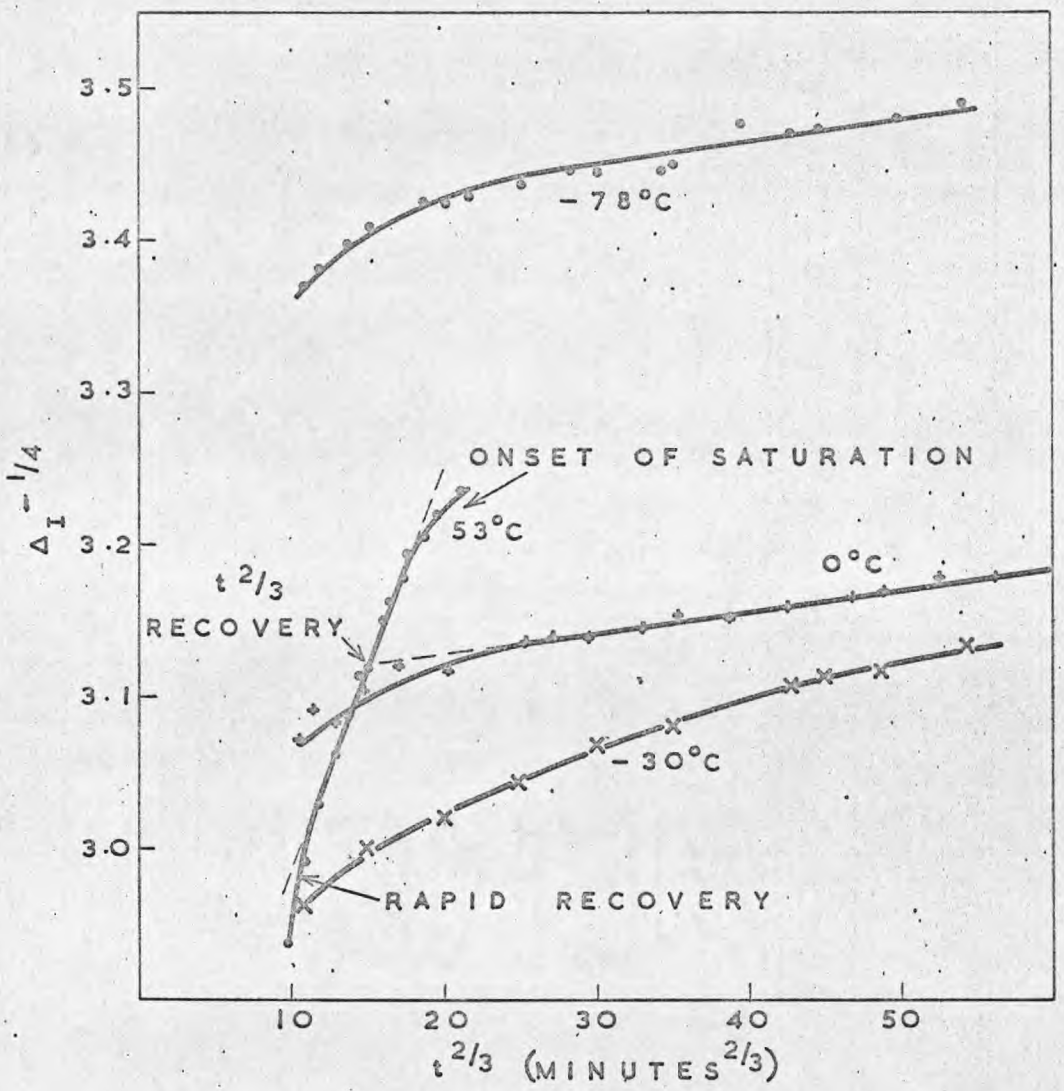

FIG. 4·4. RECOVERY OF AMPLITUDE INDEPENDENT DECREMENT AT DIFFERENT TEMPERATURES. ONLY THE 53°C DATA SHOWS ALL THREE RECOVERY STAGES. THE -30°C DATA SHOW FASTER RECOVERY THAN 0°C DATA BECAUSE THE FORMER IS COMPLETELY IN THE RAPID RECOVERY STAGE WHILE THE LATTER IS PARTIALLY IN THE SLOWER $t^{2/3}$ STAGE.

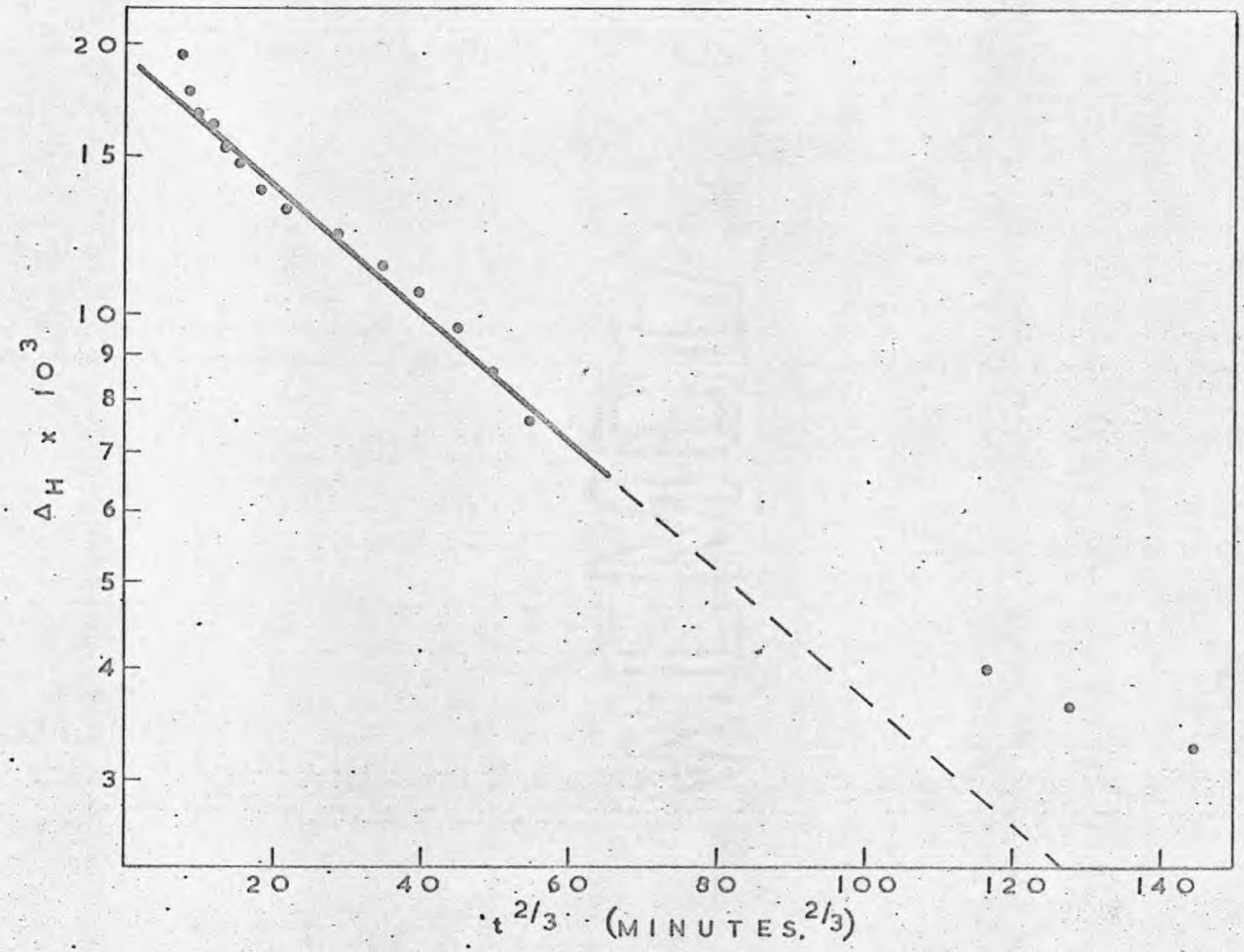

FIG. 4.5. ROOM TEMPERATURE RECOVERY OF Δ_H OF A 2% DEFORMED, ANNEALED, PURE NaCl CRYSTAL.
VIBRATION AMPLITUDE $\varepsilon = 4.0 \times 10^{-6}$

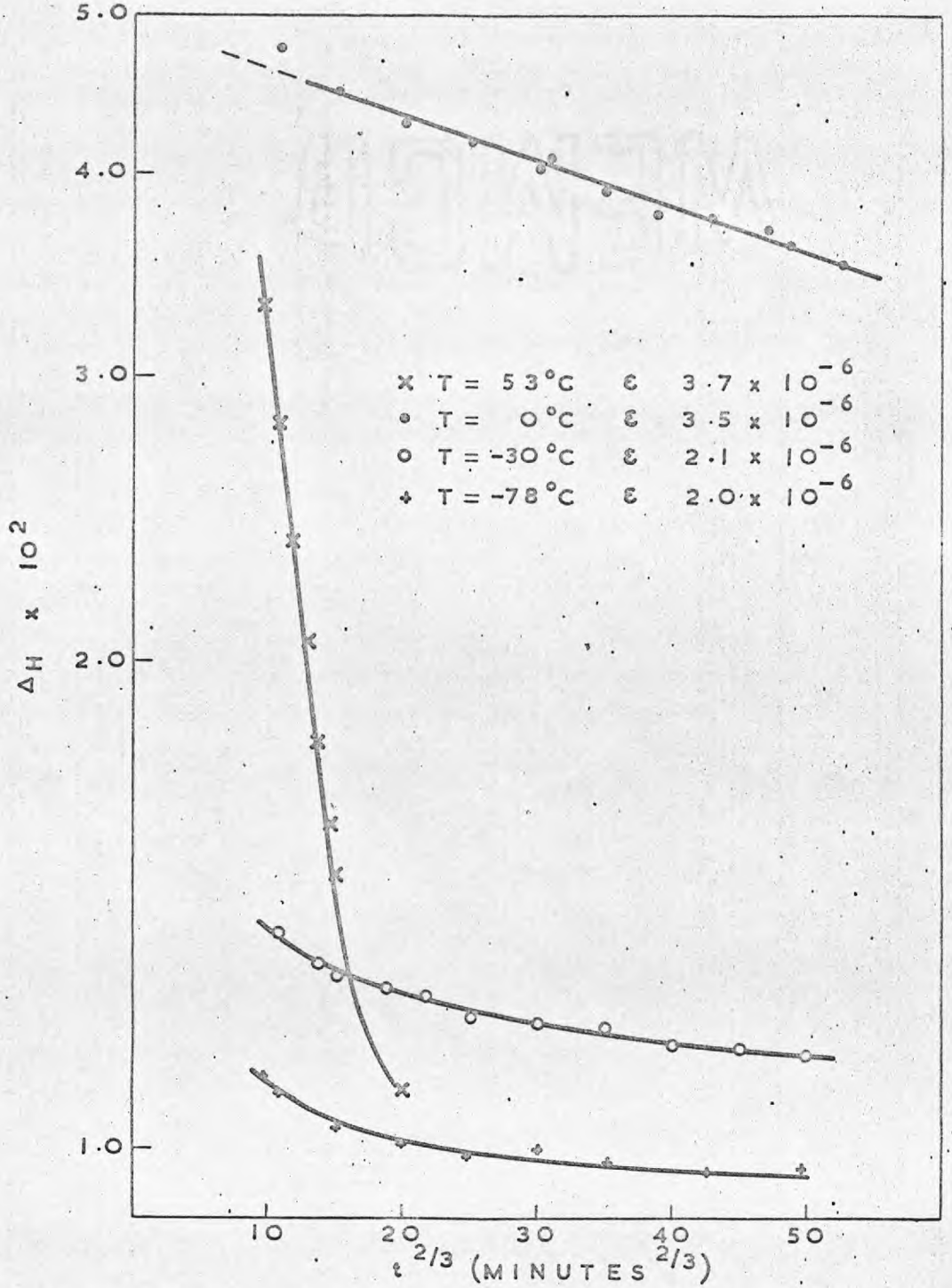

FIG. 4.6. RECOVERY OF Δ_H OF 2% DEFORMED, ANNEALED, PURE NaCl CRYSTALS BETWEEN -78°C. AND 53°C.

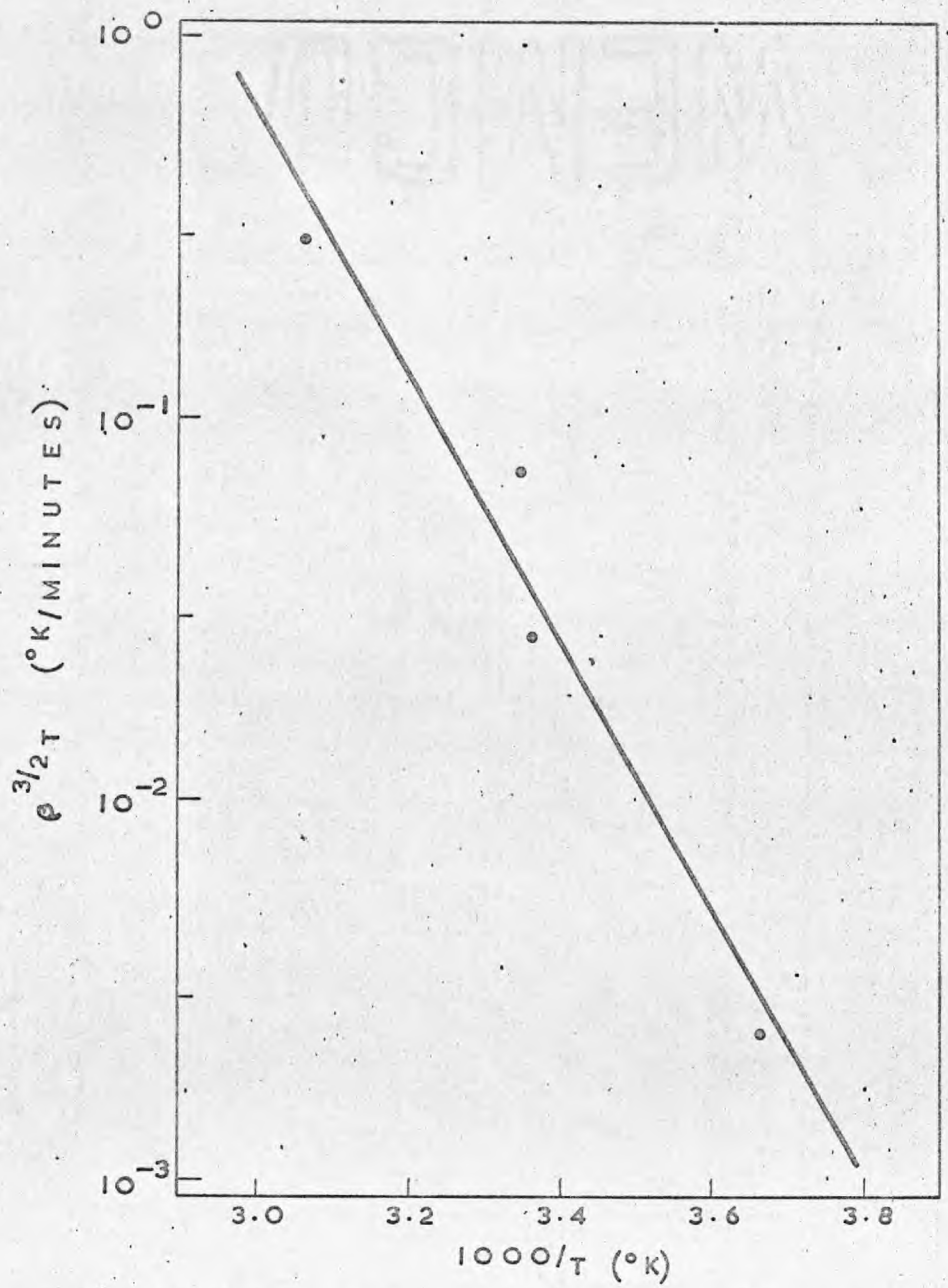

FIG. 4.7. AMPLITUDE INDEPENDENT RECOVERY PARAMETER OF 2% DEFORMED, ANNEALED, PURE CRYSTALS PLOTTED WITH TEMPERATURE

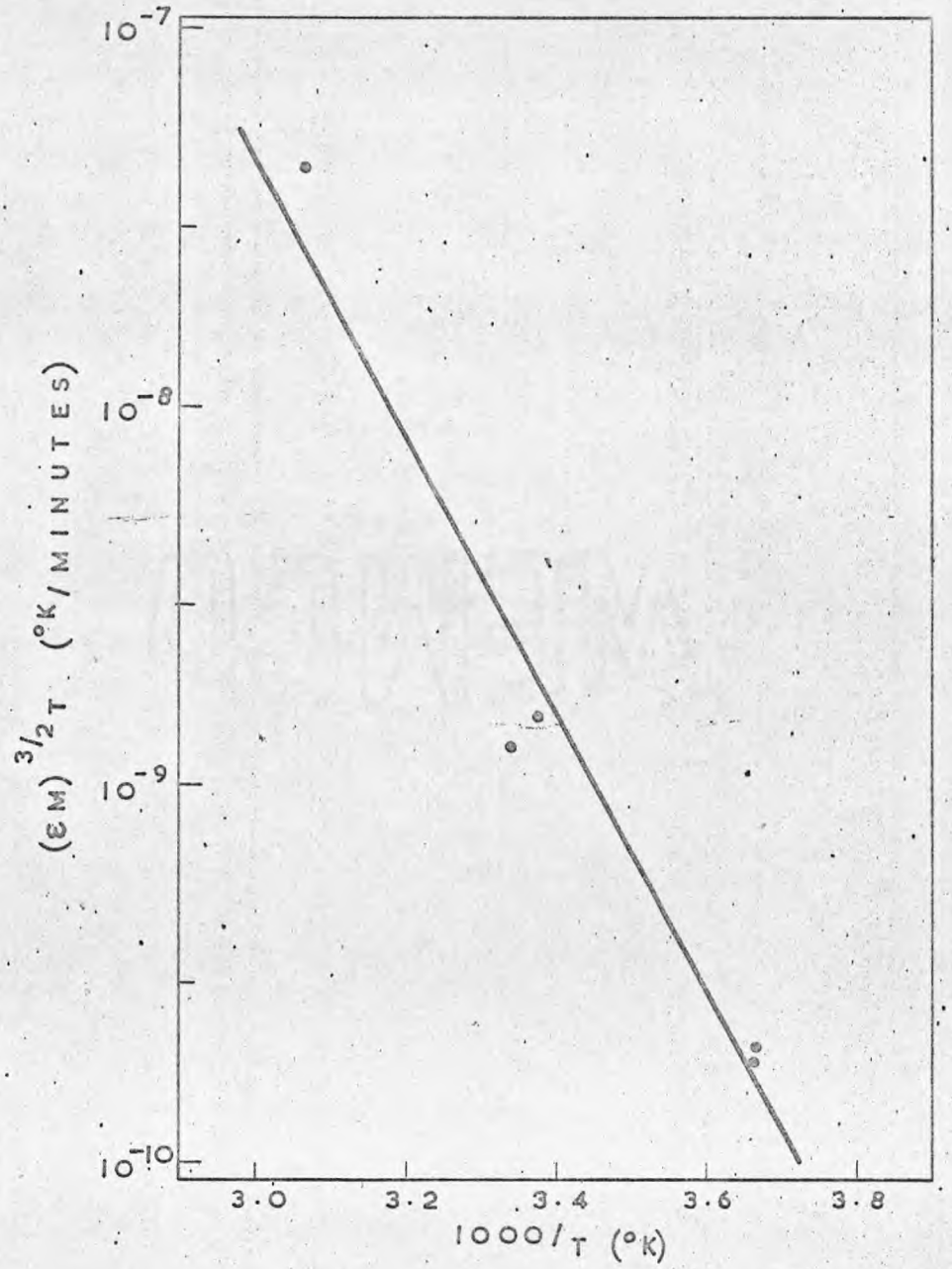

FIG. 4·8. AMPLITUDE DEPENDENT RECOVERY PARAMETER OF 2% DEFORMED, ANNEALED, PURE CRYSTALS PLOTTED WITH TEMPERATURE.

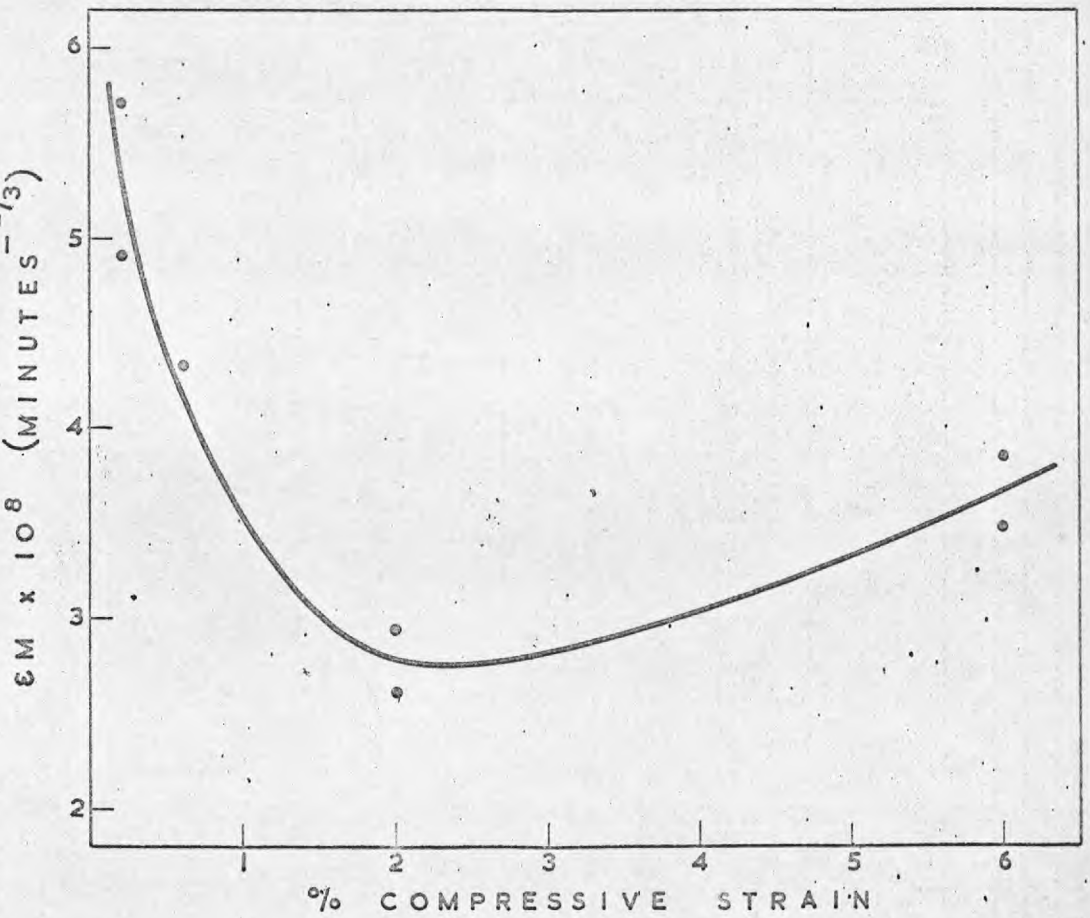

FIG. 4·9. VARIATION OF THE RECOVERY PARAMETER εM OF ANNEALED, PURE CRYSTALS WITH PRESTRAIN.

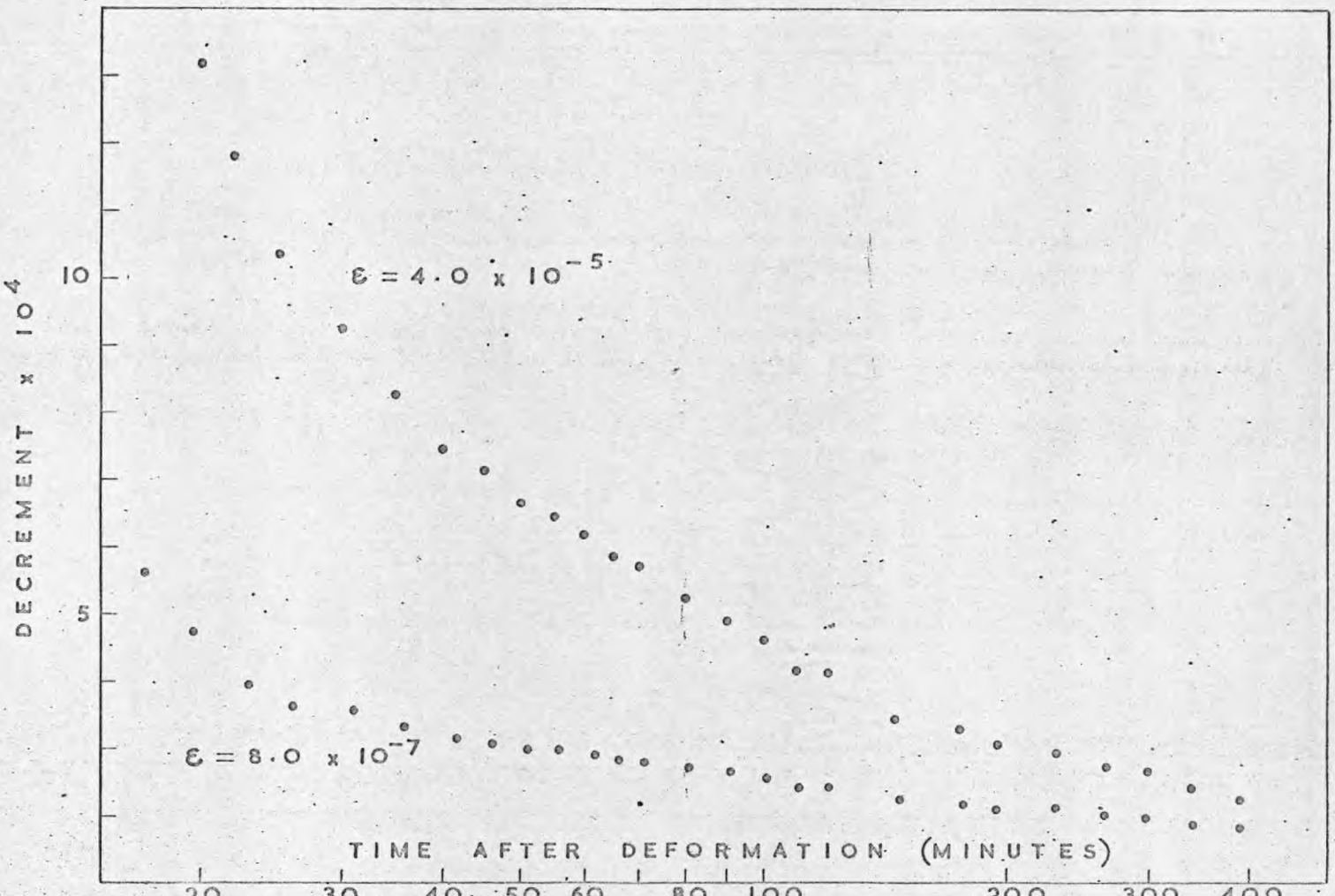

FIG. 4.10. RECOVERY OF DAMPING OF A 2% DEFORMED ANNEALED SPECIMEN CONTAINING 69 m.p.m. Cd

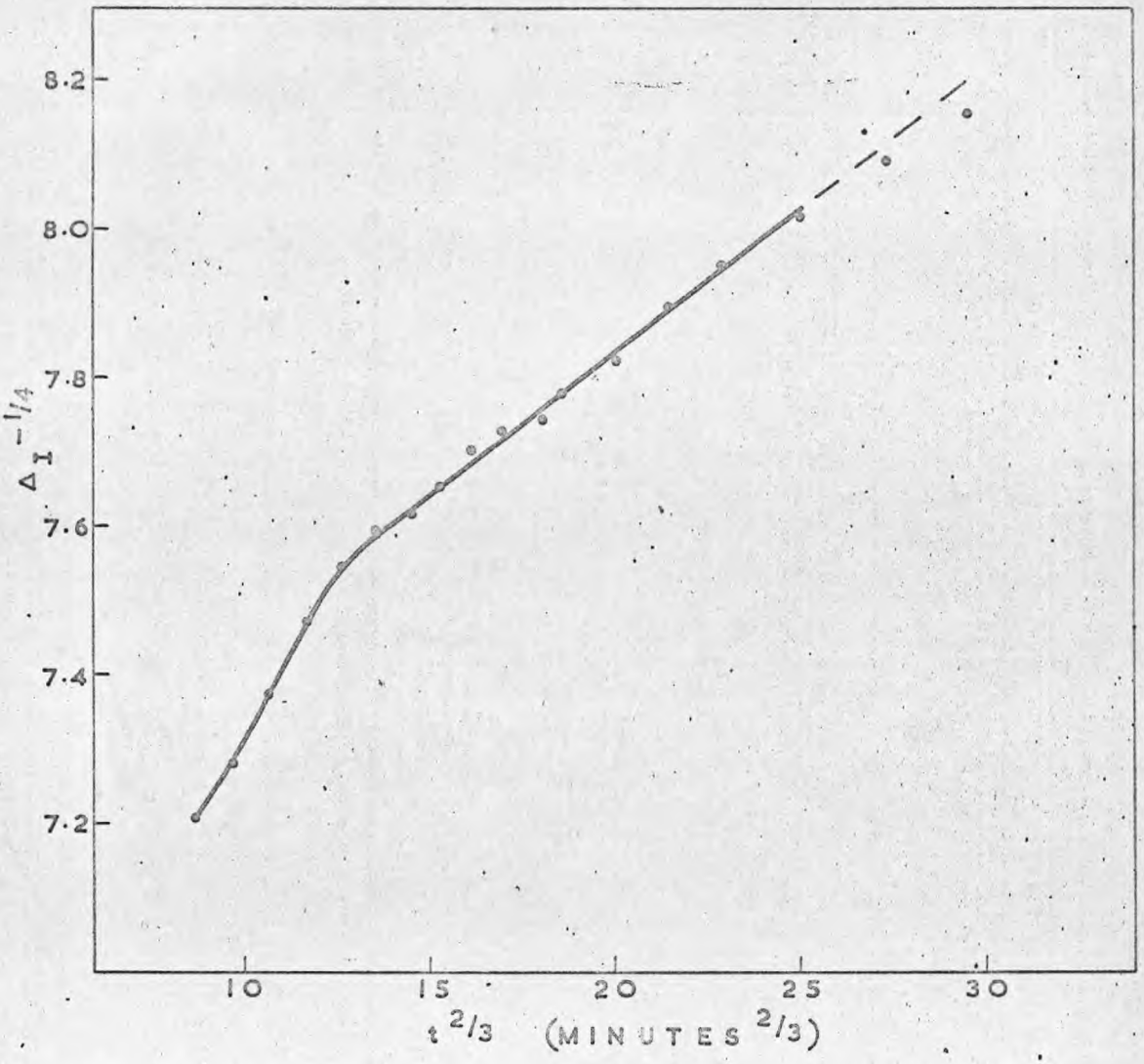

FIG. 4·11. ROOM TEMPERATURE RECOVERY OF AMPLITUDE INDEPENDENT DECREMENT OF 2% DEFORMED, ANNEALED CRYSTAL CONTAINING 69 m.p.m. Cd..

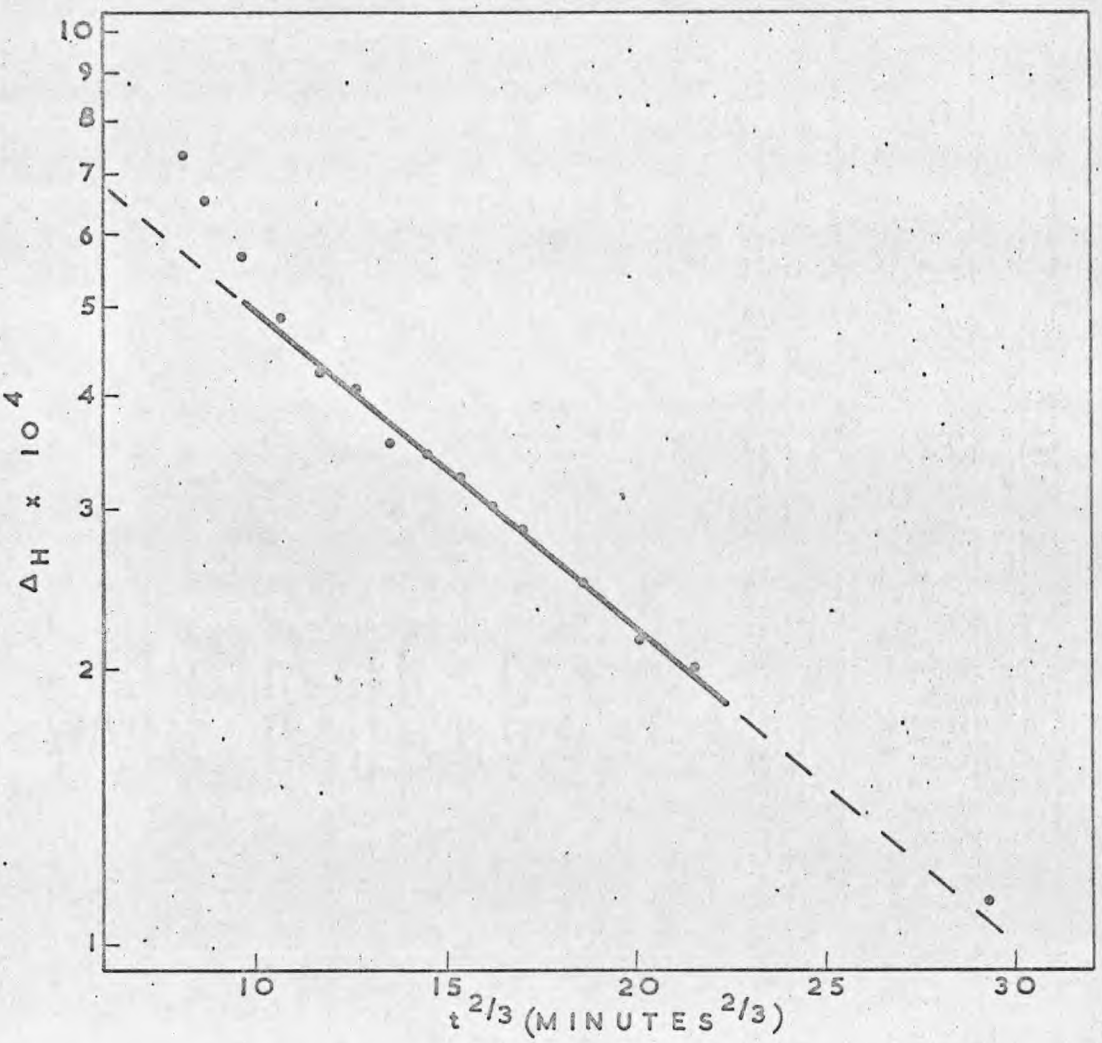

FIG. 4·12. ROOM TEMPERATURE RECOVERY OF A 2% DEFORMED, ANNEALED CRYSTAL CONTAINING 69 m.p.m. Cd. $\varepsilon = 4 \cdot 0 \times 10^{-5}$.

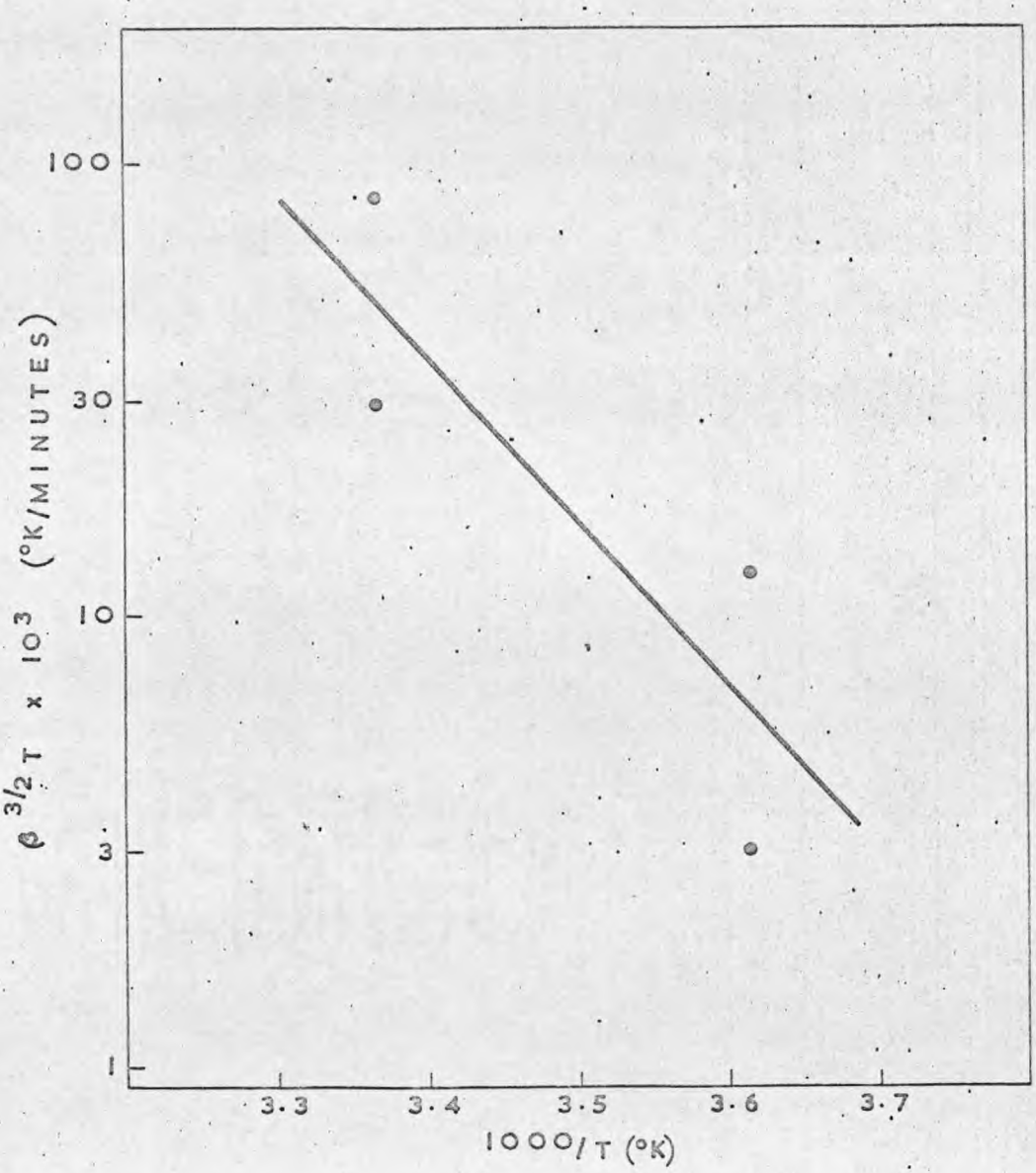

FIG. 4·13. AMPLITUDE INDEPENDENT RECOVERY PARAMETER OF 2% DEFORMED, ANNEALED CRYSTALS DOPED WITH 5·6 ±14 m.p.m. Cd, PLOTTED WITH TEMPERATURE.

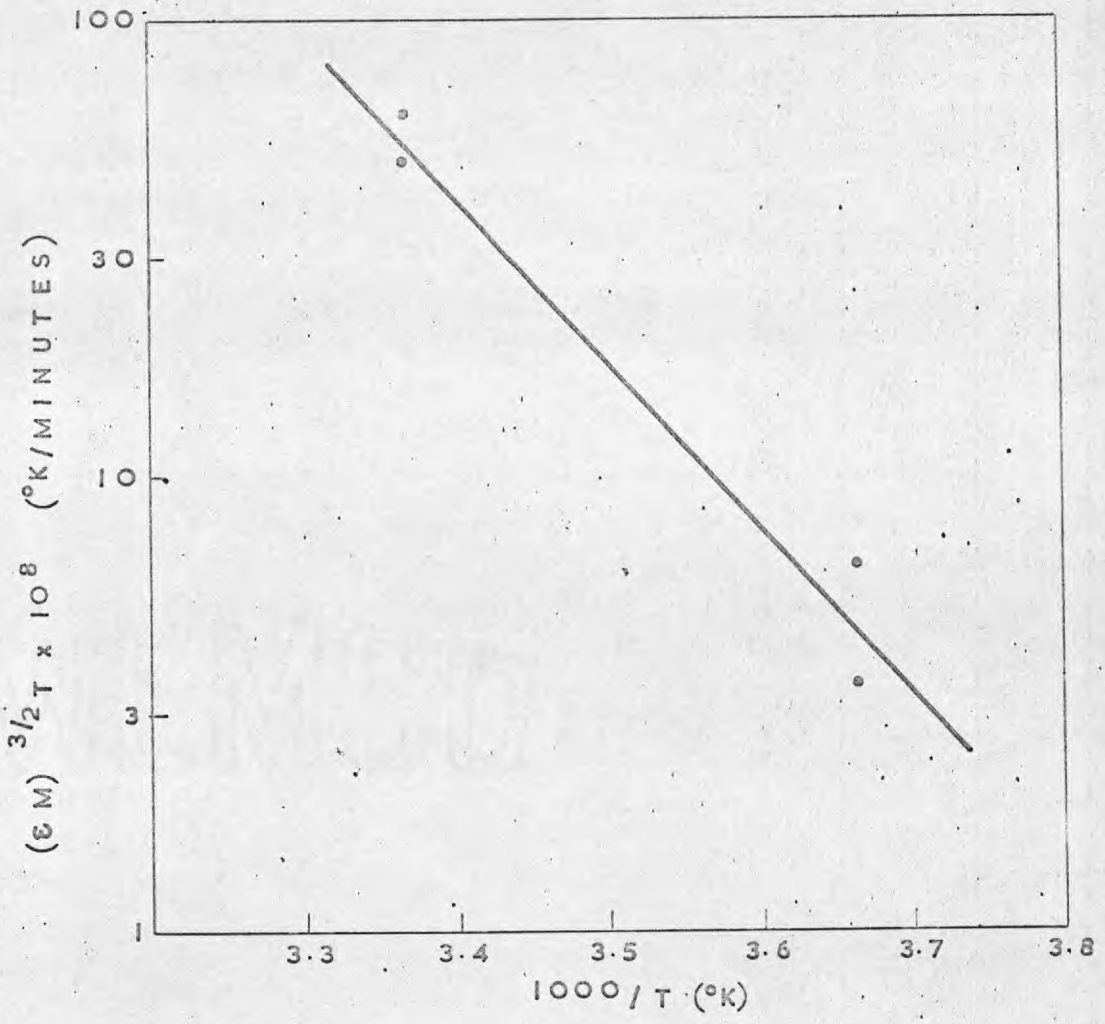

FIG. 4.14. AMPLITUDE DEPENDENT RECOVERY PARAMETER OF 2% DEFORMED, ANNEALED CRYSTALS DOPED WITH 56 ± 14 m.p.m. Cd, PLOTTED WITH TEMPERATURE.

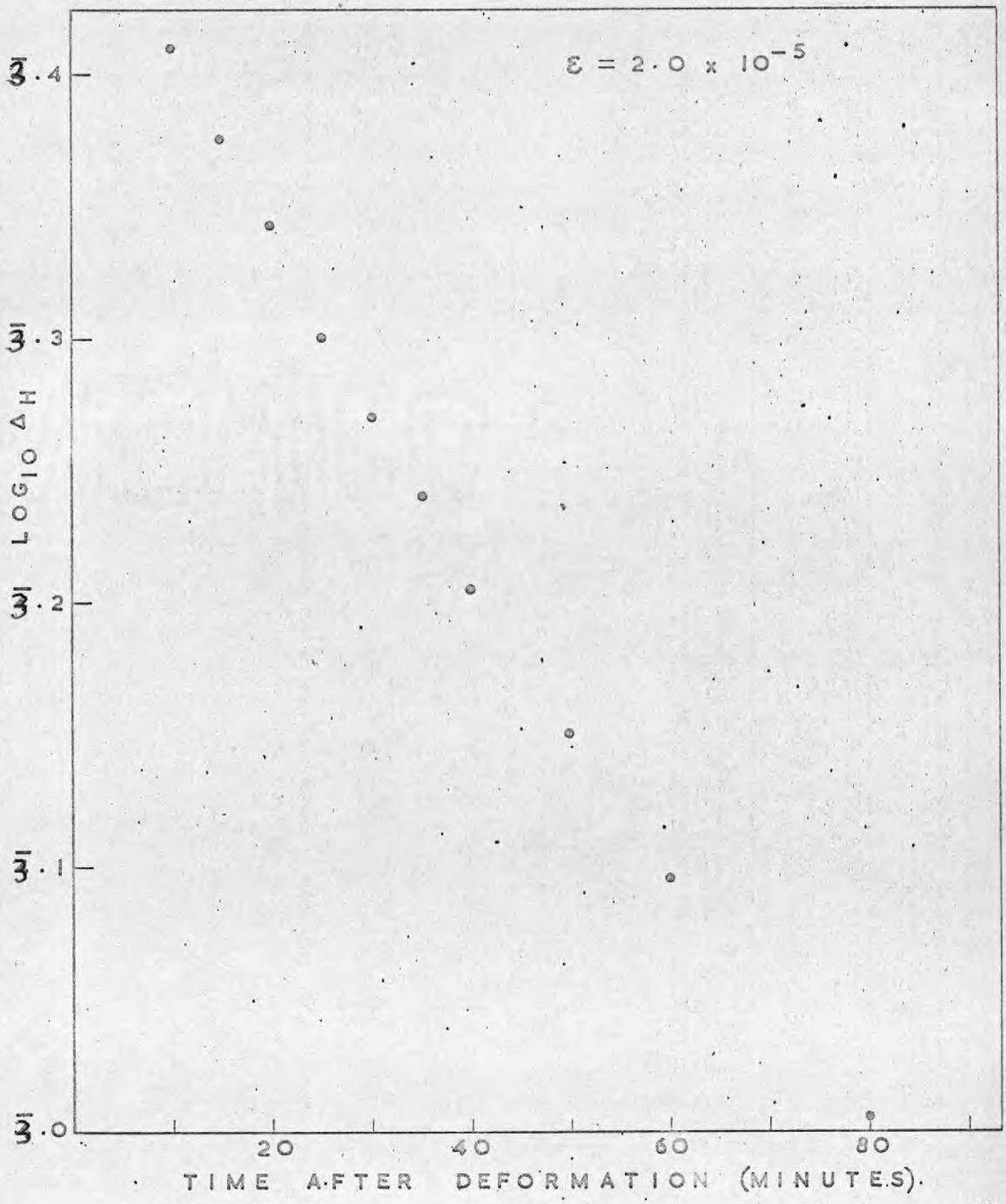

FIG. 4·15. RECOVERY OF ΔH OF AN UNANNEALED CRYSTAL CONTAINING 125 m.p.m. OF Cd.

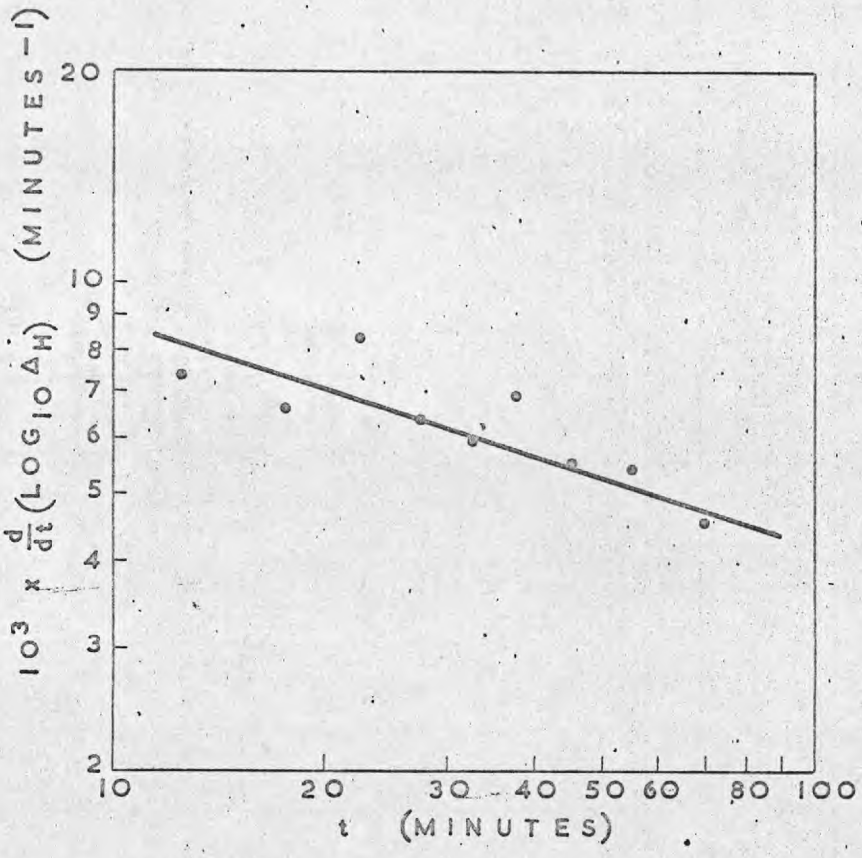

FIG. 4.16. DETERMINATION OF TIME EXPONENT

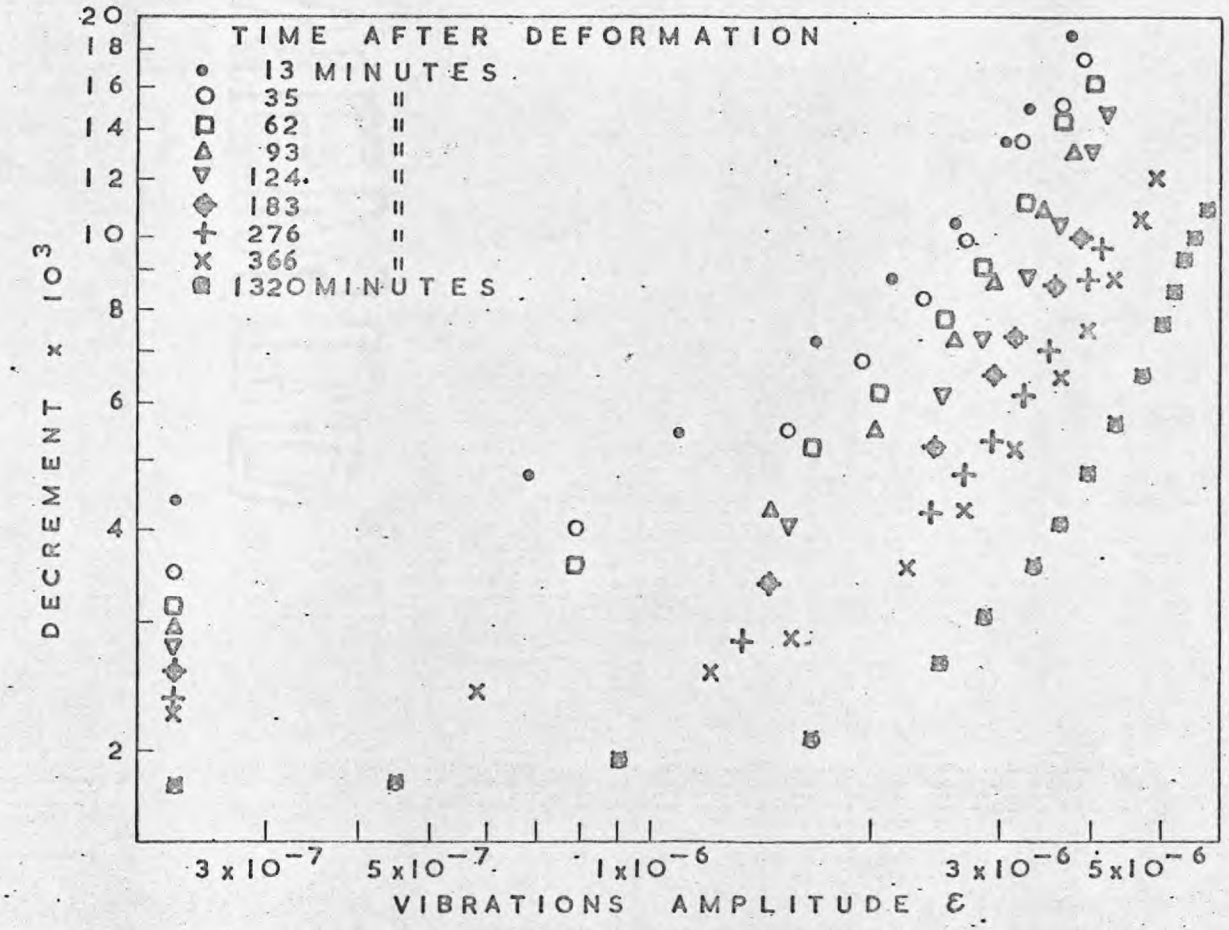

FIG. 4.17. RECOVERY OF A 2% DEFORMED, ANNEALED, PURE CRYSTAL AS A FUNCTION OF AMPLITUDE AND TIME

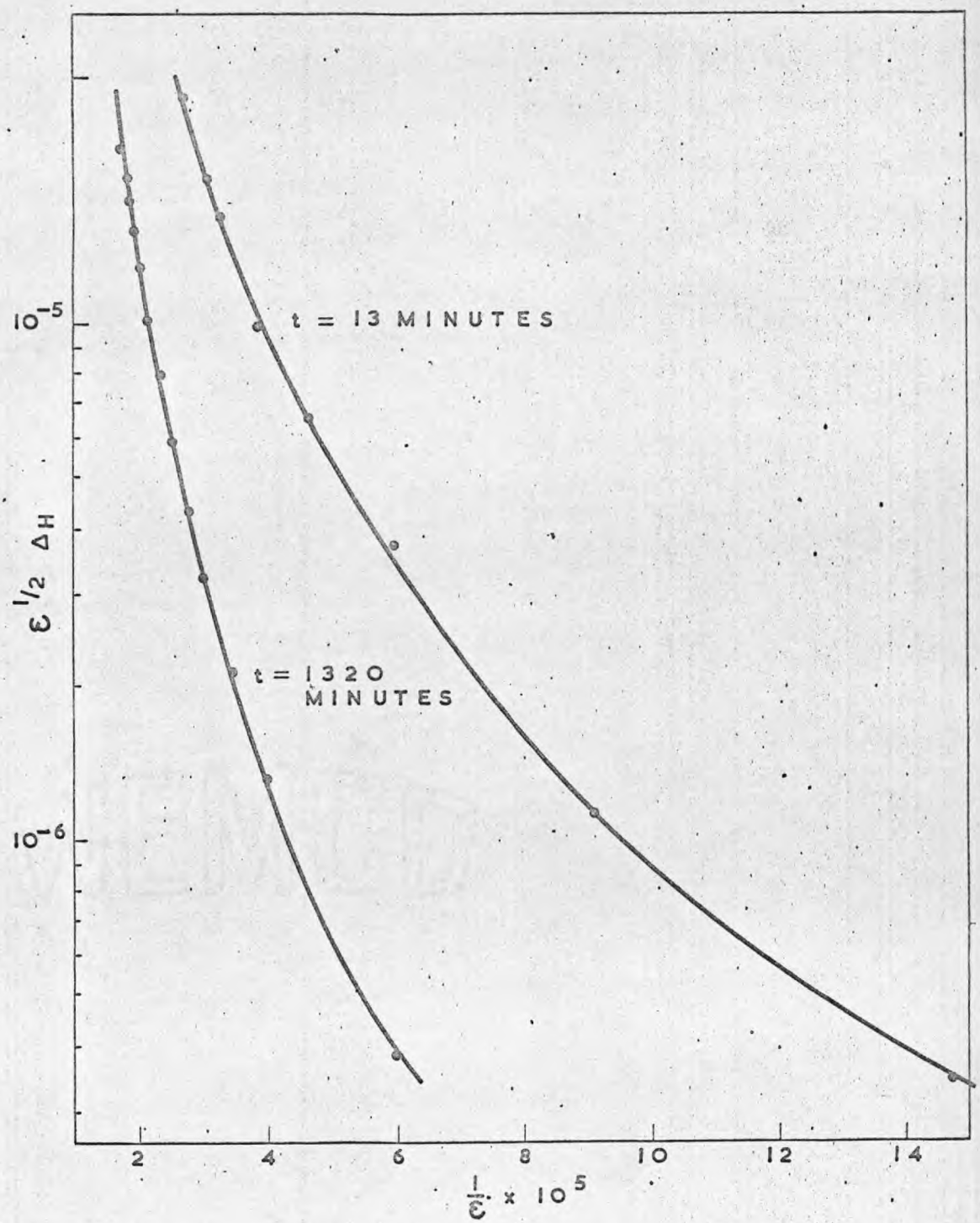

FIG. 4·18. G-L PLOTS OBTAINED FROM DATA IN FIG. 4·17.

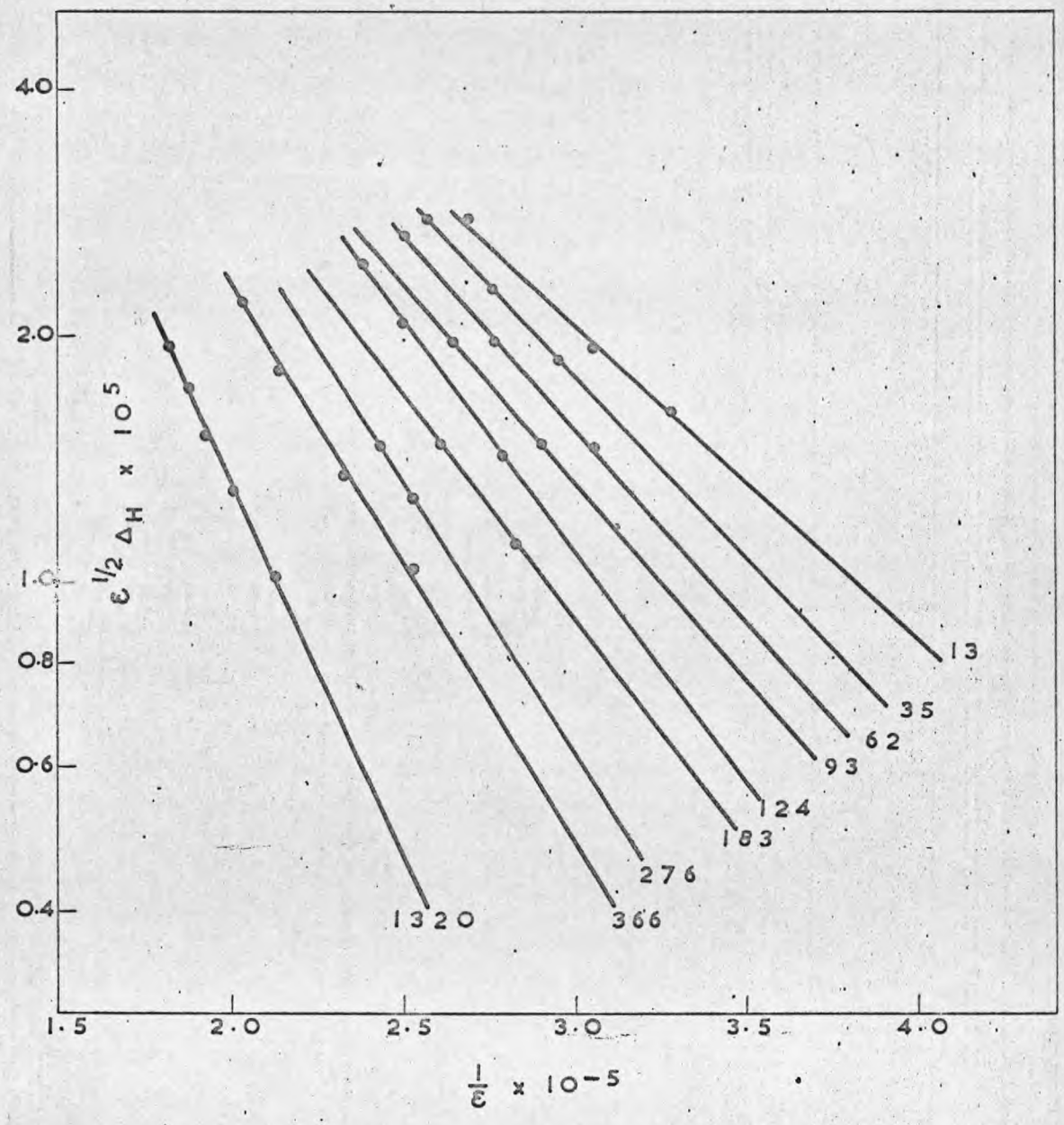

FIG. 4·19. G-L PLOTS OF HIGH AMPLITUDE DATA OF FIG. 4·17. (NUMBERS REFER TO TIME IN MINUTES)

Chapter 5

The binding energy of weak pinning defects and dislocations

5.1 Introduction

The preceding chapter has shown that the Granato - Lucke theory agrees well with the recovery of damping in Na Cl, and in particular that the negative slopes of the G-L plots of a specimen increase with ageing time as predicted. This suggests a method for measuring the binding energy between the weak pinners and dislocations. According to the theory Δ_H is related to the mean length L_c between weak pinners by

$$\Delta_H = \left(\frac{2}{\pi A_2}\right)^{\frac{1}{2}} \frac{A_1}{\varepsilon^{\frac{1}{2}} L_c^{3/2}} \exp\left(\frac{-A_2}{\varepsilon L_c}\right) \qquad 1.22$$

for a cosine strain amplitude distribution. Thus the intercept I and slope m of a G-L plot, $\ln \varepsilon^{\frac{1}{2}} \Delta_H$ v. $1/\varepsilon$, are respectively proportional to $\ln L_c^{-3/2}$ and L_c^{-1}. In general the pinning length L_c will vary with temperature because the equilibrium concentration of weak pinners which interact with the dislocation varies with temperature. If E_B is the positive interaction energy between a pinner and a dislocation then the concentration will vary as $\exp(E_B/kT)$ [52] and the pinning length will vary as

$$L_c = L_{c,o} \exp(-E_B/kT) \qquad 1.29$$

Hence

$$I = \text{Constant} + \frac{3}{2} \frac{E_B}{kT}$$

and

$$m = \text{Constant} \times \exp(E_B/kT)$$

so that a plot of I v. 1/T should have slope $\frac{3}{2} \frac{E_B}{k}$ and ln m v. 1/T should have slope $\frac{E_B}{k}$, and thus by measuring the amplitude dependence

of damping at different temperatures it should be possible to obtain E_B. It is however important that the equilibrium state between the pinners and the dislocations shall have been attained at the temperature of the test.

5.2 Experimental

Fig. 5.1 shows a set of G-L plots obtained from specimens which had been aged at temperatures between 24°C and 95°C. Each specimen was pure and annealed, and was deformed 2 % at room temperature before being mounted on the composite oscillator and heated to the testing temperature at which it was maintained for several days. It is difficult in practice to decide when an equilibrium state has been achieved between point defects and dislocations and a somewhat arbitrary criterion was used to establish this. The damping of each specimen was measured at the same two amplitudes in the amplitude independent and dependent regions every day until no discernible change occurred in the damping between successive measurements at least a day apart. It was then assumed that the pinning defects and dislocations had arrived at an equilibrium state. Damping was measured at that temperature as a function of amplitude up to the highest amplitudes at which vibration induced changes did not occur. As the test temperature was increased, the amplitude dependent region before vibration induced changes occurred decreased, and at temperatures above 100°C it was not possible to make accurate measurements of $\triangle_H$. Figs. 5.2 and 5.3 show $\log m$ v. $\frac{1}{T}$ and I v. $\frac{1}{T}$ and the best straight lines fitted to this data by a least squares method. The slopes of these lines yield values, which in terms of the above theory, are

(slopes of G-L plots) $E_B = -0.36$ eV. $\pm$ 0.08 eV.

(intercepts of G-L plots) $\frac{3}{2} E_B = -1.43$ eV $\pm$ 0.36 eV

5.3 Discussion

The values of binding energy obtained from this experiment by employing the theory outlined above immediately pose two problems. Firstly the value obtained from the slopes of the G-L plots does not agree with that obtained from the intercepts, and secondly the values are negative instead of positive which implies a repulsion between the dislocations and the pinners.

Equation 1.22 is equation 1.15 of the G-L theory modified by Granato and Lucke for a standing wave strain amplitude distribution by integrating equation 1.15 over the length of the inhomogeneously strained specimen. The effect of integration is to leave the exponential term unaltered but to alter the pre-exponential term from its dependence on $\varepsilon^{-1} L_c^{-2}$ to $\varepsilon^{-\frac{1}{2}} L_c^{-3/2}$. This alters the G-L plot from $\ln \varepsilon \Delta_H$ v. $1/\varepsilon$ to $\ln \varepsilon^{\frac{1}{2}} \Delta_H$ v. $1/\varepsilon$ and although this affects the intercept of the plot, Granato and Lucke[30] and Niblett and Wilks[19] have pointed out that it has negligible effect on the value of the derived slopes. Thus the two different assumptions about strain amplitude distribution in a specimen produce different intercepts of the G-L plots and a different dependence of the intercepts on L_c, while the slopes of the G-L plots are very much less affected and have the same dependence on L_c in both cases. It is generally assumed that the strain amplitude distribution in a specimen at resonance is described well by a simple one dimensional longitudinal

standing wave and equation 1.22 is then employed in the analysis of experimental data. Granato and Lucke[30] have warned that it is not clear how accurate this assumption is and cite analyses which indicate that the real stress distribution may be more complex. In the absence of detailed knowledge of the correct stress distribution in a specimen under the experimental conditions, the intercept data should be treated with more caution than the slope data. For this reason it is considered that the better value of E_B is

$$E_B = -0.36 \text{ eV} \pm 0.08 \text{ eV}.$$

It is however a matter for speculation whether the reasoning outlined above can altogether account for the differences in E_B obtained from the two sets of data, or whether there is a more fundamental error in the theory.

A similar experiment to that described here has been carried out by Strumane et al who also analysed their data in terms of the G-L theory. They too obtained an apparently negative binding energy but their values are an order of magnitude down on that obtained in this experiment and are -0.045 ± 0.005 eV and -0.037 ± 0.006 eV. Their experiment was not exactly the same as this one and the main differences are that they measured internal friction off specimens vibrating in a flexural mode as opposed to a longitudinal mode, and that specimens were deformed by bending to introduce an excess of edge dislocations of one sign. They do not describe the heat treatment applied to their specimens nor do they mention how long each specimen was maintained at a particular temperature before being tested, so that it is not

possible to compare how closely the specimens had attained an equilibrium state. Their lowest temperature of measurement was $-64^{\circ}C$ and the previous recovery measurements have shown that the kinetics of recovery are so slow at that temperature that a specimen must be aged for a considerable time before mobile defects stop migrating to the dislocations and an equilibrium state is attained. If sufficient ageing time is not allowed to elapse and equilibrium states are not achieved then a value of binding energy which is too low will be obtained. It is possible that this is the explanation of the discrepancy between the present value and that of Strumane et al.

The apparent negative value of the binding energy can be explained by assuming that the bulk concentration of weak pinners is temperature dependent. If the bulk concentration varies as $\exp.\left(-\frac{E_f}{kT}\right)$ where E_f is the energy of formation of the pinner, then the equilibrium concentration on the dislocation will vary as $\exp.\left(\frac{E_B - E_f}{kT}\right)$ and the pinning length will vary as $\exp.\left(\frac{E_f - E_B}{kT}\right)$ instead of $\exp.\left(\frac{-E_B}{kT}\right)$. On this reasoning

$$E_B - E_f = -0.36 \text{ eV.}$$

and the binding energy between pinner and dislocation is

$$E_B = E_f \ -0.36 \text{ eV.}$$

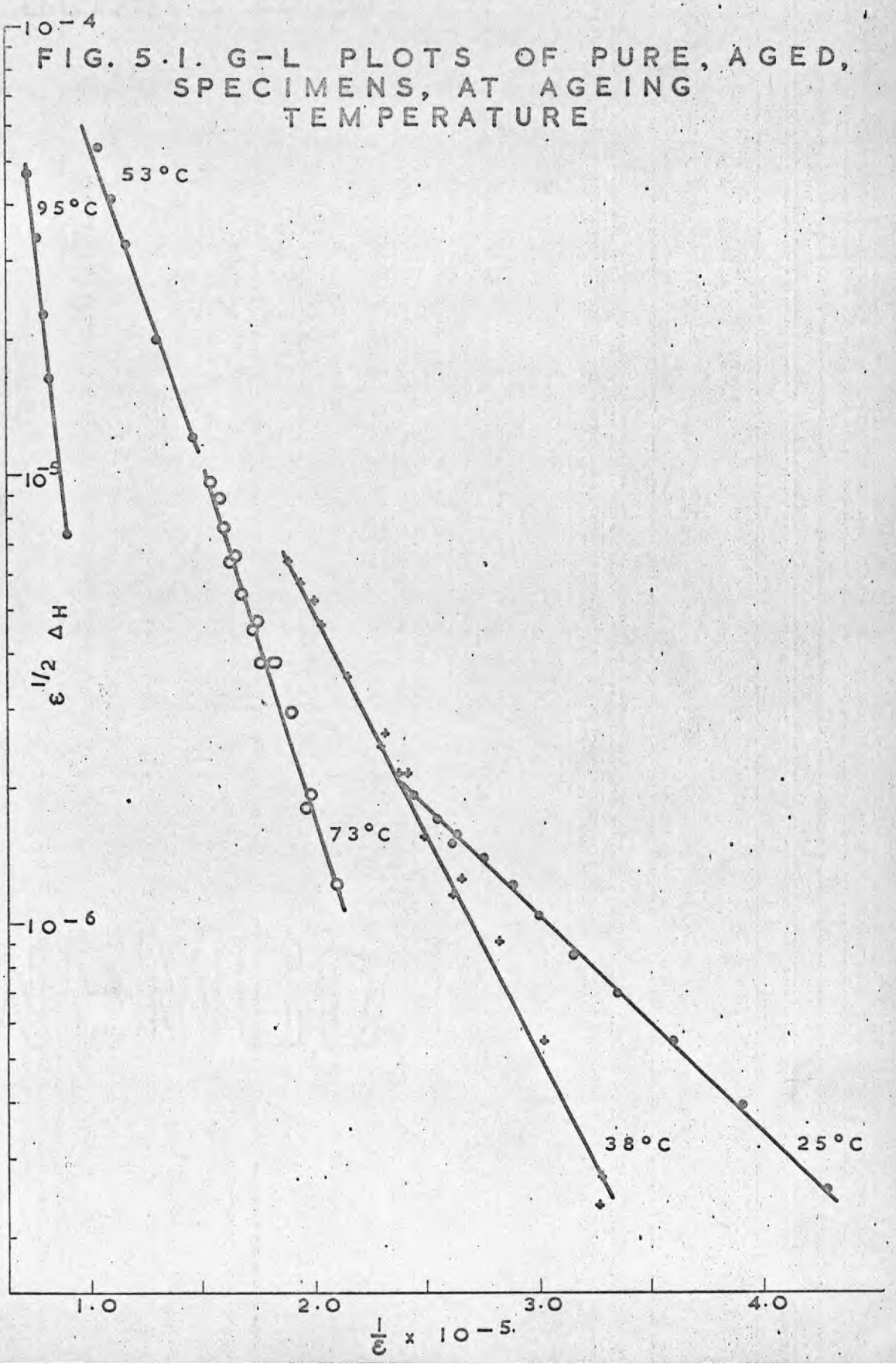

FIG. 5·1. G-L PLOTS OF PURE, AGED, SPECIMENS, AT AGEING TEMPERATURE

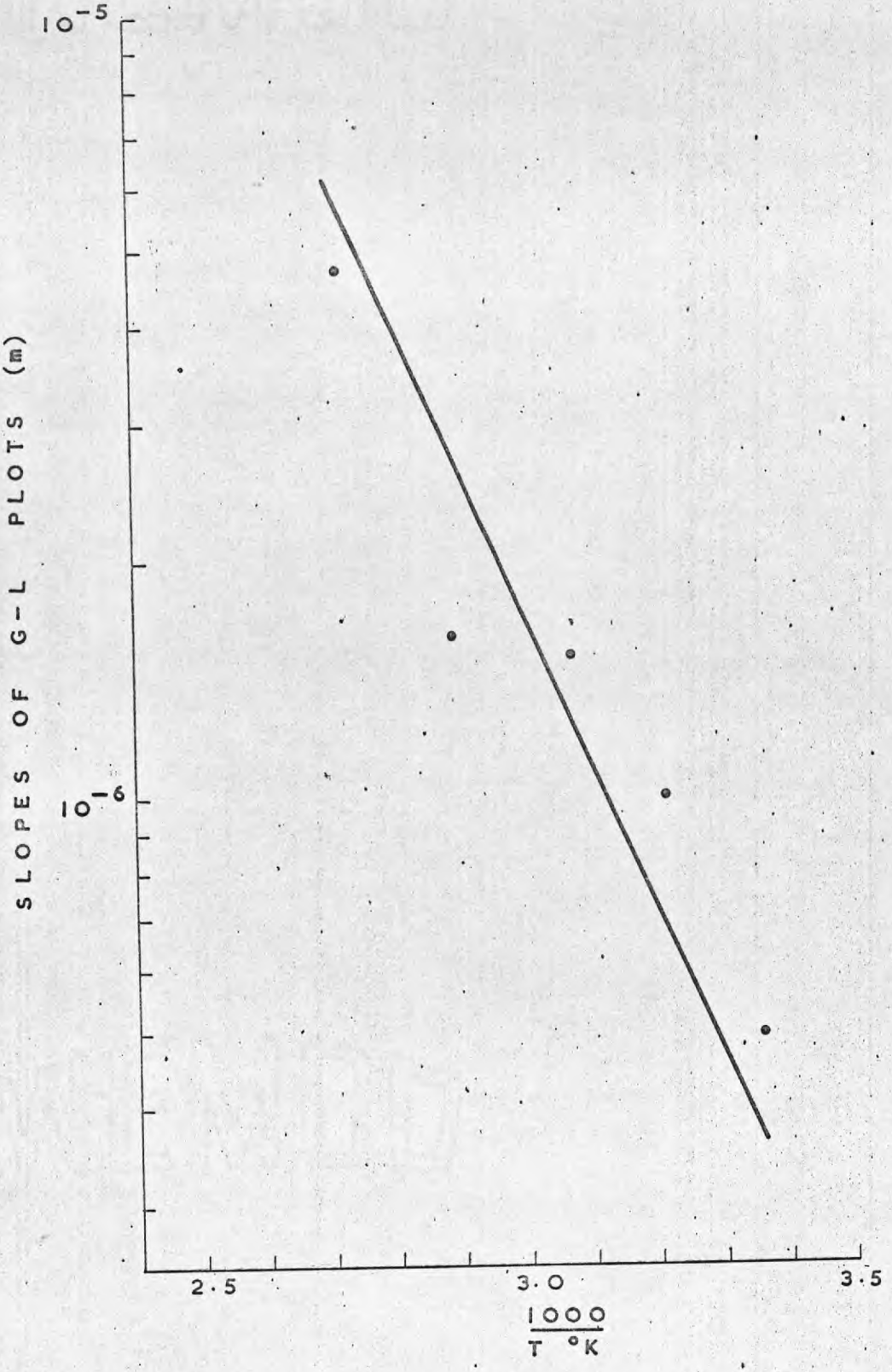

FIG. 5.2. LOG m v. $\frac{1}{T}$

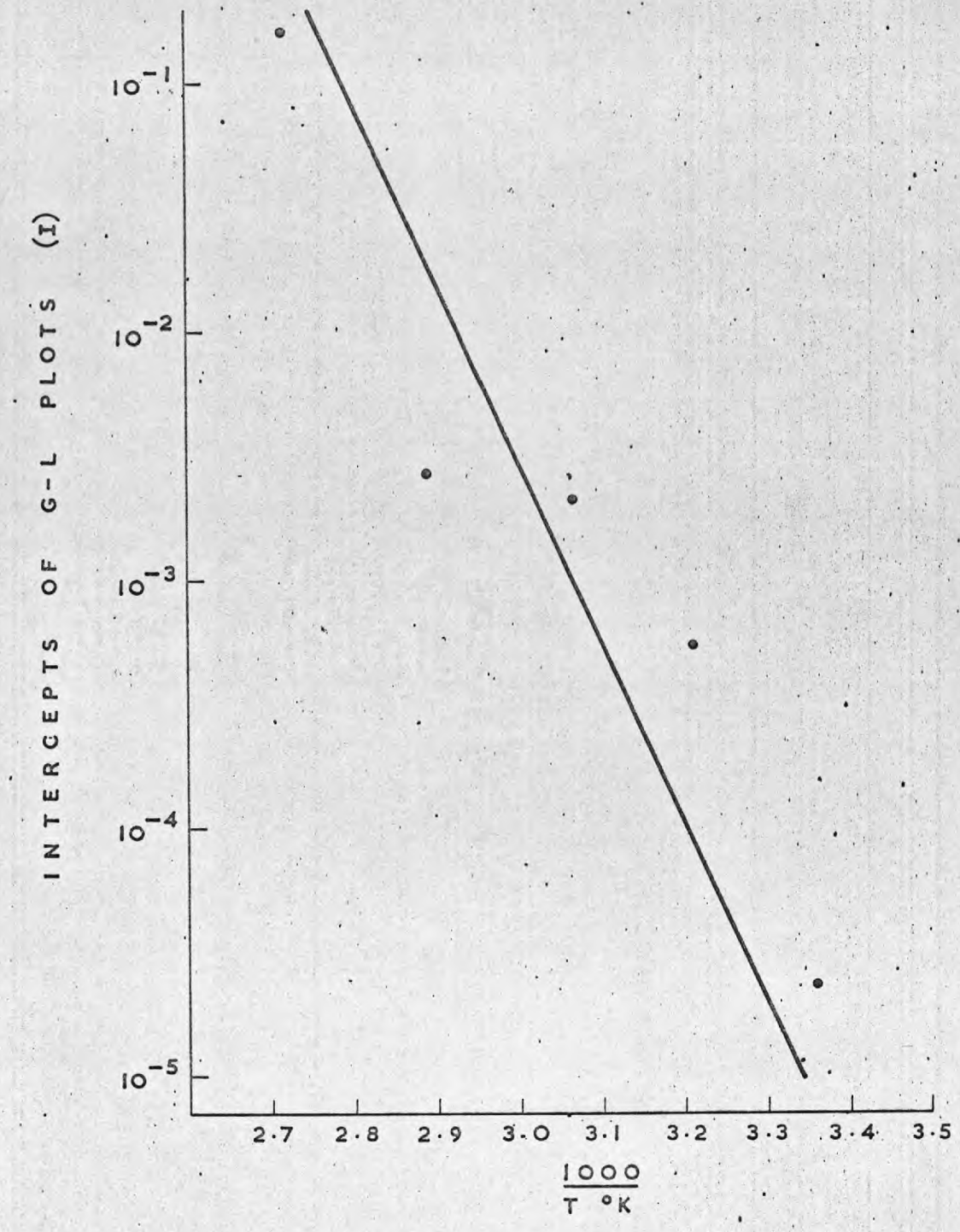

FIG. 5·3. I v. $\frac{1}{T}$

Chapter 6

The identity of the mobile pinning species

6.1 Introduction

The GHL theory predicts that the recovery parameter ξ M is proportional to the bulk concentration c_{10} of mobile pinners (equation 4.1) and this suggests a method of identifying the mobile pinner. It was shown in chapter 4 that ξ M varies widely with impurity content and thermal history of specimens which are at the same temperature and have undergone the same strain. Because of the large increase in ξ M on the addition of divalent Cd^{++} it was deduced that the mobile pinner is the divalent cation, the cation vacancy, the divalent cation - cation vacancy pair, or some higher aggregate. The higher aggregate is unlikely to be able to compete in mobility with the other three so shall be ignored. In chapter 1 it was shown that the electrical conductivity σ_c of Na Cl at room temperature is proportional to the concentration of free cation vacancies and, because the concentration of free cation vacancies equals the concentration of divalent cations at this temperature, thus to the concentration of free divalent cations. Further, the maximum in the dielectric loss peak, obtained by plotting tan δ v. frequency, is proportional to the concentration of divalent cations and cation vacancies associated on near lattice sites. Hence if ξ M is measured for a series of specimens with varying impurity content and thermal history it should be possible to correlate these values with the conductivities or dielectric loss maxima of similar specimens. If the vacancy or the metal ion is the pinner then there will be a correspondence between the values of ξ M and conductivity. If the dipole is the pinner there will be a correspondence between the values of ξ M and the maxima of the dielectric loss peaks. Accordingly a

series of dielectric loss and D.C. conductivity measurements have been made on similar specimens to those whose ξ M values are given in tables 4.1 and 4.2.

6.2 Dielectric loss measurements

The experimental details of these measurements have been described in section 2.3 (c). Fig. 6.1 shows the dielectric loss peak of a specimen containing about 60 m.p.m. of Cd^{++}, obtained 3 hours after quenching from 350°C to room temperature and measured at 36.5°C. Unfortunately it was not advisable to measure the peak at room temperature because it was then centred about a lower frequency and the accuracy of the measurements was greatly decreased. The drawn curve is a fitted Debye curve and the good fit indicates that the peak is due to a single type of defect. No such peak was observed on quenching a pure specimen and on quenching a more heavily Cd^{++} doped specimen a similar but higher peak was observed. On ageing a quenched specimen at 36.5°C the peak initially rapidly decreases in height in a similar manner to that of the dipole peaks observed in Ca^{++} and Mn^{++} doped Na Cl by Quin[17] and Cook and Dryden.[9][15][16] The close proximity, but not exact superposition, of the peaks in the Cd^{++}, Ca^{++} and Mn^{++} doped materials indicates that the peaks are not due to associated pairs of cation vacancies. Hence it is concluded that Fig. 6.1 shows the dielectric loss behaviour due to associated Cd^{++} ions and cation vacancies, but there is insufficient evidence to suggest whether it is a nearest neighbour dipole peak or a next nearest neighbour dipole peak.

Fig. 6.2 shows the dielectric loss peaks of two annealed specimens one of which contained about 55 m.p.m. and the other about 110 m.p.m. of

Cd^{++} The height of the peaks of annealed doped specimens decreased negligibly in a day indicating that the bulk concentration of dipoles decreased only a small amount in this time. However no peak was observed in the specimen containing about 55 m.p.m. of Cd^{++} which had been previously aged at room temperature for a year, which indicates that in this time the dipoles had associated to form higher aggregates. The sensitivity of the apparatus was such that 5 dipoles per million molecules of Na Cl could be detected, and the absence of a peak means that there was less than this amount present.

Table 6.1 shows the measured, maximum tan δ values.

6.3 Conductivity measurements

The experimental details of these measurements have been described in section 2.3 (b). Table 6.2 shows the measured conductivity values(MEASURED AT ROOM TEMPERATURE)

6.4 Discussion

Table 6.3 compares the relative values of ε M, σ_c and $(\tan \delta)_{max}$.

If the free cation vacancy or divalent metal ion is the predominant mobile pinner over the whole range of doping and heat treatment, then $\varepsilon M/\sigma_c$ should be constant. Alternatively if the dipole is the predominant mobile pinner then $\varepsilon M/(\tan\delta)_{max}$ should be constant. No attempt was made to measure the scatter in ε M values of similar specimens under similar conditions, but in those cases when ε M was measured on two similar specimens under similar conditions, the maximum differences from the mean value was about 20 % and usually a lot less, as can be seen in tables 4.1 and 4.2. The uncertainty in ε M in table 6.3 has been taken to be 20 % but this is probably an

overestimate. Similarly the maximum difference in conductivities was about 20 % and this too has been assumed to be the uncertainty in conductivity. Thus the quoted uncertainty of ± 40 % in the $\mathcal{E}M/\sigma_c$ column is almost certainly an overestimate but, even so, the values of $\mathcal{E}M/\sigma_c$ do not agree within these limits but vary by an order of magnitude. The information in the $\mathcal{E}M/(\tan\delta)_{max.}$ column is less explicit than that in the $\mathcal{E}M/\sigma_c$ column because it was only possible to measure $(\tan\delta)_{max.}$ of the annealed and quenched doped specimens, but the two definite values of $\mathcal{E}M/(\tan\delta)_{max}$ agree within experimental error and the other values give lower bounds which do not disagree with them. The evidence thus suggests that the mobile pinner is not the cation vacancy or divalent metal ion but the associated pair.

Brown and Pratt,[50] in their work on strain ageing in Cd^{++} doped Na Cl, concluded that the most plausible model for strain ageing in Cd^{++} doped Na Cl is the migration of divalent ion - vacancy complexes to the dislocations. This work agrees with that conclusion. Fleischer[53] has considered the interaction between screw dislocations and point defects of tetragonal symmetry and has shown that for certain relative orientations of dislocation and defect, the interaction energy has a spatial dependence $E_B \propto 1/d$. Such a spatial dependence would lead to a $t^{2/3}$ time dependence of recovery. This therefore provides a possible mechanism by which pinning can take place. In any case, whatever the actual pinning mechanism, it seems clear that pinning is due to an interaction between dislocations and the dipoles rather than by the interaction of a vacancy with a dislocation to form

a charged half jog which is immobilised by the surrounding compensating charge cloud.

Table 6.1

$(\tan\delta)_{max.}$ values

Specimen	$(\tan\delta)_{max.}$
Pure specimens, annealed and quenched. Doped specimens containing 110 ± 7 m.p.m. Cd^{++} aged for 1 year.	No detectable peak, therefore less than 8.6×10^{-5}
Doped specimen containing 57 ± 7 m.p.m. Cd^{++} quenched from 350°C and measured after (a) 30 minutes (b) 3 hours	(a) $(11.9 \pm 0.9) \times 10^{-4}$ (b) $(8.7 \pm 1.1) \times 10^{-4}$
Doped specimen containing 110 ± 7 m.p.m. Cd^{++} shortly after annealing	$(5.6 \pm 1.1) \times 10^{-4}$
Doped specimen containing 57 ± 7 m.p.m. Cd^{++} shortly after annealing	$(4.0 \pm 1.0) \times 10^{-4}$

Table 6.2

Conductivity values. (σ_c) AT ROOM TEMPERATURE.

Specimen	Conductivity $ohm^{-1}\ cm^{-1}$
Annealed pure specimens	1.76×10^{-16} 2.37×10^{-16}
Pure quenched from 350°C	3.56×10^{-16} 2.37×10^{-16}
Unannealed specimens, aged at room temperature for 1 year, containing 110 ± 7 m.p.m. Cd^{++}	9.89×10^{-16} 1.08×10^{-15}
Specimens containing 57 ± 7 m.p.m. Cd^{++} quenched from 350°C	5.36×10^{-15} 6.65×10^{-15}
Specimens containing 110 ± 7 m.p.m. Cd^{++}, annealed	2.80×10^{-15} 2.64×10^{-15}
Specimens containing 57 ± 7 m.p.m. Cd^{++}, annealed	2.21×10^{-15} 2.45×10^{-15}

Table 6.3

Comparison of εM, σ_c and $(\tan\delta)_{max.}$

Specimen	$\frac{\varepsilon M}{\sigma_c}$	$\frac{\varepsilon M}{(\tan\delta)_{max.}}$
Annealed pure specimens	$(1.3 \pm 0.5)\times10^{8}$	$>3.23 \times 10^{-4}$
Pure quenched from 350°C	$(6.9 \pm 2.8)\times10^{8}$	$>2.38 \times 10^{-3}$
Unannealed specimens containing 110 ± 7 Cd^{++} m.p.m and aged at room temperature for 1 year	$(4.8 \pm 1.9)\times10^{8}$	$>5.59 \times 10^{-3}$
Annealed specimens containing 57 ± 7 m.p.m. Cd^{++}	$(6.5 \pm 2.6)\times10^{8}$	$(3.8 \pm 1.7)\times10^{-3}$
Annealed specimens containing 110 ± 7 m.p.m. Cd^{++}	$(15.5 \pm 6.2)\times10^{8}$	$(7.5 \pm 3.0)\times10^{-3}$
Specimen containing 57 ± 7 m.p.m. of Cd^{++} quenched from 350°C and measured within 30 minutes	$>8.5\times 10^{8}$	$>4.2 \times 10^{-3}$

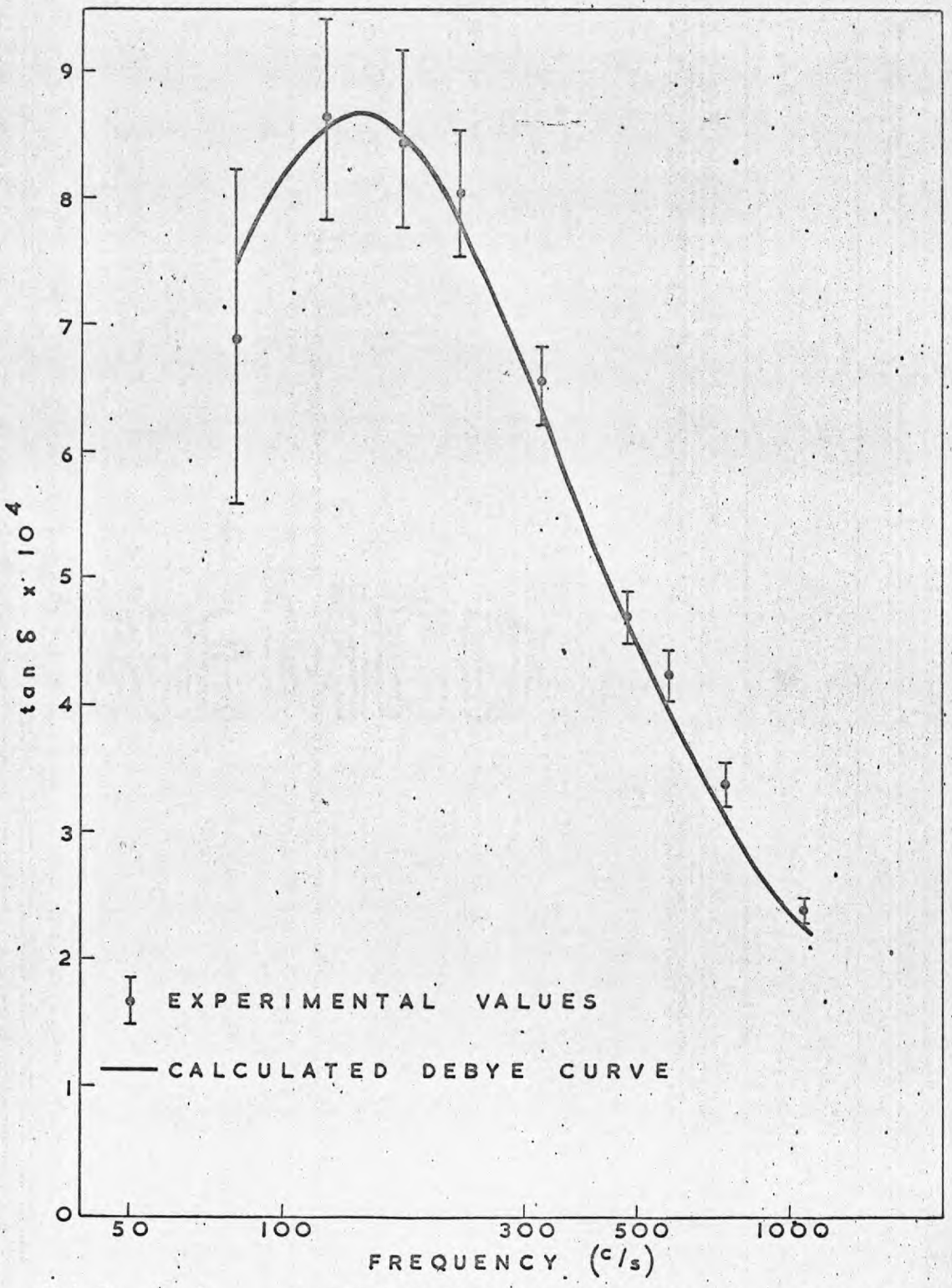

FIG. 6·1. DIELECTRIC LOSS PEAK IN SPECIMEN CONTAINING ABOUT 57 m.p.m. Cd MEASURED AT 36·5 °C, 3 HOURS AFTER QUENCHING FROM 350 °C.

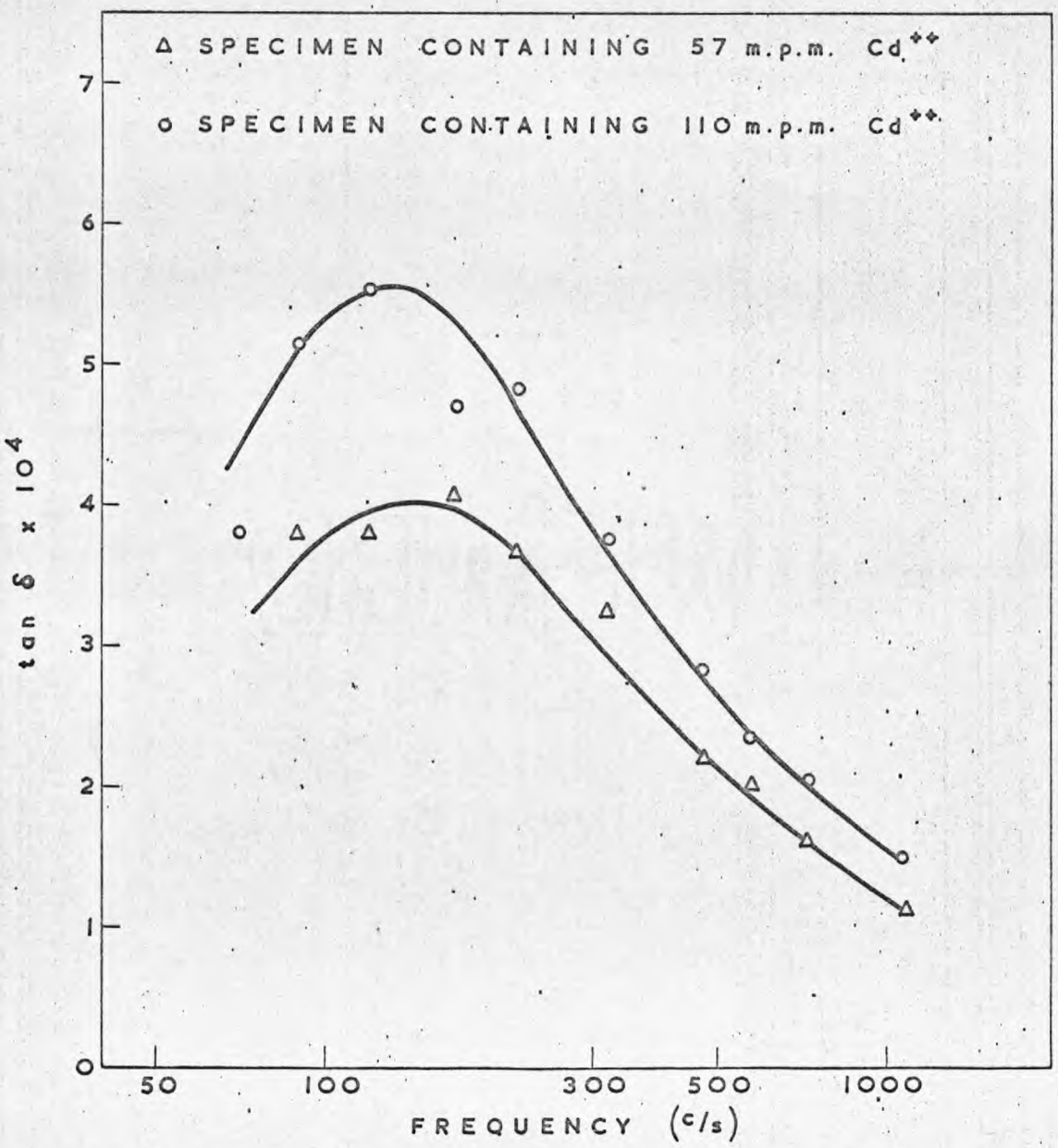

FIG. 6·2. DIELECTRIC LOSS PEAKS IN SLOW COOLED SPECIMENS

Chapter 7

Conclusions and suggestions for future work

The recovery of damping in Na Cl obeys the functional relationships predicted by the GHL theory and this has been interpreted as suggesting that the GHL model is basically a correct description of the recovery mechanism. By employing this theory the mobile weak pinning species has been identified as the divalent cation and cation vacancy associated pair and the migration energy has been calculated to be $E_m \simeq 0.70$ eV. The calculation has implicitly assumed that the bulk concentration of mobile weak pinners c_{10} is temperature independent for if it were not so then equations 1.27 and 4.1 would contain this temperature dependence in different relationships. This is because $\beta \propto c_{10}/(c_{10} + c_{20})$ and $\varepsilon M \propto c_{10}$. If the GHL theory is a good description of recovery of internal friction then the G-L theory should be a good description of internal friction with the reservations expressed in Chapter I. Employing the G-L theory an attempt has been made to measure the positive binding energy of weak pinning defects and dislocations and an apparent negative value has been obtained. Following Strumane et al[38] it has been shown that the apparently negative value can be explained if it is assumed that the bulk concentration of the weak pinning species is temperature dependent. This assumption leads to a positive binding energy provided the energy of formation E_f of weak pinners is greater than 0.36 eV $\pm$ 0.08 eV. There is here an obvious anomaly, for in the calculation of the migration energy E_m it has been assumed that the bulk concentration of mobile weak pinners is temperature independent, while the binding energy measurements suggest that the bulk concentration of the weak pinning species is temperature dependent. This anomaly might be simply resolved by inserting $c_{10} = (c_{10})_o \exp.[-E_f/kT]$ into equations

1.27 and 4.1. However if this is correct then log $\beta^{3/2}$ T and log $(\varepsilon M)^{3/2}$ T when plotted against 1/T as in Figs. 4.7 and 4.8 should not both lead to straight lines with the same slope unless $(c_{10} + c_{20}) >> c_{10}$ in the temperature range of these measurements. However, as was pointed out in Chapter 4, if this last condition is correct then the value of β should vary as much from pure to doped specimens as do the εM values and Figs. 4.7 and 4.13 show that this is not so. It is perhaps worth noting that on theoretical grounds it is certain that the concentration of associated divalent cation - cation vacancy pair is temperature dependent. Thus it is to be expected that if the mobile pinning defect is the associated pair then the calculated energy of migration (0.7 eV) should be corrected because of this dependence. If this correction is not made then the calculated value will be an underestimate and the correct value should be greater than 0.7 eV. Brown and Pratt[50] have obtained an activation energy of migration of the associated Cd^{++} ion - cation vacancy pair of 1.04 ± 0.11 eV, and the present work does not disagree with this value.

It is clear that very many more measurements must be made of the recovery parameters as a function of temperature to clarify the temperature dependence, and also measurements as a function of doping to determine more accurately their dependence on impurity concentration.

A more rigorous test of the GHL theory than has previously been applied is possible when all the data from a given specimen are combined. This will be carried out for a 2 % deformed, annealed, pure crystal. Fig. 7.1 shows $\log_{10} \triangle_{II}$ and $\log_{10}(\triangle E/E)_H$ plotted against $t^{2/3}$. According to equation 1.24 these should be coincident, or nearly

coincident, straight lines with slope $M = \frac{K\eta}{\mathcal{E}} c_{10} \frac{8\alpha}{a^2} \left(\frac{AD}{kT}\right)^{2/3} \log_{10} e$ and intercept $\log_{10}\left[\left(\frac{2L}{\pi A_2}\right)^{\frac{1}{2}} A_1\right] - \frac{K\eta}{\mathcal{E}}(c_{10} + c_{20}) \log_{10} e$. They are in fact parallel within experimental error, but displaced so that $r = \Delta_H / \left(\frac{\Delta E}{E}\right)_H \approx 3$. The slopes of these lines, together with other relevant data quoted in this analysis, are given in table 7.1. Fig. 4.3 shows the amplitude independent decrement of this specimen plotted as $\Delta_I^{-\frac{1}{4}}$ v. $t^{2/3}$, ($\mathcal{E} = 2.0 \times 10^{-7}$), and from this can be obtained (equation 1.25) β and $\left[\frac{120\,\Omega\,\Lambda\,B\omega}{\pi^3\,c}\right]^{\frac{1}{4}} \frac{a}{c_{10} + c_{20}}$. Equation 1.26 predicts that $\left(\frac{\Delta E}{E}\right)_I = 2\,\frac{(f_{el.} - f_I)}{f_I} = \left(\frac{6\Omega\Lambda}{\pi^2}\right) \frac{a^2}{(c_{10} + c_{20})^2} \frac{1}{(1 + \beta t^{2/3})^2}$ and because the true resonant frequency f_{el} of the specimen under elastic conditions is not known, it is necessary to employ the value of β obtained from the Δ_I data to test this relationship. Fig. 7.2 shows f_I plotted against $(1 + \beta t^{2/3})^{-2}$ and from this can be obtained $\frac{6\Omega\Lambda}{\pi^2} \frac{a^2}{(c_{10} + c_{20})^2}$. The data, encouragingly, display a fairly linear relationship. Finally Fig. 7.3 shows the G-L plot obtained 20 minutes after deformation. The slope of this is $K\eta(c_{10} + c_{20}) \times (1 + \beta t^{2/3}) \log_{10} e$ and the intercept is $\log_{10}\left[\left(\frac{2L}{\pi A_2}\right)^{\frac{1}{2}} A_1\right]$. Taking $\eta = 0.1$, $\Omega = 0.1$ and $\mathcal{E} = 2 \times 10^{-4}$ dynes[34] and assuming that the measured dislocation density $\Lambda = 5.8 \times 10^6$ cm^{-2} is the appropriate value to use, it is possible to calculate $(c_{10} + c_{20})$, the damping constant B and the factor K.

Firstly it is possible to calculate several values of $K(c_{10} + c_{20})$. Thus from (i) and (iii), (Table 7.1), $K(c_{10} + c_{20}) = 3.1 \times 10^{-4}$; from (ii) and (vii) $K(c_{10} + c_{20}) = 1.5 \times 10^{-4}$ and 2.0×10^{-4} ; and from (vi) $K(c_{10} + c_{20}) = 7.5 \times 10^{-5}$. These five values of $K(c_{10} + c_{20})$ have been derived from various combinations of intercepts and slopes of data obtained as a function of amplitude at constant time, and as a function of time at constant amplitude. They agree within a factor of 4 and this does not seem intolerable. From (v) $(c_{10} + c_{20}) = 3.3 \times 10^{-4}$ or 330 parts per million. This seems too high a value to be attributed to impurities (v. Chapter 2) in the crystals, but the value of $c_{10} + c_{20}$ has been calculated on the assumption that the measured dislocation density is the appropriate one to insert into the equation. If the correct value is less than the measured value, then $(c_{10} + c_{20})$ is decreased. From (v) the damping constant $= 6.5 \times 10^{-4}$ and this is larger than that predicted by theories of dislocation damping. Finally, K lies between 0.25 and 1.0, which is an order of magnitude greater than assumed by Granato and Lucke. The value of K has been discussed in Chapter I and both K and β have been discussed in some detail by Granato and Lucke[30] and will not be considered here.

It is probably fair to conclude that the GHL theory is a useful description of recovery although it is by no means completely accurate.

Apart from the suggestions already made concerning future work, a study of the vibration induced changes in internal friction would be useful. If this is associated with the diffusion of pinners along dislocations it should be possible to obtain the parameters which describe impurity diffusion along dislocations.[35] Moving outside the

field of internal friction, electron spin resonance studies of Mn doped Na Cl might elucidate the nature of the weak pinner in divalent doped Na Cl, since the paramagnetic ion might display a resonance which is shifted in frequency when associated with a dislocation. This is a faint hope however as order of magnitude calculations show that 0.1 m.p.m. of impurity can saturate the dislocations in a Na Cl crystal and it does not seem likely that a resonance associated with this quantity of material could be detected.

Table 7.1

(i) Slope of $\log \Delta_H$ and $\log\left(\frac{\Delta E}{E}\right)_H$ v. $t^{2/3}$ $\frac{K\eta}{\varepsilon} \; c_{10} \; \frac{8\alpha}{a^2}\left(\frac{AD}{kT}\right)^{2/3}$	1.0×10^{-3} secs$^{-2/3}$
(ii) Intercept of $\log \Delta_H$ and $\log\left(\frac{\Delta E}{E}\right)_H$ v. $t^{2/3}$ $\log_{10}\left[\left(\frac{2L}{\pi A_2}\right)^{\frac{1}{2}} A_1\right] - \frac{K\eta}{\varepsilon}(c_{10}+c_{20})\log_{10} e$	$\Delta_H \rightarrow$ - 1.7 $\left(\frac{\Delta E}{E}\right)_H \rightarrow$ - 2.2
(iii) Δ_I data $\beta = \frac{c_{10}}{c_{10}+c_{20}} \; \frac{8\alpha}{a^2} \; \left(\frac{AD}{kT}\right)^{2/3}$	1.4×10^{-4} secs$^{-2/3}$
(iv) Δ_I data $\left[\frac{120\,\Omega\Lambda\beta\omega}{\pi^3 c}\right]^{\frac{1}{4}} \; \frac{a}{c_{10}+c_{20}}$	2.6×10^{-1}
(v) $\left(\frac{\Delta E}{E}\right)_I$ data $\frac{G\Omega\Lambda}{\pi^2} \; \frac{a^2}{(c_{10}+c_{20})^2}$	8.8×10^{-3}

Table 7.1 (Continued)

(vi) Slope of G-L plot $K\eta (c_{10} + c_{20})(1 + \beta t^{2/3}) \log_{10} e$	3.3×10^{-6}
(vii) Intercept of G-L plot $\log_{10}\left[\left(\frac{2L}{\pi A_2}\right)^{\frac{1}{2}} A_1\right]$	- 3.4

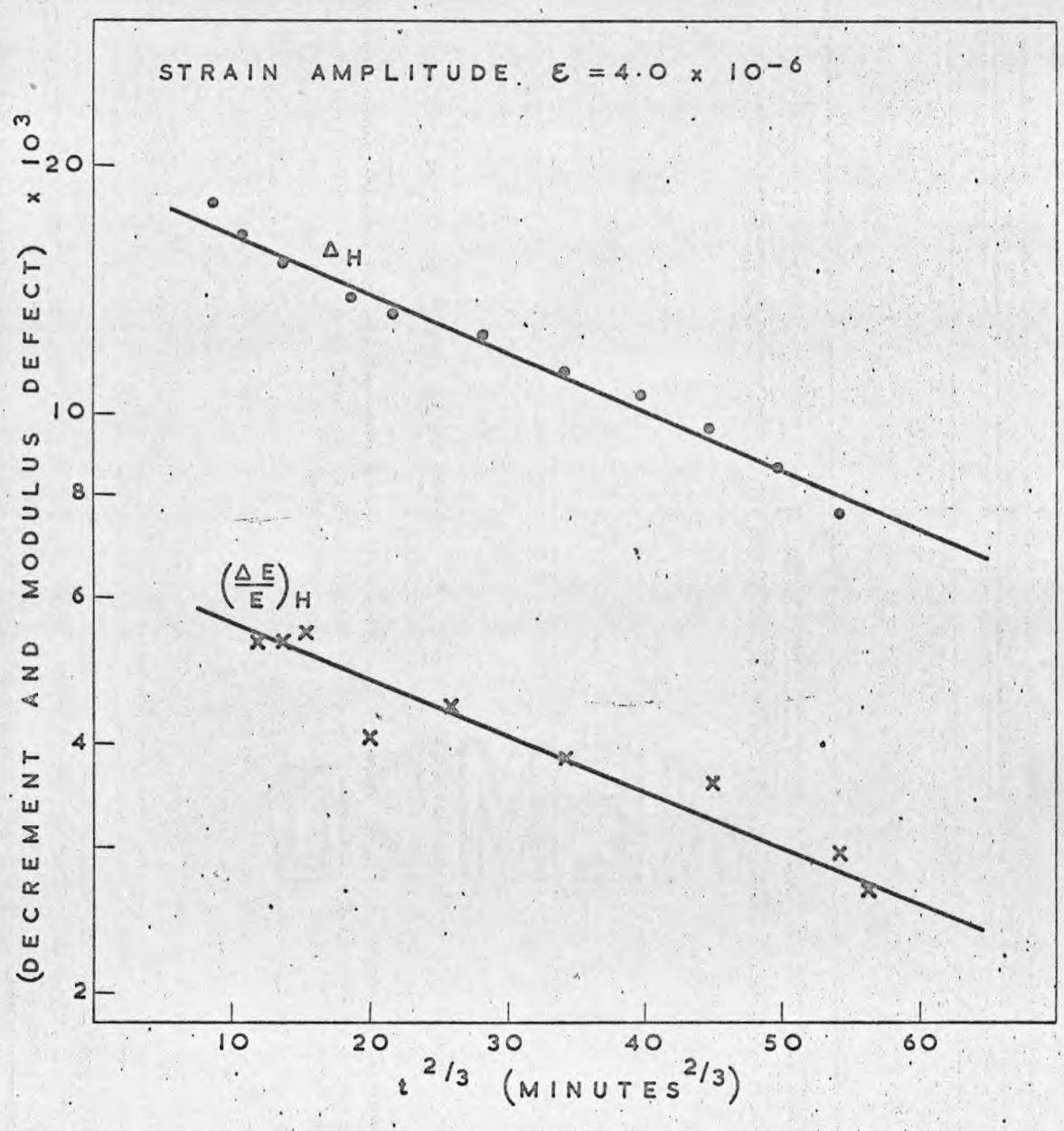

FIG. 7·1.
AMPLITUDE DEPENDENT DATA

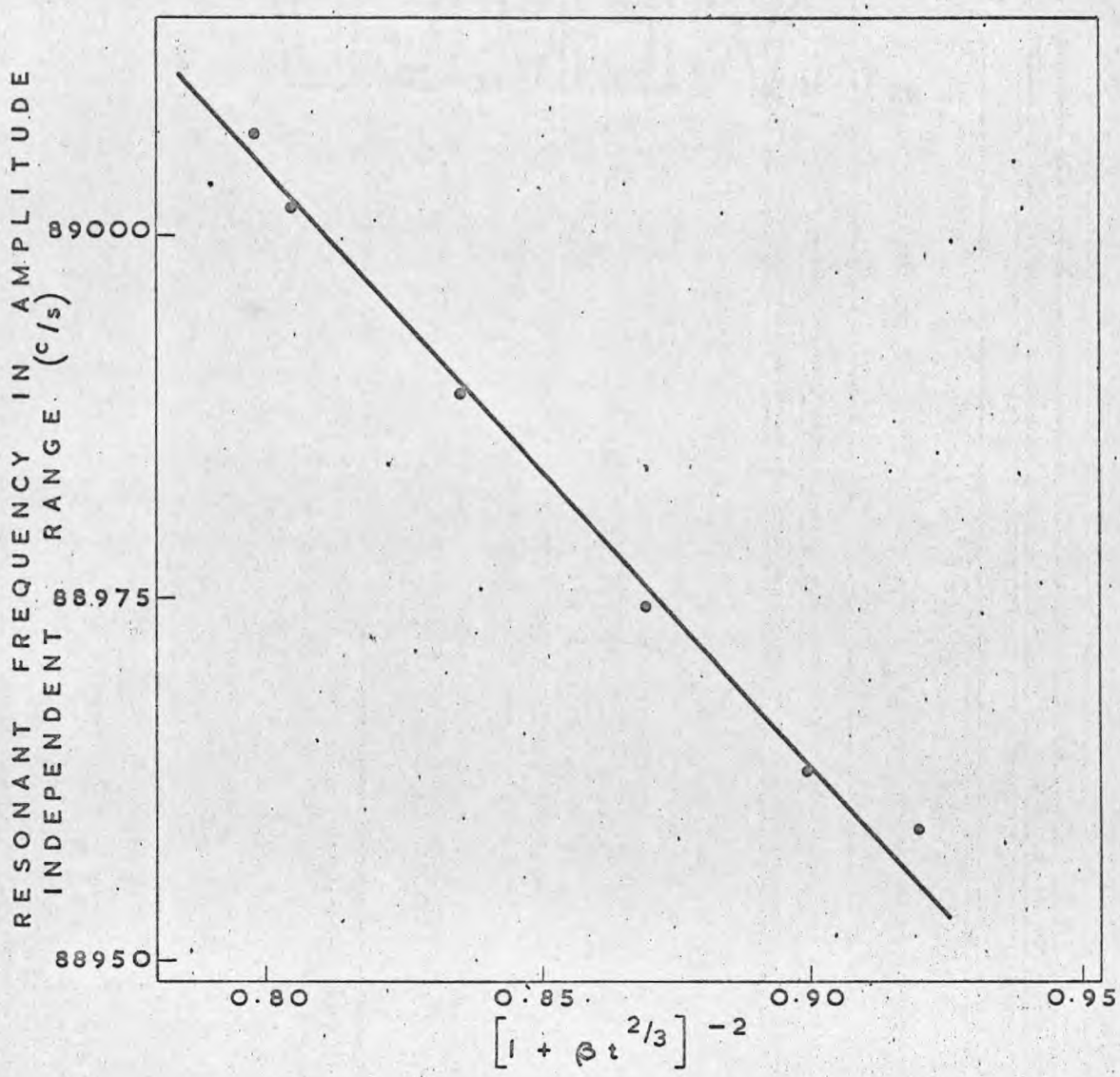

FIG. 7·2. AMPLITUDE INDEPENDENT FREQUENCY DATA

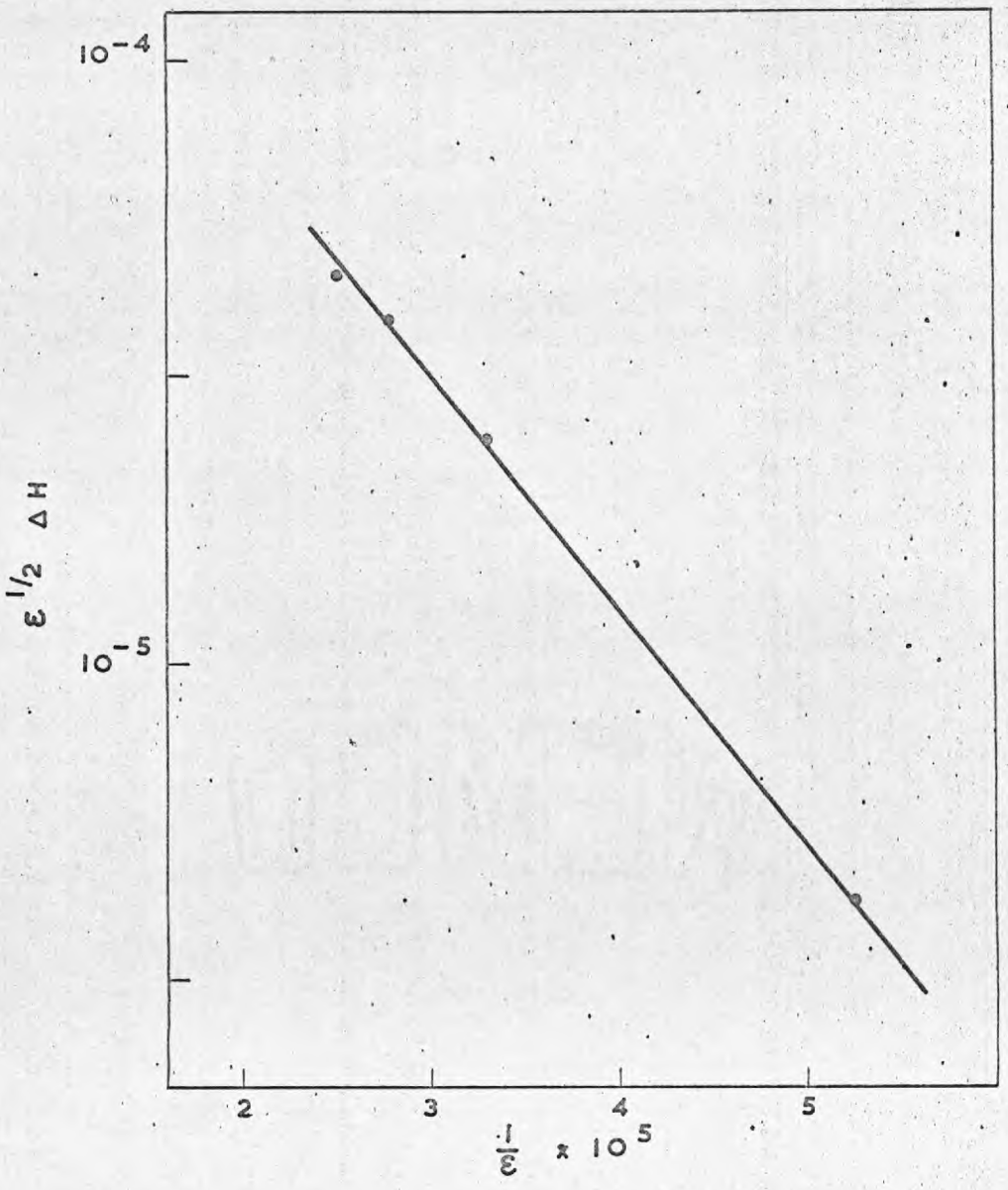

FIG. 7·3. G·L PLOT AFTER 20 MINUTES

Acknowledgements

This work has been carried out in the Department of Metallurgy at Imperial College, and I am grateful to Professor J.G. Ball for the provision of research facilities. I would like to extend my sincere gratitude to Professor P.L. Pratt who introduced me to the subject of internal friction in ionic crystals and supervised this research. I am indebted to him for his encouragement and advice during the period in which this work was carried out.

I have benefited from many stimulating discussions with past and present members of the ionic and ceramic crystals research group. In particular Dr. R.W. Whitworth for his advice about internal friction apparatus, Dr. J. Quin, Dr. D.L. Kirk and Dr. A.G. Evans.
Mr. H. Haddow gave invaluable practical assistance.

I express my sincere thanks to my wife for her patience and encouragement during this research and the preparation of this thesis.

Finally, my thanks are due to A.E.R.E. Harwell for providing financial support from October 1964 to October 1967.

References

1. See for example, R.C. Evans, An introduction to crystal chemistry, Cambridge University Press, 1964.
2. P.L. Pratt, Acta. Met., 1953, 1, 103.
3. R.W. Davidge and P.L. Pratt, Phys. Stat. Sol., 1964, 6, 759.
4. B.H. Kear, A. Taylor and P.L. Pratt, Phil. Mag., 1959, 4, 665.
5. A. Taylor and P.L. Pratt, Phil. Mag., 1958, 3, 1051.
6. R.W. Whitworth, Phil. Mag., 1965, 11, 83.
7. J.D. Eshelby, C.W.A. Newey, P.L. Pratt and A.B. Lidiard, Phil. Mag., 1958, 3, 75.
8. P.L. Pratt, Symposium on vacancies and other point defects in metals, Institute of Metals Monograph and Report Series No. 23, 1958.
9. J.S. Cook and J.S. Dryden, Australian J. Phys., 1960, 13, 260.
10. R.W. Dreyfus and R.B. Laibowitz , Phys. Rev., 1964, 135, A 1413.
11. A.R. Khan, Ph.D. Thesis, University of London, 1967.
12. K. Suzuki, J. Phys. Soc. Japan, 1961, 16, 67.
13. H.W. Etzel and R.J. Maurer, J. Chem. Phys., 1950, 18, 1003.
14. R.W. Dreyfus and A.S. Nowick, Phys. Rev., 1962, 126, 1367.
15. J.S. Cook and J.S. Dryden, Proc. Phys. Soc., 1962, 80, 479.
16. J.S. Dryden, Proceedings of an international conference on crystal lattice defects 1962, Conference Journal of the Physical Society of Japan, 18, Supplement III, 129.
17. J. Quin, Ph.D. Thesis, University of London, 1967.

18. A.S. Nowick, Progress in Metal Physics, 1953, 4, 1.

19. D.H. Niblett and J. Wilks, Advances in Physics, 1960, 9, 1.

20. K.M. Entwistle, Met. Rev., 1962, 7, 175.

21. D.R. Frankl, Phys. Rev., 1953, 92, 573.

22. R.W. Whitworth, Phil. Mag., 1960, 5, 425.

23. R.B. Gordon and A.S. Nowick, Acta Met., 1956, 4, 514.

24. C.L. Bauer and R.B. Gordon, J. Appl. Phys., 1960, 31, 945.

25. J.M. Sivertsen, Acta Met., 1962, 10, 401.

26. A.S. Nowick, J. Appl. Phys., 1954, 25, 1129.

27. J. Weertman, J. Appl. Phys., 1955, 26, 202.

28. L.J. Teutonico, A.V. Granato and K. Lucke, J. Appl. Phys., 1964, 35, 220.

29. A.V. Granato and K. Lucke, J. Appl. Phys., 1956, 27, 583.

30. A.V. Granato and K. Lucke, J. Appl. Phys., 1956, 27, 789.

31. C.R. Heiple and H.K. Birnbaum, J. Appl. Phys., 1967, 38, 3294.

32. D.H. Rogers, J. Appl. Phys., 1962, 33, 781.

33. G. Alefeld, J. Appl. Phys., 1965, 36, 2642.

34. A.V. Granato, A. Hikata and K. Lucke, Acta Met., 1958, 6, 470.

35. K. Yamafuji and C.L. Bauer, J. Appl. Phys., 1965, 36, 3288.

36. G. Alefeld, Phil. Mag., 1965, 11, 112.

37. R.W. Whitworth, Phil. Mag., 1961, 6, 1115.

38. R. Strumane, R. De Batist and S. Amelinckx, Phys. Stat. Sol., 1963, 3, 1379.

39. A.A. Blistanov, A.V. Panov and M.P. Shaskol'skaya, Soviet Physics - Solid State, 1963, 5, 1994.

40. A.A. Blistanov and M.P. Shaskol'skaya, Soviet Physics - Solid State, 1964, 6, 568.

41. A.A. Blistanov, I.V. Troitskii and M.P. Shaskol'skaya, Soviet Physics - Solid State, 1965, 7, 1492.

42. W.J. Johnston, J.S. Nadeau and R.L. Fleishcher, Proceedings of an International Conference on Crystal Lattice Defects, 1962, Conference Journal of the Physical Society of Japan, 18, Supplement III, 7.

43. C.L. Bauer and R.B. Gordon, J. Appl. Phys. 1962, 33, 672.

44. J. Marx, Rev. Sci. Instruments, 1951, 22, 503.

45. R.P. Harrison, Ph.D. thesis, University of London, 1965.

46. C.W.A. Newey, Ph.D. thesis, University of Birmingham, 1958.

47. R.W. Whitworth, Phil. Mag., 1967, 15, 305.

48. E.Y. Gutmanas, E.M. Nadgornyi and A.V. Stepanov, Soviet Physics - Solid State, 1963, 5, 743.

49. H.K. Birnbaum, Acta Met., 1955, 3, 297.

50. L.M. Brown and P.L. Pratt, Phil. Mag., 1963, 8, 717.

51. R. Bullough, U.K.A.E.A. report, 1964, A.E.R.E. - P.G.E.C./L.33.

52. A.H. Cottrell, Report on strength of solids, P.30, Phys. Soc., London, 1948.

53. R.L. Fleischer, Acta Met., 1962, 10, 835.